# Biosensors' Utility in Mammalian Cell Culturing

Parth Malik, Rachna Gupta, and Tapan Kumar Mukherjee

**Abstract**

Over the past three decades, sensors have swiftly emerged as the fundamental requirement for ascertaining the progress of molecular events. Biosensors prevail as a formidable member under this umbrella, wherein biological entities or engineered biomaterials are used as a probe to primarily screen biological interactions. The potential of biomaterials as molecular sensing moieties draws inspiration from their renewable nature, along with the possibility of being functionalized in diverse regimes. The distinguishing aspect of biomaterials as sensing probes prevails in terms of their specificity through which their involvement in the screened interactions is minimized. A blossoming aspect in this regard pertains to the development of robust shape and size-dependent nanomaterials (NMs) whose integration with biomaterials imparts a further precision enhancement to the screening of molecular events. The architecture of noncovalent self-assembly with van der Waals forces as stabilizing factors manifests as the key prospect of biological sensing. The development of nanobiomaterials has therefore catalyzed a robust screening of biological interactions as the NMs with enhanced surface area exhibit tremendous functionalization potential. This chapter is, therefore, focused on the utility of mammalian cells or the products thereof as biosensing probes with the most emergent applications of disease diagnosis and handheld devices.

P. Malik
School of Chemical Sciences, Central University of Gujarat, Gandhinagar, India

R. Gupta
Department of Biotechnology, Visva-Bharti Shantiniketan, Bolpur, India

T. K. Mukherjee (✉)
Amity University, Noida, Uttar Pradesh, India



T. K. Mukherjee et al. (eds.), *Practical Approach to Mammalian Cell and Organ Culture*,
https://doi.org/10.1007/978-981-19-1731-8_18-1

**Keywords**

Biosensors · Quantum confinement · Biomaterials · Surface plasmons · Shape and size dependent properties · Dynamic light scattering · Luminescence · Quantum dots · Nanocrystals · Functionalization · Surface engineering · Miniaturization

## 1 Introduction

Biological materials endow smart responsive behavior, characterized by their dynamic patterned structures attuned to specialized functioning and incorporation of natural bioactive compounds. These remarkably efficient architectural designs of biomaterials have been optimized ever since the origin of life on earth, thanks to stimulus-sensitive transport and mechanical properties thereof. Such attributes propel biomaterials as attractive candidates for flexible electronic sensing technologies. The most important criterion relates to the effect of the biological activity of biological materials, which aids in superseding the limited bioavailability and restricted morphology of materials involved in the fabrication of traditional flexible electronic devices. Mounting requirement for monitoring the nativity of biological interactions has necessitated the need for robust biomaterials, capable of specified biological efficacy, along with the modulation of screened interaction into a readable and modifiable electronic impulse. Conventional materials cease to be suitable here owing to their concurrent nonresponsiveness to biological stimulus and concurrent interactions. Conventional sensing makes it extensively preoccupied with inorganic/organic compound-based entities, such as carbon materials, metal oxide semiconductors, and polymers. Despite significant improvement in material attributes of these entities, their intrinsic mechanical properties, high cost, and non-biocompatibility arrest the biological stimulus detection feasibility of these materials. Biological materials are complex actuators and possess manifold attributes suitable in this regard, such as extraordinary topography, adequate in situ tailorability (capable of being adapted to a particular function) of chemical composition, and splendid mechanical properties. Apart from structural features, readily available natural biological materials have additional advantages in being renewable, cost-effective, water-soluble, biodegradable, self-adhesive, biocompatible, nontoxic, antimicrobial, and having good adsorption. A unique characteristic of natural biological materials is their natural optimized state, manifested since the inception of evolution, harnessing acquaintance for specified requirements. For instance, our immune system comprises several nano-biointerfaces having cancer cell recognition ability. Similarly, lotus leaves have superhydrophobic surfaces enabling self-cleaning properties, along with low water adhesion. Likewise, insect-eating plants are conferred with an immensely accurate sensing mechanism for enclosing their prey. Thereby, the master class on the natural phenomenon has plenty to ponder new insights from nature for deigning further novel materials. Some other prominent natural biological entities include their natural 3D structure (like in honeycomb and

natural cellular materials), imparting tunable elastic modulus to provide exceptional mechanical flexibility, such that the material can effectively and congruently assort to manifold curved and dynamic surfaces and interfaces, such as human organs and biological organism. The feasibility of affording a wide variety of functionalities (i.e., recognition, selective adsorption, and sensing) comprising several functional groups, such as –OH, –COOH, $–NH_2$, and $–NH_3$ groups, confers the properties that are seldom ever noticed in synthetic and man-made materials.

This chapter focuses on the above-briefed and related attributes of biomaterials capable of propelling them for sensing applications. Emphasis has been laid on the detection of redundant and immunologically critical disorders such as cancers, diabetes, cardiovascular complications, and several others.

## 2 Suitability/Principles of Biological Materials as Sensing Agents

Mechanical interactions cement a highly fundamental locus from biological concern. Mechanical forces resulting from chemical interactions elucidate the equilibrated distribution of kinetics (motility) and potential energy exchange (adhesion) on the cellular scale. These factors subsequently emerge as decisive factors for regulating molecular scale transport and affinity. Sensing through biological entities offers manifold significant opportunities to quantify the binding forces (BFs), displacements, and mass changes emanating out from cellular and subcellular events. In course of monitoring chemical interactions, concurrent specifications urgently press for monitoring of dynamic structural simulations as a result of varying interactive stoichiometries.

Natural biological materials have viciously emerged as frontrunners in such applications owing to the remarkable receptiveness of their physicochemical and biological characteristics. A thorough understanding of such attributes can revolutionize the applications of biological materials by enhancing a practical understanding of the amalgamated possibilities from different research fields. Biological materials endow splendid performance attributes through natural selection, enabling perfection in adapting to their surrounding environments. Therefore, we discuss the fundamental properties of biological materials with an emphasis on the latest advances suitable for sensing applications. A mandatory assumption here is that not all properties of biological materials are entirely well-defined. The discussion broadly focuses on the interaction of biological materials with the stimulus of varying nature, which would ideally enable sensing of the stimulus in as much unaltered form as possible (mandating no chemical interactions between the biological sensing agent and the stimulus to be detected). Owing to a legal binding on not including more than 50 references, readers are suggested to refer to the 2017 review article by Wang and colleagues for the details of referred studies included in this section. The literature source focuses on the electronic properties of biological materials and is published in *Chemical Society Reviews*.

## 2.1 Organized 3D Biological Assemblies

- Structure-driven properties are known for multiple specialized functions in natural creations and have inspired several technological innovations. Biological materials are inherently complex composites exhibiting structural diversity spanning several orders of magnitude in length. The exceptional characteristics are the outcomes of functional adaptation of their structure at distinct hierarchical platforms. In particular, organized 3D structures exhibit extraordinary replication of their constitutional design ingredients such as small fibers, tubes, open and closed foams, and plates.
- These structures span into eight distinct categories, having been thoroughly investigated by Meyers and subsequently reviewed by Espinosa and colleagues. The classification includes fibrous, helical, gradient, layered, tubular, cellular, suture, and overlapping structures. The most common entity herein is wood (fundamentally a composite) comprised of open spaces (lumens) and interconnected cells (tracheids), having a natural cellular structure. The varied arrangement and interior structure of spaces are responsible for the different porosity of various wood species. For instance, softwood species are characterized by uniform and closely packed rectangular cells, facilitating infiltration of solutions through the porous structure, whereas a large number of closely packed (1–100) μm ranged tubular cells, including growth ring boundaries, earlywood vessels, latewood vessels, fibers, rays, and axial parenchyma cells in marginal bands, have been traced in hardwood species (such as poplar) (Wang et al. 2017).
- Tissues from several different plants and animals are richly bestowed by their multiple architectural traits for desired transport and mechanical requirements. These structural characteristics comprise the spatial and geometrically specific distribution with 3D topography and the explicit arrangement of building blocks. Hierarchical entities from nature (e.g., seashells, bones, wood, bamboo, exoskeletons) possess numerous pores in their structures. Their high specific surface areas, extraordinary permeability, storage capability, and mass transfer properties make them structurally unique. Together, these features are highly useful in several inter- and cross-disciplinary applications, ranging from catalysis, adsorption, separation processes, sensors, energy security, confronting low food grain output, and ensuring their high shelf-life.
- Two illustrations of such capability quite amicably elucidate the multifunctional abilities of self-hierarchical structures. A gecko foot, for instance, is composed of a large number of well-configured microsized hairs with a 500 $mm^{-2}$ approximate density. The assembly portrays a unique assorted structure with the hairs comprised of numerous smaller nanoscale structures (carrying 100–1000 single hair in density). The multiscale structure hierarchy in gecko feet lends them manifold functions and abilities, including extraordinary adhesiveness, and super-hydrophobic and self-cleaning nature (Fig. 1).
- Erstwhile structures exhibiting hierarchical arrangements include seashells with two layers of distinct microstructures. These layers can be divided into peripheral prismatic calcite layers while the outer layer has a greater susceptibility toward

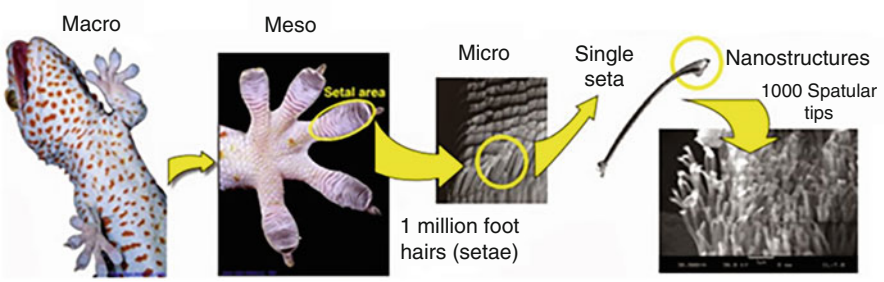


**Fig. 1** Pictorial view of the gecko foot hair structures, where each seta is divided into hundreds of split ends, spatulas. Such provisions facilitate infinitesimal intermolecular forces as van der Waals forces to provide the needed adhesion. (Figure included after taking inputs from http://bioimicryreport.blogspot.com/2014/02/gecko-feet.html)

brittle failures and the soft inner layer of nacreous aragonite can withstand comparatively greater inelastic deformation. Apart from this, there is a third layer consisting of self-assembled mesoscale that attributes to a significant dissipation of mechanical energy. The inner layer in this assembly consists of multiple microscopic aragonite polygonal tablets with (5–8) μm diameter, 400 μm thickness, and (20–30) nm organic material constituting a thick region (Wang et al. 2017).

## 2.2 Biological Activity

Biological materials in the relevant size range and corresponding activity possess several properties on par with those of synthetic materials. Biological material research has emerged as a most productive research domain in nanobiotechnology through the remarkable interlinking of biological, physical, and chemical sciences for developing advanced tools having the potential to revolutionize wearable and flexible electronics. The characteristic properties responsible for the expansion of biological materials into diversified areas are as follows:

- Remarkable mechanical strength and flexibility for obtaining wearable electronic-grade biological materials.
- Altered colored appearances of biologically suited materials are capable of forming specified platforms to make sensors suited for optical transduction. Such materials can revolutionize the diversified requirements of anti-forgery devices, optical gas sensors, and biosensors for the detection of cancer and air pollution.
- With remarkable water-resistant ability contributing to self-cleansing and a meager water adhesion, the biological materials provide several benefits for use in printing, optical transduction, ultra-precision sensors, and energy storage batteries.

- Robust adhesive properties of biological materials over several 3D surfaces manifest a smart system for further conjugating bonding encompassed with alluring functionalities.
- Nearly all biological materials are antimicrobial, exhibiting suitability for making implantable antimicrobial materials in medical devices (such as artificial electronic skin).

***The following sections describe the abovementioned properties of biological entities about their sensing amicability.***

## 2.3 Mechanical Properties

The major mechanical features conferring suitability of sensing applications to biological materials include flexibility, stiffness, strength, and fracture toughness, imparting them robustness for applications in multiple domains.

The traits of flexibility, toughness, and tensile strength imbibe biological materials toward fascinating wearable green electronics. Some critical aspects of these are as follows:

- Well-ordered 3D hierarchical structures having nano- to microscale dimensionality. The mechanical properties are inherently defined by the microstructure, wherein distinctive character allows biological materials to function as active units capable of meeting specific demands. Meyers and coworkers discuss these structural design prospects leading to diverse mechanical properties of biological materials. For instance, chitosan exoskeletons consist of well-organized repetitive hierarchical structures with remarkable mechanical flexibility, comprising several discrete levels (Fig. 2). These exoskeletons can be further divided into a large number of smaller fragments. The combination of overlapping segments herein depicts an improved mechanical response arising out of overall flexibility and spontaneous internal movements (refer Wang et al. 2017 for discussed studies).
- The overlapping structures confer consistent modified responses, such as bending, deformation, and drape, the last one serving as a motivational breakthrough for several researchers toward designing novel biological composites equipped with splendid mechanical flexibility for developing flexible green electronics. Such overlapping structures could be easily located in shark skin, fish scales, butterfly wings, seahorse tails, and pangolin plates, and decisively impart efficient joined flexibility and working potential.
- Highly efficient flexible electronic devices could be easily available as such from animals, such as natural spider silk (having micron-scale diameter) is a highly apt example of an assorted structure comprising numerous aligned fibers. Fibrous structures are also very finely fitted entities for strength, high tension, and effectively low to null compression. Molecular configurations of natural silk present another befitting framework for dynamic response channeling. At low-stress levels, natural-grade silk responds via entropic folding of amorphous

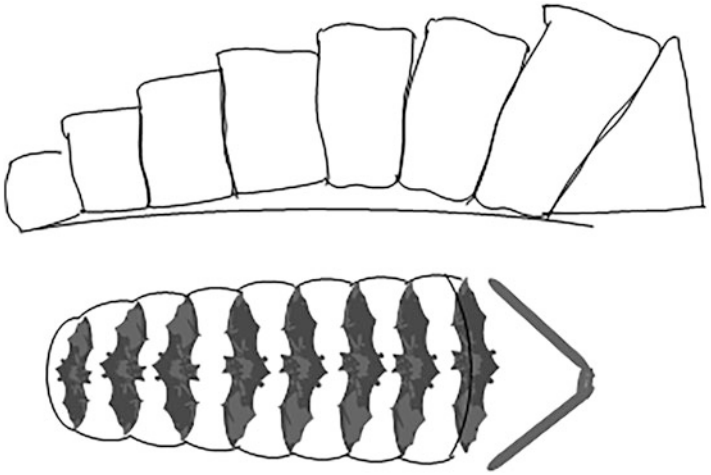

**Fig. 2** Partly covered structures from chitin (Polyplacophora) represent a range of biological hierarchies for improved biological sensing

strands (uncoiling and straightening of protein strands). Contrary to this, at high pressure, the major interactions are weak hydrogen bonds so that the crystalline domains can sustain the load.

- The credit for illustrating the intricate stress–strain correlation of fibrous assemblies under physical stimulus goes to Meyer's group. Its quantitative version is as depicted in Eq. 1:

$$\sigma = K_1 \varepsilon^{n+1} + H(\varepsilon_c) E(\varepsilon - \varepsilon_c) \tag{1}$$

where $\sigma$ is the stress, $K_1$ is a material parameter, $\varepsilon$ is the strain, and $n$ varies as per the chosen material. The constant as an exponent, n being 1, relates to the mechanical response of collagen support, and $H$ is the Heaviside function and is usually activated at the beginning of the second regime ($\varepsilon = \varepsilon_c$, the strain corresponding to entirely extended geometry of fibers; refer Wang et al. 2017 for discussed studies).

- So, natural silk as a remarkable fibrous material exhibits high tensile strength or unidirectional stiffness apart from having robust mechanical properties and insulating nature. These attributes make natural silk a highly useful entity for being used as biocompatible passive support and packaging material for flexible electronic devices. Readers are suggested to refer the rigorous contributions of Meyer's group, where the authors have described the quantitative profile of mechanical properties of several other biological materials, along with their structural advantages.

## 2.4 Structural Coloring

The colored features of living organisms generated on account of iridescence, pigmentation, or superposition of two distinct colors are in themselves a kind of boost for sensing-based applications. Among these several modulations, structural color is a distinctive natural trait exhibited by the interaction and transport of ordered structures with light. The hierarchical structural arrangement in biological structures serves as an incentive for efficient light absorption unlike that of pigmentation. Some notable aspects regarding this property are as detailed next:

- Structural color is a source of tunable energy transformation, and, most importantly, it is environmentally friendly as it does not involve external mediation of chemical dyes. Perhaps, tunable structure exhibition is used by many living organisms as the means of adapting to the surrounding environment such as using communication, predation, camouflage, and several other modulations.
- Several instances can be found supporting the response monitoring via color development. Butterfly wings, hormonal and stimulus responses of plants, flowers, and leaves, environmental adaptation mechanisms of a chameleon, insectivorous plants, and hibernation patterns of certain birds are some other traits. Butterfly wings comprise multiple beautiful and purely (by themselves) iridescence appearances owing to their hierarchical and ordered repetitive structural constitution. For instance, the butterfly *Morpho sulkowskyi* bears a tempting dual color (blue) on the top and (camouflaged brown) beneath the wing's surface. The distinctive blue and brown appearances are noticed in the flying and landing stages; such characteristics if replicated using pressure equilibration modulations can be the remarkable basis of a piezoelectric biosensor. Apart from being fascinating, the shiny butterfly colors are unique because of the seeing-through (transparent character) ability of their wings. Glasswing butterflies have a characteristic of this ability where the glassy sections of wings confuse their predators, the time lapse in which butterflies fly away. This ability is often recognized as optical transparency, implying that all light that goes into the wing continues out of the other side. A closer look at the transparent regions of glasswing butterflies using a scanning electron microscope (SEM) shows numerous randomly sized patterns of nanopillars (Fig. 3). The exclusive source of the transparent character of butterfly wings (irrespective of directional view) is the random size and shape of pillars. Among the noted erstwhile functions of butterfly wings are their extraordinary hydrophobic and self-cleaning abilities. The significance of hydrophobicity for butterfly wings stems from the inherent ability to resist a rainstorm in the absence of which the residual water on butterfly wings makes flying difficult. The water droplets are unable to penetrate the hydrophobic pockets due to stronger interactions of water molecules than those between water and air. Furthermore, the air pockets have an internal pressure that resists water from permeating through.
- Similarly, *Aphrodite* (a kind of trivial humid water worm) hair possesses intense structural colors derived from front cylinders, which collectively diffract light due

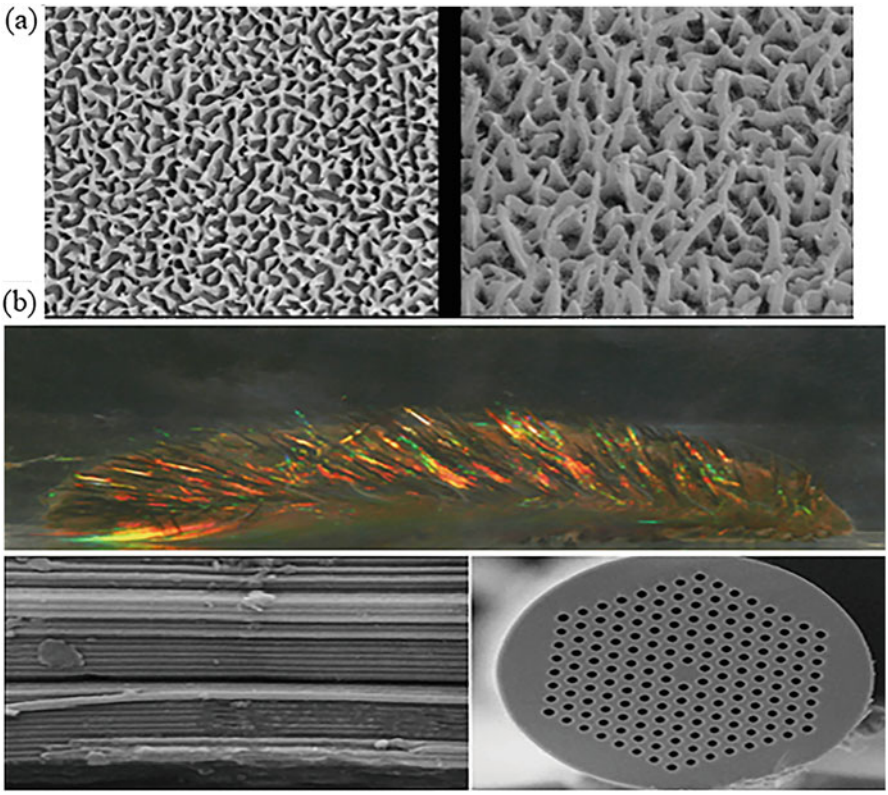


**Fig. 3** (**a**) Surface topography of transparent regions of glasswing butterfly. (**b**) The tiny spines of Polychaeta, *Aphroditidae*, are just like inherent photosensitive crystalline materials. The cross-sectional image depicts their closer view, typically comprising regular configured hollow channels with chitin walls (bottom left), the red color of spectrum incident on *Aphrodita* spine. Alternate heating and retrieving the bundles of glass capillaries can be a simpler method to obtain similar synthetic photonic fibers. (Parker et al. 2001; Russell 2003; Siddique et al. 2015; image reproduced with permission)

to substantial longitudinally oriented, closely packed, and 230 nm in diameter. These hairy structures make up tubular structures constituted of hexagonally configured hollow cylindrical channels that are a few nanometers across and are made up of chitin. These arrays act as 2D photonic crystals that reflect light strongly in the long wavelength region of the spectrum. These structures confer the *Aphrodite* spine, a deep, iridescent red color. Whether the optical properties of polychaete spines have a biological function remains poorly understood, but the applications for light-manipulating fibers in optical technology are indeed immense. Such observations could be traced to the efforts of Phillip Russell and collaborators, who fabricate the assemblies by stacking glass capillaries into hexagonally packed bundles and drawing them out under heat into narrow fibers laced across with perforations. If "defects" are introduced into an array of

tubular channels (either via including a wider capillary or a solid rod in the bundle), light can pass along the defect while being excluded from the photonic crystals. This creates an optical fiber cladding that is essentially impermeable to the light wavelengths within the band gap. Photonic crystal fibers of such configurations can guide light around the tighter bands than normally possible with conventional fibers, having comparatively weakly confined light due to internal reflection at the fiber surface. Hence, these fibers are anticipated to function better for guiding light in tightly confined spaces, such as on optical microchips.

- Similar examples of such biological structures are the wings of peacocks and the varied appearances of *Hercules* and *Tortoise* (beetles). Monitoring the track record for color-specific tolerated stimulus can be a crucial breakthrough in the utilization of these natural biological mechanisms for optical, electronic, and calorimetric sensing.

## 2.5 Hydrophobic Receptivity

Hydrophobicity is the most important natural characteristic of natural biological agents (in particular, for the aquatic regime) and endows a sharp dependence on surface topology and morphology (Fig. 4).

Superhydrophobic materials are in typically high demand owing to their potential significance in printing, microfluidic devices, nanoparticle assembly, batteries, high-sensitivity sensors, and optical devices. The following points illustrate the significance of superhydrophobicity in improving the sensing mechanism:

- Feasible strategies toward a progressive replacement of traditional synthetic materials are of key significance. Several natural biological materials are known to possess superwettability. The most fabulous example of natural superhydrophobic biological material is lotus leaves exhibiting superhydrophobicity toward the water with nearly 150° water contact angles and self-cleaning properties. These self-cleaning attributes are immensely useful for the removal of dust and dirt particles through the motional activities of water droplets. Apart from self-cleaning properties, Mele and Feng groups independently reported *Strelitzia*

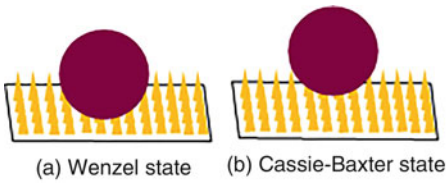


**Fig. 4** Surface topology and morphology-driven hydrophobic sensitivity. Due to the larger contact area in the Wenzel state, the role of the surface is more prominent in the functional activities

*reginae* and *Oryza sativa* leaf surfaces to be composed of parallel microgrooves, and also exhibit superhydrophobic features (Wang et al. 2017).

- The anisotropy of superhydrophobic properties enables the displacement of droplets in a direction parallel to that of microgrooves. This response could be a much-needed boost for the development of amicable fluid-transport systems, enabling the assessment of relative aqueous interactions of distinct chemical surroundings of a surface region(s).
- Other fine examples of superhydrophobic biological material are the wings of the *Morpho* butterfly, which exhibit directional adhesion. The nonwetting ability of these structures facilitates easier shedding of water droplets from a butterfly's wings upon a slight shake, thereby facilitating rain flying. These wings can be easily used to quantify the drying extent of a biological specimen, which is often the requirement for sophisticated characterization sample preparation.
- The genesis of hydrophobicity is manifested through the existence of an air layer trapped inside the rough surface, which can reduce the liquid and ion penetration alongside facilitating efficient heat transfer. Studies have illustrated the making of pollen comprising electronic skin as a hydrophobic biological material with a contact angle of nearly 100°, subsequently elucidating a strong influence of hydrophobic on the electronic signal stability. Investigations focusing (0–30) min water penetration of pollen material also revealed no significant variation in water droplet physicochemical and flow behavior concerning time.
- Modulating the interlayer frictional forces and interlocked structures of e-skin materials through increasing the relative pollen content enabled enhancement in elasticity (a highly important requirement for flexible electronic agent). Thereby, this response illustrated that biological materials are bestowed with several attributes as active units that require consistently good mechanical and hydrophobic properties.

### 2.5.1 High Adhesion

Smart adhesive materials with flexible surfaces capable of being engineered for various applications are being provided by biological entities. To name a few, biomolecules of amphibian and aquatic organisms (waterproofing ability), the skin of animals, and certain plants are the tissues that meet robust needs. The following points describe such features of several living tissues:

- Owing to strong adhesion or cohesion abilities, biological materials of natural origin are not easy to be de-eliminated from integrated assemblies and are therefore widely used in making multicomponent assembled stable devices. Dauskardt and colleagues provided extensive illustrations of organic semiconductors and devices in terms of their adhesive and cohesive energies, noting the dependence of the former on chemical bonding, van der Waals interaction, and chain entanglements. It must be emphasized here that adhesion may also refer to the contact between two dissimilar molecules/surfaces, whereas cohesion essentially involves interaction between two similar species (which could be the

subcomponents of two independent systems) (refer Wang et al. 2017 for cited studies).

- Polydopamine (PDA), herein, is the most famous natural adhesive, depending on both noncovalent and covalent bonding. This material strongly adheres to organic surfaces through covalent coupling under alkaline conditions via appropriate addition or coupling reactions. The process depends on the typical oxidation of catechol (present in polydopamine) to quinines. Steadfast PDA addition has created significant interest in the fabrication of hybrid materials and functional substrates. The past 10 years have witnessed overwhelming importance being conferred to gecko lizards to adhere to surfaces with different orientations and frictional coefficients. Being a neurotransmitter, such attributes of PDA have revolutionized its use toward efficient binding to its signaling mediators. The relative frictional extents could be therefore utilized in ascertaining the nature of the bound stimulus, keeping the database as standard.
- A 2011 study by Helbig and colleagues revealed the ability of *T. bielanensis* to detect *Candida albicans*, *Staphylococcus aureus*, and *Escherichia coli*, comprising significant diversity in fungi, and Gram-negative and Gram-positive bacteria. Analysis showed no visible culture deposition even after 4 days. In general, terpenes are known to confer protection from plants and insects to safeguard the cuticular surface from microbial adhesion (refer Wang et al. 2017 for cited studies).
- Separate investigations showed that the lipid layer is not covalently connected with the epicuticle and could be therefore extracted using carefully chosen dissolving solvents or mechanical shedding in the form of dust particles through animal movement. Lipids gradually transit to the surface and recover the coating. In this process, the lipid film could be used as a sacrificial layer that is regularly reproduced to avid microbial invasion. So, there is no need to provide nonspecific reaction control from an external agency (to keep microbial contamination arrested) and the growing *T. bielanensis* in itself is capable of protecting against such interference.
- Natural oligomeric proanthocyanidin (OPC), a standard anti-inflammatory drug, can combat neurodegenerative disorders through multiple therapeutic mechanisms. The semihydrophilic OPC assists the self-adhesion of nanohydrogels via acting as a structural stabilizer through its structural architecture and abundant –OH groups, which gradually develop into a biologically stable 3D anti-inflammatory neural interface. So, the adhesion ability of OPC provides a strategy for the nanofiber-like protective ability of the hydrogel network via distributing its structural layers and extending the anti-inflammatory impact on the assorted neurons and their exaggerated confirmations.
- Recent studies of the Chen group elucidate a novel 3D nanocarrier utilizing natural antioxidant OPC reagents derived from natural grape (Fig. 5). Consequently, this nanocarrier possesses exceptional antifouling properties as an OPC-coated neural probe, developing lower impedance alongside exceptionally higher signal stability compared to a nanocoated probe after short-range and continual in vivo implantation.

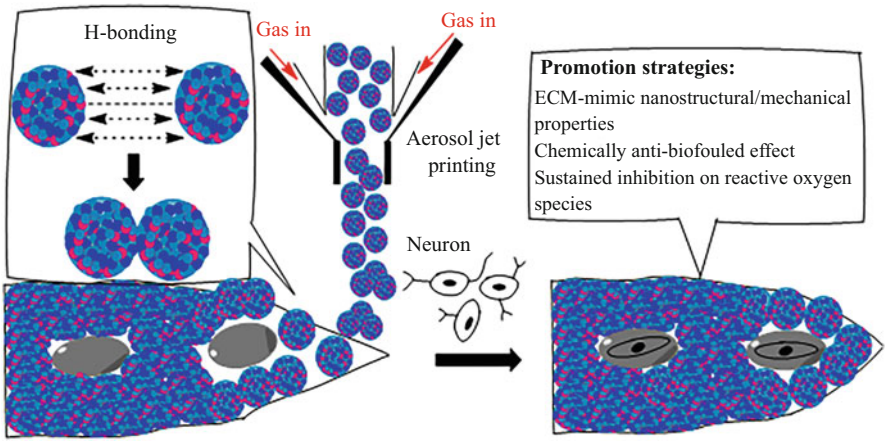


**Fig. 5** Schematic procedure of an oligomeric proanthocyanidin (OPC) neural probe fabrication having an anti-inflammatory interface. A native semihydrophilic receptivity of OPC aids in the self-adhesion of nanohydrogels by acting as a structural stabilizer. The aromatic architecture and abundant –OH groups are the key controls for developing a biologically compatible 3D anti-inflammatory neural interface

- Inspection of this implanted assembly through immunostaining revealed a reduced astrocyte population around the implanted site through a protective functioning of an OPC-based probe. Apart from decreased astrocyte population, significant reductions were noticed in activated microglia, paving the way for improved survival 28 days after being implanted. Thus, this study presents another remarkable advance through the potentiated antioxidant activity of implanted OPC reagents, which is not only a biological source but also biological essence (as noted through its implantable ability).

## 3 Sensor and Biosensor Distinctions

### 3.1 Sensors

A sensor is a device used to detect any variations in physical, chemical, and biological extents quantified through changes in light intensity, force expression or exertion, pressure, locus-defining coordinates, sonication impacts, gases, specificity, and functional activities of proteins, microorganisms, cells, and others (Fig. 6). Enhanced precision of sensing mechanism depends on specificity, sensitivity, accuracy, cost-effectiveness, and capability to respond in different environmental conditions. While the sensor monitors the interaction of any kind of stimulus (resulting in varied physical, chemical, optical, electronic, or acoustic responses), a biosensor exclusively tracks the changes in the biological response of the scrutinized entity.

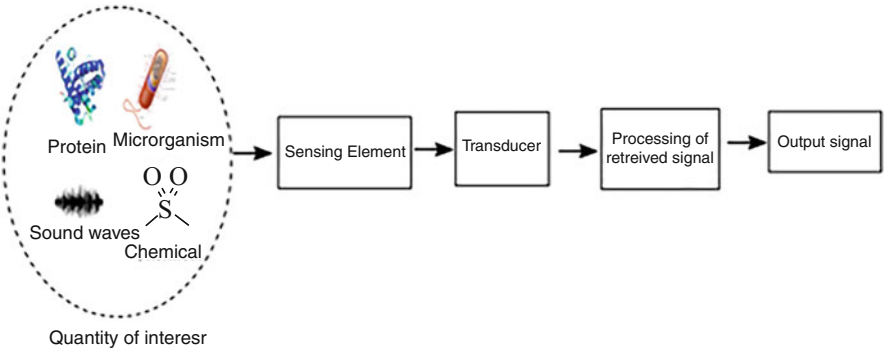


**Fig. 6** Flow diagram of sensor functioning

Based on the physical positioning of the sensing probe and analyte, the following categories of sensors are known to prevail:

- **Contact**: The sensors of this mode necessitate physical contact with probe moiety to sense them. Coziness and biocompatibility are prominent considerations to be kept in mind concerning sensor functioning in contact mode, wherein time-bound responses monitor the characteristic performing aspects (of the analyte). A persistent aspect of concern here is the minimization of fouling effects that persist for prolonged durations. *Measuring thermometer.* The most common examples of such sensors include the waterheating electrical rod and temperature. Both of these mandate their residence with their respective sensed moieties (water and body of the host, respectively). Some diagnostic procedures working through noncontact mode include electrocardiography (ECG), electromyography (EMG), and electroencephalography (EEG).
- **Noncontact**: This mode of sensing does not necessitate any direct contact between analyzing probe and the analyte. The most common example of such sensing devices is magnetic retrievers (which attract iron or magnetically sensitive material without physical contact with them). Biological instances of such sensors include the identification of a substrate (among many) by enzyme and antigen (among many) by its specific antibody. These sensors are mostly utilized in ambient applications like passive infrared (PIR) spectroscopy, having less impact on the environment or quantity of interest. A comparative advantage of these sensors over the contact mode sensing devices is that there are much fewer chances (as well as maintenance of provisions) mandating moderation of interaction between probe and analyte, resulting in a better reliability of sensed response.
- **Sample elimination**: This is only a specified domain of noncontact sensors, wherein the prediction of toxins or a threshold extent of a biochemical aspect could be maintained. The purpose of such tracking is not limited to detection but also to entirely squeeze out the undesired proportions. Ascertaining *E. coli*

contamination of water or excessive blood glucose extents are some illustrations of such sensing mode.

### 3.1.1 Working Components of a Sensor

- Certain working parameters of a sensor form the defining aspects of its classification, such as sensitivity, stimulus range, constitutional material, detection means, conversion phenomena, the field of applications, and stimulus being intercepted (Tables 1, 2, 3, and 4).

**Table 1** Functional attributes of a sensor having a key role in the typical performance

| | |
|---|---|
| Sensitivity | Stimulus range (span) |
| Stability (short and long term) | Resolution |
| Accuracy | Selectivity |
| Speed of response | Environmental conditions |
| Overload attributes | Linearity |
| Hysteresis | Dead band |
| Operating life | Output format |
| Cost, size, and weight | Input control |

**Table 2** The diversity of input stimulus describes a sensor's functioning

| | |
|---|---|
| Acoustic | Wave amplitude, phase, polarization, spectrum, and wave velocity |
| Biological | Microbes, enzymatic activity. antigen–antibody interaction, and biomass driven |
| Chemical | Specific constitutional state of stimulus |
| Electric | Charge, current, potential difference (mV), electrostatic potential, electric field (amplitude, phase, polarization), and electrical permittivity |
| Magnetic | Magnetic field strength (amplitude, phase, polarization), magnetic flux, susceptibility, and permeability |
| Optical | Wave amplitude, phase, polarization, spectrum, wave velocity, refractive index, emissivity, reflectivity, and absorption |
| Mechanical | Position, acceleration, force, stress, strain, shear, mass, density, torque, shape, roughness, orientation, stiffness, and viscosity |
| Radiation | Energy, intensity, penetration ability |
| Thermal | Temperature, flux, specific heat, and thermal conductivity |

**Table 3** Sensor configuration based on sensed and percept energy stimulus

| Sensor configuration | Perceived energy stimulus |
|---|---|
| Physical | Thermoelectric, electroelastic, photoelectric, thermomagnetic, photomagnetic, thermooptic, magnetoelectric, photoelastic, electromagnetic, thermoelastic, and combinations |
| Chemical | Chemical conversion, physical conversion, electrochemical process, spectroscopic modulation, and combinatorial phenomenon |
| Biological | Biochemical conversion, physical conversion, the influence of test organism, and combinations |

**Table 4** Sensor classification is based on specific applications

| | |
|---|---|
| Civil engineering | Domestic and structural applications |
| Distribution, commerce, and finance | Environment, meteorology, and security |
| Energy and power | Information and telecommunication |
| Health and medicine | Marine |
| Manufacturing | Recreation and toys |
| Military | Space |
| Scientific measurement | Robotics, bioelectronic, risk perception, safety assessment, and several others |

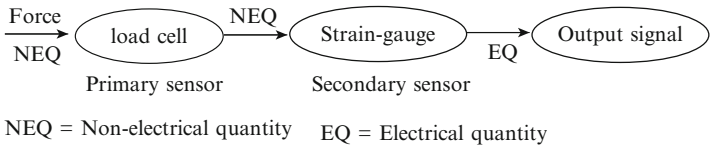


**Fig. 7** Distinction of primary and secondary sensors

- Sensor performance is a combination of optimized fitting of multiple factors, which are more authentically understood as the classification criterion.

### 3.1.2 Classification of Sensors

*The sensor classification is described as follows:*

Classification based on the application method
Classification based on the energy conversion
Classification based on the output signal form

*Here is a brief discussion about them:*

**Classification Based on the Application Method**

- **Primary sensor**: Here, the input is directly detected by the sensor. For example, load cell is used to extend the weight of the object.
- **Secondary sensor**: In this case, the output of the primary sensor is sensed by another sensor whereby the nonelectrical stimulus is converted into an electrical signal (Fig. 7).

**Classification Based on the Energy Conversion**

- **Active or self-generating sensors**: Generates output signal in response to external excitation (Fig. 8a). Examples are LVDT and a photovoltaic cell.
- **Passive sensor**: This produces an output signal without any external excitation. Examples are thermistor and strain gauge produce resistance to temperature and length variations (Fig. 8b).

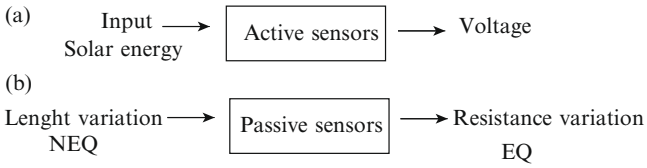


**Fig. 8** (**a**) Working diagram of the active sensor. (**b**) Working of a passive sensor

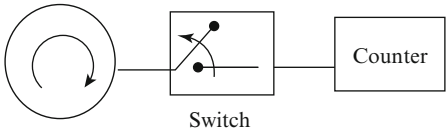


**Fig. 9** The switching actions are counted through an electronic counter

**Classification Based on the Output Signal Form**

- **Analog sensors**: Provides varied continuous output signal *vis-à-vis* input changes. In addition, within the sensor's range, the output signal can have infinite values.
- **Digital sensors**: In contrast to analog, digital sensors have a discrete form of output with finite values. Here, the data are digitally converted and transmitted through an electronic counter. For example, the switching actions of a revolution counter (Fig. 9).

### 3.1.3 Terminological Distinction of Sensors

Though all sensors are exclusively confined within contact and noncontact regimes, some terminologies do refer to them in consideration of their specific property ascertaining. For instance, the optical sensor may indirectly refer to any of the spectrometric techniques. Similarly, ultrasonication subjection could be the means to know about the extent of cavitation meted out for a fixed duration of sound waves persistence in a medium. Figure 10 depicts an approximate distribution of different properties analyzed by the above sensor classification domains through their working modes, energy conversion efficacy, and output signal form. Salient sensor types with their advantages and disadvantages are listed in Table 5.

### 3.1.4 Sensor Characteristics

- Typically, a sensor response and functioning are described by its characteristic behavior corresponding to static and transient responses toward an input stimulus. These include static and dynamic characteristics.
- The **static characteristics** defining a sensor functioning encompass all properties of a system post-steady-state manifestation of all transient effects, such as accuracy, discrimination, precision, errors, drift, sensitivity, linearity, and hysteresis. The dynamic attributes describe the immediate or instantaneous response of a

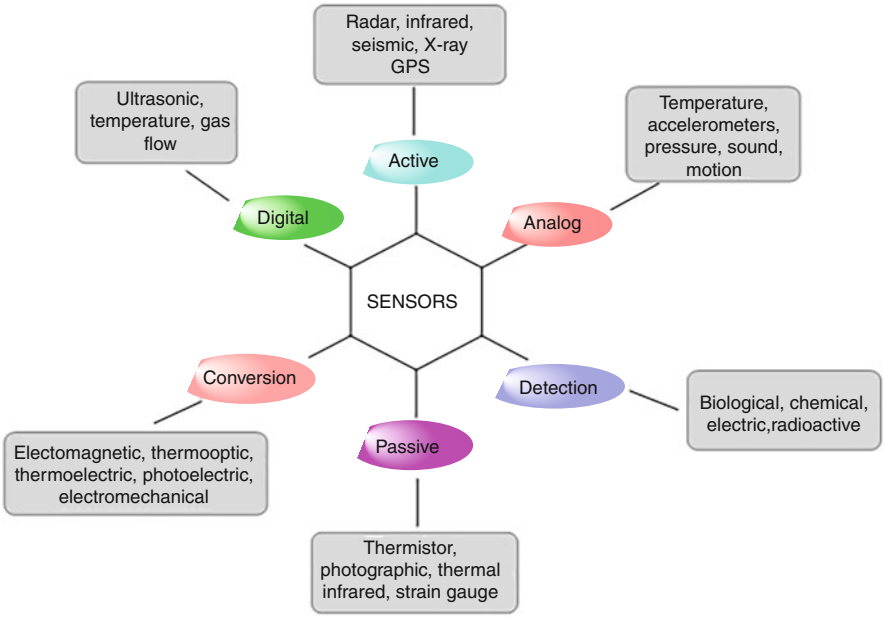


**Fig. 10** Brief outline of the sensor types

system to the input. A system can be, therefore, zero, first, or second order in functioning. The following points provide a basic idea of different static and dynamic sensor parameters.

- **Dynamic characteristics**: The response of a sensor to a particular variable input is quite distinct from the one exhibited when the input signals are constant. Dynamic characteristics of a sensor arise due to the presence of energy-storing elements, that is, inertial (masses, inductances) or capacitances (electric or thermal). These parameters are determined by ascertaining the sensor response toward a family of varying input waveforms, such as impulsive, step-based, sinusoidal, or white noise comprising.

A brief explanation of salient static and dynamic sensor characteristics is as follows:

- **Accuracy**: This property of a sensor ensures the retrieval of an output close to that of the true value of the measured quantity. The determination of accuracy is related to the deviation of repetitive measurements and involves absolute and relative errors (Eqs. 2 and 3).

$$\text{Absolute error} = \text{Result-True value} \tag{2}$$

$$\text{Relative error} = \frac{\text{Absolute error}}{\text{True value}} \tag{3}$$

**Table 5** Characteristic sensor types with advantages and disadvantages

| Sensor types | Advantages | Disadvantages |
|---|---|---|
| Optical | Low cost, small size, and ability to operate over large distances | Short-lived stability |
| Temperature | Accuracy, flexibility, higher reliability, and sensibility | Resistance error, vibration, and a high response time |
| Magnetic | High sensitivity, low noise, high switching speed, and reduced power consumption | Shock performance, magnetic metals disturbance, and magnetic field affect the trip point |
| Image | Reduced energy consumption, security, and digital lock | Slow speed and vulnerability to heating and distortion |
| Motion | Available at low cost, higher security, and save energy | Sensitive to environment changes, short distance coverage and undesired triggering of motion sensors can occur when it is installed near a light source |
| Pressure | Easy to rearrange, no parallax inaccuracy, steady readings even at a high vibration, and does not need any operators | The error occurs due to oscillating values, requires a power supply, and is not easy to observe full-scale and trend |
| Proximity | Well established, easy to operate, high switching rate, insensitive to environmental conditions, and accuracy | Limited operating range, noisy interface, and suffering from the object surface |
| Ultrasonic | High penetrating power, low cost, high frequency, and sensitivity | It can be affected by environmental changes or conditions |
| Radar | Insensitive to environmental conditions, direct measurement of vehicle speed, accurate, and reliable | Expensive, difficulty in discriminating between the close objects and color of the objects |
| Infrared | Effective in detecting defects, and accurate measurement of vehicle speed and position | Incapable of detecting multiple objects having minimum temperature difference and expensive |

- **Resolution**: This is defined as the least variation in the input needed to effect a detectable output change. In case the initial limit is "zero," the resolution is termed a "threshold."
- **Precision**: This is defined as the progressive ability to repeatedly provide unchanged results instead of a similar input under the definite prescribed conditions. This parameter indicates agreement and coherence between the successive measurements and nowhere means the nearness to the true value. Hence, despite being a necessity for accuracy, it is never a sufficient characteristic.
- Repeatability and reproducibility are the two parameters closely based on precision. The repeatability implies a precision of a set of measurements taken within a short time interval while reproducibility infers the precision of a measurement set taken over a long time interval or the results of experiments done by distinct operators using dissimilar instruments or in distinctive working environments.

- **Errors**: Error could be defined as the deviation from the expected ideal working state for which manifold factors could be responsible. Two major kinds of errors in experimental measurements are systematic and random.
- The systematic errors result from a variety of factors such as modifying variables (i.e., temperature), variations in chemical structure that manifest interactions with the probe, human error (amidst sample loading), and transmission-attributed signal attenuation. These errors could be corrected with the compensation methods (i.e., feedback or filtering).
- Random errors arise due to a signal that is devoid of any information (noise). Factors contributing to the generation of noise include repeatability of experimentalist (could be aggravated by the abnormal height of a rough surface), environmental noise, and transmission noise (typically in the order of 60 Hz).
- For a minimized generation of random errors, the signal-to-noise ratio (SNR) should be $\gg 1$.
- **Sensitivity**: This is ascertained as the slope of the calibration curve (discussed in the subsequent section) and should be ideally large and constant. Mathematically, the sensitivity of a sensor is calculated by taking the first derivative of the calibration curve equation.
- **Linearity**: The resemblance extent of the calibration curve to a specified straight line.
- **Hysteresis**: The difference between two outputs corresponding to the same input, depending on the trajectory followed by the sensor.

### 3.1.5 Sensor Calibration

- The output of a sensor analysis (in response to one or more input stimuli) is usually obtained as a transfer function. Calibration implies checking, adjusting, or determining via comparison with a standard. This infers a comparison between multiple measurements.
- Typically, a sensor calibration involves the application of a range of known physical inputs and subsequent recording of a system's response. The calibration provides desired justification for proper functioning by recording the outputs to manifold input values other than the inputs used in course of calibration. Some potential methods of sensor calibration are as follows:
- Estimation to obtain well-fitted points with the chosen calibration coordinates (curve fitting via computational assessments of nearest trends followed)
- Modification of the sensor properties to fit with determined transfer function
- Optimization of the acquired data by fitting them to a normalized distribution function
- Design of a sensing-specific reference provision having resemblance with select calibration stages

### 3.1.6 Biosensors

A biosensor is a specific sensor that utilizes biologically derived materials such as an antibody, enzymes, protein, nucleic acid, living cells, and tissues as the recognition

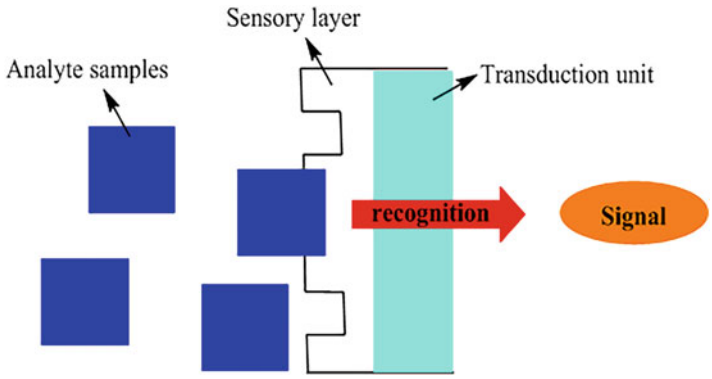


**Fig. 11** Schematic representation of biosensor components, wherein analyte samples bind to the probe. The mechanism of sensing is, no doubt, similar to the one depicted in Fig. 6, wherein the recognition element is immobilized using membrane entrapment, covalent or noncovalent binding, which maintains its bioactivity. Apart from this, an indirect process can also be used where a biochemical reaction arises between the analyte and the biomaterial element that results in product formation via the evolvement of heat, gas, ions, and electrons, which are subsequently measured by the biorecognition element (sensory layer) to generate a specific chemical stimulus. The transducers convert this chemical signal into an analogous electrical signal, which is further amplified by the detector circuit

element in the transduction process to measure certain chemical concentrations in a biological system (Fig. 11).

## 3.2 Developmental Background of a Biosensor

- The first-ever use of biosensor terminology was made in 1906 when M. Cremer demonstrated that the acidic load of a liquid varies directly with the electrical potential difference between the separated zones partitioned by a glass membrane.
- Subsequently, in 1999, the concept of pH (hydrogen ion concentration) was unveiled by Soren Peder Lauritz Sorensen and an electrode for pH measurement was designed in 1922 by W.S. Hughes (1922). Between 1909 and 1922, Griffin and Nelson were the first to demonstrate the immobilization of invertase on aluminum hydroxide and charcoal (Griffin and Nelson 1916).
- The first major attempt in the direction of a true biosensor development was put in 1956 by Leland C. Clark Jr., who explained the detection of oxygen. In course of his experiments, investigator Clarke fabricated an "oxygen electrode" that is still recognized as the "Clark electrode" and fetched the regard of "Father of Biosensors Development" Sir Clark (Heineman et al. 2006). This paved the way for the making of amperometric electrodes working on an enzymatic titer basis to quantify glucose in 1962. Eventually, the first-ever potentiometric biosensor was

designed by Guilbault and Montaly Jr. in 1969 for the detection of urea (Guilbault and Montalvo Jr. 1969).

- With gradual developments, the first commercial biosensor was made public in 1975, developed by Yellow Spring Instruments (YSI). Subsequently, with the advances in miniaturized sensing precision, the handheld human blood biosensor was designed by i-STAT in 1992, indicating an era of remarkable progress for biosensor development.
- The subject domain of "biosensors" remains a formidable multidisciplinary research area, involving experts from all branches of basic sciences (physics, chemistry, and biology) and their intensified merger with nanotechnologists, microbiologists, and pharmacists. The decade from 2005 to 2015 lists >80,000 studies on biosensor fabrication and their diversified application domains.

## 3.3 Classification of Biosensors

- Biosensors are classified into two broad bases, either nature of biological element or transducer type, briefly discussed in Fig. 12. The transducer-driven classification is more rigorous of the conventions as it has an exclusive say to the working efficiency of the biological sensing. Fundamentally, a transducer converts the intervening modifications prevailing in course of interaction between the biological probe and analyte into a measurable signal such as optical or electrical current. The most common transducers for biosensors are electrochemical, optical, piezoelectric, and thermometric.
- Fundamentally, a transducer converts the intervening modifications prevailing in course of interaction between the biological probe and analyte into a measurable signal such as optical or electrical current. The most common transducers for biosensors are electrochemical, optical, piezoelectric, and thermometric.

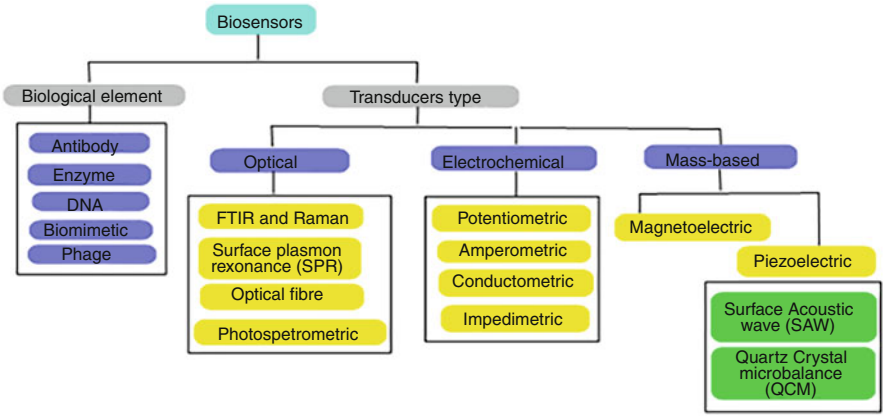


**Fig. 12** Biosensors classification criterion

## 3.4 Biosensors Variations Through the Distinctive Transduction Mechanisms

### 3.4.1 Electrochemical Transducers

- **Potentiometric biosensors** measure potential differences between two reference electrodes separated by a semipermeable membrane. These biosensors are based on an ion-selective electrode and ion-sensitive field-effect transistors (FETs). For example, glucose oxidase can be immobilized on the surface of a pH electrode.
- **Amperometric biosensors** are used to determine the electric current developed via biochemical redox reaction. The working principle of these biosensors involves either the generation or consumption of an electroactive species as the oxidation of glucose in presence of glucose oxidase forms gluconolactone. Scrutiny of the sensor using a Clark oxygen electrode is used to monitor the depletion of oxygen that is countercompensated by glucose oxidation.
- **Conductometric biosensors** function at comparatively lower amplitude, changing potential difference, and do not mandate the inclusion of reference electrodes. These biosensors eliminate the Faraday principle on electrodes, which generally remains unaffected by light. The best explanation of this biosensing principle is provided by the initial biosensors designed to monitor the kinetics of enzymatic hydrolysis of urea via assessing urease actions in 1965. The functional configuration of this biosensor is comprised of two pairs of the platinum plate, each placed in its explicit measuring cell (with and without enzyme, each). The distinction in the signal response from both cells was monitored through which the possibility of random errors (arising from temperature, buffer, and concentration changes) was reduced. The screening range of urea concentration was within (1–75) mM while that for urease activity was within (0.04–2.5) units per ml.
- Impedance-based biosensors (the principle also being referred to as impedimetric) are made via immobilizing a biological recognition moiety onto a conductive and biochemical electrode. The analyte presence in this configuration was ascertained via monitoring variations in the interfacial impedance. Using biological probes for these sensors involves the administration of a small-amplitude AC potential difference to the sensor electrode. This is followed by measurement of in/out of the phase current response as a function of frequency. The analyte molecules could vary among the antibodies, receptor proteins, single-stranded DNA, aptamers, and peptides.

### 3.4.2 Optical Transducers

- Based on fluorescence, absorption, internal reflection, surface plasmon resonance (SPR), luminescence, and light scattering intensity.
- In these biosensors, a bound biological moiety on optical fiber interacts with its target analyte and forms a complex having different optical behavior. For example, an immunosensor with SPR activity could be used to detect casein in milk.

### 3.4.3 Mass-Based Transducers

- In piezoelectric biosensors, crystalline materials such as quartz, gallium nitride, or cadmium sulfide(s) are subjected to elastic deformation or mass variation under the influence of electric potential. This ultimately generates resonant frequency variations in the crystal. Bulk acoustic wave (BAW) and surface acoustic wave (SAW) are two major propagation transducers used in such biosensors. Mechanistically, an acoustic wave is converted into a mechanical wave under the influence of an electric field that propagates either through the surface (SAW) or substrate (BAW). For instance, immobilized monoclonal antibodies (MAbs) interact with their complimentary antigen, resulting in mass density variation as a function of changing the resonant frequency.
- Thermometric and calorimetric biosensors measure the heat generated in enzyme-catalyzed reactions and are exothermic. Measuring heat capacity can be used to determine analyte concentration and also rate of reaction.

#### Biosensors Classification Is Based on Distinct Biological Elements

Based on the nature of biological entities, biosensors are subcategorized as enzyme sensors, DNA sensors, protein sensors, microbial sensors, and others. Above 80% of the biosensors are electrochemical in nature. Here, biological entities act as a recognition element, having the ability to recognize a single substrate among a group (with different masses).

- **Enzymatic Biosensors**

In these biosensors, the substrate or product of an enzymatic reaction is electrochemically active and capable of being reversibly oxidized or reduced on an electrode upon the application of a suitable potential. They are of two types, namely, substrate and inhibitor biosensors. The former is used to determine specific reaction substrates while the latter is used to screen the agents reducing an enzyme's activity. For example, glucose oxidase biosensor acts as substrate biosensor that determines the glucose, whereas organophosphorus pesticide determination acts as an inhibitor biosensor inhibiting acetylcholinesterase activity.

- **Immunosensors**

Immunoglobulins or antibodies are the proteins generated in response to foreign particles (antigen) by an organism. These antibodies act as receptors and form a strong complex on binding with antigens. Such biosensors are used to detect antibodies having high specificity and selectivity. For instance, the existence of immunoglobulins in the blood sample indicates infection emanated from certain toxic constituents.

- **DNA Biosensors**

Apart from antibodies, aptamers are synthetic nucleic acids that interact with proteins, cells, small molecules, and others. Their high specificity and affinity have made them a promising protein recognition element. Compared with antibodies, aptamers are highly stable and easy to synthesize. These biosensors are used to identify infectious diseases via hybridization between the immobilized oligonucleotide probe and a complementary target sequence, on an electrode. Moreover, DNA sensors are also used to expose several anticancer drugs, tumor markers hampering DNA, and other regulatory proteins.

- **Microbial Biosensors**

In these biosensors, microorganisms are used to detect a target substrate and convert the generated biological response into a physiological, electrical, or biochemical response. Their sensing mechanism depends on conventional optical, electrochemical, and sensory regulated devices. In contrast to the response of enzymes or antibodies, the responses of microorganisms vary as per the culture medium chemical composition. So, in microbial sensors, the biological element is parted from the recording device. These sensors are almost similar to enzymatic sensors, but the only difference is the group of enzymes that take part in converting substrate rather than a single one. These sensors are also known as respiratory biosensors as their respiratory response varies during the assimilation of organic substances. Such sensors are used in determining the concentration of oxidizable organics as well as antimicrobial agents. Other domains of application include toxicological estimation and optimizing the antibiotic dosages. In addition, their enzyme activities and stability can be enhanced using genetically engineered microorganisms. The best example of these sensors is toxin determination through luciferase inhibition, a microbial enzyme catalyzing the substrate with luminescence production. Hence, the different biosensors have significant commercial importance for their wide applications.

***To reach everyone's hand, a typical biosensor model should have the following features***:

- The biocatalyst should be stable under normal storage conditions and highly specific for the analyses determination.
- Their reaction should be free of physical parameters such as pH, temperature, stirring, and others.
- The response should be accurate, defined, reproducible, and linear over the analytical parameter without dilution or concentration.
- The signal processing unit in the biosensors should be free from any arbitrary electrical noise.
- For clinical studies, these sensors must be biocompatible and sterile.
- Finally, the model should be simple, low cost, portable, and be easily operable by semiskilled operators.

### Characteristics of Biosensors

As discussed for sensors (above), certain parameters and properties are mandatory to be optimized for the best biosensor performance. These parameters are therefore recognized as the character traits of a biosensor.

- The working description of biosensor operation is described by its selectivity, reproducibility, stability, sensitivity, and linearity, which are together summed up as the characteristics or "performance-defining" parameters. The following points briefly describe these parameters with the intent to drive an optimum biosensor working efficacy.
- **Selectivity**: Perhaps the most critical characteristic of the typical working mode of a biosensor, selectivity could be defined as the exclusive ability of a biological probe to screen the analyte in varying chemical environments. Thereby, the presence of contaminants of varying chemistry cannot affect the efficiency of detecting a particular molecule. The best illustration of selectivity is provided by antigen–antibody reaction, wherein immobilized Abs on the surface of a transducer are perceived discretely by the antigen comprising solution.
- **Reproducibility**: This characteristic of a biosensor relates to the generation of similar responses corresponding to the detection of an analyte in distinctive chemical environments. The high reproducibility of a biosensor inevitably depends on the precision and accuracy of the transduction phenomenon and electronic sensitivity. Precision implies the ability to generate unaltered outcomes corresponding to multiple attempts of screening an analyte. Contrary to this, accuracy infers a sensor's ability to generate an average output (in multiple attempts) nearing the absolute value instead of multiple measurements. Reproducible outcomes of biosensing are the indicators of high reliability and stimulus adjustment of a typical analysis.
- **Stability**: This property of a biosensor quantifies the susceptibility corresponding to the alterations of distinct sample configurations. These deviations together culminate as differences in the output signals from the standard results (estimated from the database in response to a specific analyte). As a result, estimated titers are accompanied by errors, affecting the precision and accuracy. This property of a biosensor working holds significant relevance for the analysis mandating optimum incubation or monitoring. The operational working of transducers and electronics digitalization must remain unaffected by temperature and other likely involuntary deviations in the vicinity. Thus, appropriate adjustment of electronics is a mandatory requirement to ensure a stable response of the sensor. The affinity of the bioreceptor (the extent to which an analyte binds the bioreceptor) is another factor that could affect biosensor stability. Bioreceptors with high affinities usually result in aggressive electrostatic bonding or covalent linkage of the analyte that compromises biosensor stability. So, it must be ensured that binding activities do not at all induce any structural insult to the native analyte and sensing element configuration. It must also be ensured that the chosen bioreceptor does not undergo any degradation over a due passage of time.

- **Sensitivity**: This refers to the minimum extent of analyte that can be detected by a biosensor probe, also considered the limit of detection (LOD). Several applications from medical sciences to environmental contamination monitoring and others mandate the analyte detection to the extent of nano or even lower ranges per ml of the analyzed fluid. The lower the determined extent, the higher the sensitivity, and ultimately least chances of contamination would remain. For instance, the general recommendation of biopsy tests by doctors in response to prostate cancer is made subject to a minimum 4 ng•ml$^{-1}$ prostate-specific antigen (PSA) blood concentration.
- **Linearity**: This characteristic of a biosensor ascertains the accuracy of a measured response (corresponding to a set of measurements in response to varying analyte concentrations). Ideally, a graphical dependence of the output signal on the analyte concentration is deemed as a straight line, $y = mx$, where y is the output signal, x is the analyte concentration, and m is the biosensor sensitivity. The linearity of a biosensor is associated with its resolution and the range of analyte concentrations being examined. Resolution of a biosensor could be defined as the smallest change in analyte concentration deemed suitable to effect a response variation. Although it varies with the application concerned in general, a good resolution argues well for biosensor performance as the use of biosensor not only pertains to analyte detection but also determining its concentration over wide working ranges. Extensive studies monitoring a biosensor response define the corresponding linear range, which refers to the range of analyte concentrations corresponding to which a biosensor response varies linearly with concentration.

## 4 Improving the Working Efficacy of a Biosensors

The typical working efficacy of a biosensor is discretely affected by the optimal contribution of each of its above characteristics. In convention, the electrically active mammalian cells cultured on extracellular electrode arrays are used to detect bioactive agents. As cells are easily affected by varying environmental conditions, environmental and biochemical variations can easily trigger cellular responses that contribute to noise in a mammalian cell-driven biosensor. Thus, it is highly essential to maintain the growth supporting pH, temperature, and osmolarity so that the native detection sensitivity of living cells is not altered and could be rightly exercised. It is observed that the response of a growing mammalian cell is significantly distinct through its different growth stages, owing to growth or instantaneously specific biochemical secretion by a host cell. Other than environmental and biochemical factors, the performance efficacy of a biosensor is also affected by the distinct recognition of two closely resembling stimuli. For example, distinct recognition of microbial stains collected from the air and infected sufferer is significantly cumbersome and the one from the air is easily accepted to be much more heterogeneous. Similarly, the detection of proteins produced by a microbial cell and an agricultural crop plant mandates the right selection of distinctive markers for optimum assay design. Thus, for a distinct recognition, it is a must to identify distinguishable

markers in the screened cells. With the advancement in characterization techniques, it has become quite handy to screen the distinctive markers among multiple sources of a similar biostimulus. Apart from discrete markers, efficient and prompt functioning of recognition and transduction domains of a biosensor is highly desired.

***The following are some aspects of the modulation of which the rapid and implicit response from a biosensor could be optimized***:

1. Enhancing detection sensitivity
2. Incorporation of nanomaterials
3. Reduced detection time and analyte quantity
4. Reusable substrate–analyte interactive platforms

*A brief discussion of all these parameters is provided next.*

## 4.1 Enhancing Detection Sensitivity

Detection sensitivity (DS) infers the minimal intensity of the input signal distinctly recognized by a sensing probe. This could also be considered as the least count extent of a designed sensing configuration. In practice, every scientific instrument or probe has a defined workable range, and sometimes for the measurements beyond these extents, accessories in the functional setup are combined. A perfect example of DS-based biosensors differentiation could be the distinctive diagnosis protocols for screening more than one kind of infection. The protocol used for screening jaundice provides a negative response if used for diagnosing dengue or typhoid. The programmable mechanisms of each diagnostic kit are tuned specifically concerning characteristic antigens and are highly optimized for specific responses. Now, if we compare the detection mechanisms specified to a particular response, we notice that the recognition efficacy of two or more probes differs from each other, like the response time of human and mouse brains to a similar external shock or even between two human beings belonging to a different geography. Likewise, the time taken by an electric rod and gas heater to heat two water samples having identical initial temperatures is quite different, owing to the dissimilar DS. So, the distinctive probe configuration concerning screened analyte manifests the presumably distinctive DS. Some primitive aspects of DS are described next.

- The probe–analyte interactions in a biosensor working are strictly physicochemical and therefore highly delicately influenced by probe geometry (size and surface area). However, detection is not merely dependent on physical contact and is perceived only by the generation of a signal in response to the perceived signal. A fine illustration of DS could be gathered by the understanding of the Vernier caliper (VC) and a simple plastic scale. While both are designed to measure length, the former has a lower least count. Similarly, chemical indicators (used for screening acidity or alkalinity) respond variably to a reached or modulated pH level.

- We observe that in both instances the probes provide varying inputs, although they are prepared to perceive a similar quantity. Interestingly, the response time in screening a stimulus is not at all dependent on the analyte configurations but on the programmed working algorithm of the probe.
- While both the discussed instances involve physical entities (electric heater-rod and Vernier caliper-plastic ruler), the mammalian cell-based sensors are quite distinct as the living cells are to be used as probes. The typical response in such cases is the outcome of implicit probe–analyte interactions, and it is obvious to anticipate a faster response for a stronger analyte–probe interaction. So, if an analyte interacts strongly with a probe, it is very much likely that it would be perceived easily. For example, glucose oxidase perceives glucose from the blood and several other mixed solutions, and thereby the DS of a mammalian cell-based sensor working through glucose oxidase as a probe would be highest for glucose than other carbohydrates or proteins.
- The analyte concentration and texture are crucial parameters affecting the DS of a probe. Although the probe is implicitly specific to an analyte, the latter's high proportion in the scrutinized sample serves as a positive factor for prompt detection. The morphology or texture of the analyte is a highly vital prospect affecting an analyte DS, wherein a nano-thin analyte layer is much easier to be detected rather than its bulk form. This is because the energy levels in a nano-material are continuous and the possibilities of intramolecular transitions are much higher.
- Enhanced DS is of critical importance in diagnostic purposes as the distinctive ascertainment of physiological infections is of paramount importance to advise or suggest the cure. So, the right interaction of probe and analyte forms the key to providing a reliable detection response. It is practically very much infeasible to expect that two or more biosensing responses develop similar DS with the same probe. Though, it is possible that certain modifications of the probe could reduce the detection time of analyte recognition. This is attained through nanotechnological interventions, wherein NMs having infinitesimal closer energy levels (owing to a feasibility prevalence of quantum mechanics) could perceive even a slight change in the surrounding environment with a prompt change in their characteristic response. The following section discusses the various NMs being used to improve the sensing probe detection efficacy via prompt recognition and substantially reduced times.

## 4.2 Incorporation of Nanomaterials

- The realm of materials chemistry accompanied by sophisticated characterization tools forming most fundamental links to explore the possibilities at atomic-scale resolution has been the reason to make the best use of enhanced surface area and reduced activation energy of NMs for accomplishing a faster response generation.
- Manifold NMs such as metal nanoparticles (NPs), carbon NMs (carbon nanotubes, fullerenes, quantum dots), and functionalized assemblies of distinctive

materials are being used with increasing interest to fasten the sensing interactions and reduce the response times for a prompt detection mechanism.

- A prominent feature of all NMs is their high specific surface area (surface area to volume ratios), which aids in the attainment of the enhanced extent of bioreceptor units. While using NMs with the biosensors, a consistent challenge has been the immobilization-driven conjugation of a biospecific entity over the NMs. Readers are suggested to refer Putzbach and Ronkainen's 2013 contribution to the different biofunctionalization mechanisms of NMs.
- The major noncovalent approaches to mediate the conjugation of nanomaterial and biological entities are electrostatic interactions, π–π stacking, polymeric entrapment, and van der Waals forces. These binding interfaces exhibit the desired properties of a nanomaterial as well as a biomolecule. While the covalent binding is often recognized as the regulatory force for biomolecules–nanomaterial attachment, distinguished via stability, reproducibility of surface functionalization besides decreasing nonspecific physisorption. A potential concern with covalent biomolecule–nanomaterial linkage is the unrestrained anchoring that is probable to affect the recognition determining domain.
- Immobilization of biomolecules by supramolecular or coordinative interactions has garnered significant recognition over the past few years for assisting the binding of biological species to surfaces. A familiar instance applied for biosensor engineering comprises biotin/avidin (or streptavidin) system (Wilchek and Bayer 1988). This mechanism works by the attachment of biotinylated molecules to biotinylated surfaces via avidin bridges. Other affinity configurations are also reported such as nitrilotriacetic acid (NTA/$Cu^{+2}$/histidine complex) or the host–guest system (adamantine/β-cyclodextrin) (Haddour et al. 2005). The preferred benefits of such systems over other immobilization methods include reversibility and the possibility of regenerating the transducer component. The functionalized transducer surface and altered bioreceptor configuration could be separately prioritized on a one-to-one basis, thereby assuring reproducibility.
- Depending on specific chemical compositions, nearly all NMs can be functionalized either via the direct route (during the synthesis) or by coating functional polymers without altering their specific characteristics (Biju 2014). Thus, the functionalization in NMs not only enables a reproducible immobilization of receptors but also improves biocompatibility.
- A major advantage of the use of NMs in biosensing is the progress of label-free transduction mechanisms, together contributing to obvious signal amplifications upon being used as labels. Such ability of NMs resolves the hurdles caused by no direct detection of recognition event by the used transduction technique (the usual observation in course of antigen–antibody immunoreactions or amidst the hybridization of complementary DNA strands). In both these cases, biologically specific constituents (secondary antibodies or DNA strands) modified with optical or electrochemical transduction-compatible labels need to be used.
- Most well-documented and reported NMs used to improve the performance of the biosensor include gold (Au) NPs, quantum dots (QDs), magnetic nanoparticles (MNPs), and the nanostructures of carbon.

- The salient aspects of each of these entities concerning improved biosensor performance are described next.

### 4.2.1 Gold Nanoparticles

- The major reasons for the increasing application of gold (Au) NPs in biosensor development are their relatively high biocompatibility, size and shape tunable optical and electronic properties, robust preparation methods with significant reproducibility, and, most importantly, the ease of being functionalized with several biomolecules.
- Belonging to the 11th group and the 6th period of the periodic table, Au has a stable electronic configuration with a filled 5d orbital (10 electrons) and a half-filled 6s orbital. Several methods are known for the preparation of Au NPs, of which the most prominent is the approach proposed by Turkevich and coworkers. This method uses $HAuCl_4$ as the Au precursor salt and trinitrate as a reducing agent. The method is a chemical reduction approach, and its several modifications (using distinct reducing agents) are also known. In the mechanism proposed by Turkevich and colleagues, it is well reported that varying the combination stoichiometry of precursor (here, $HAuCl_4$) and the reducing agent could provide variations in the sizes of generated NPs. A lower size generally argues for a greater nanoscale effect (high energy conversion) due to greater manifested quantum confinement. It is due to high native stability that NPs of Au exhibit significant potential to immobilize mammalian cells with minimal risk of cross-reactivity and toxic responses (Turkevich et al. 1951).
- Among the manifold sensing incentives of Au NPs is the optical behavior, wherein irradiation with a specific wavelength of light oscillates the electrons in the conduction band, referred to as resonant surface plasmons. Of note, every material comprises an energy barrier separated by valence and conduction bands. At the ground state, all constituent electrons lie in the valence band but on gaining energy (as temperature, interacting moieties, etc.) these gain entry in the conduction band. The mechanism by which size-dependent optical attributes of Au NPs aid in obtaining an improved sensing response is optimized by the interaction of incident light wavelength with smaller particle size.
- The interaction of such a smaller NP size with the incident wavelength forbids the propagation of oscillating electrons along the surface (unlike conventional SPR). This results in the electron density polarization on one side of the particle with a simultaneous oscillation of plasmons in resonance with the light frequency (Fig. 13). This experience is sensitively dependent on NP size and shape as well as the dielectric constant of the environment.
- The environmental dependence of such light–matter interaction comprises a substantial gain for bioanalytics as the recognition can result in varied oscillation frequency that ultimately results in a color change of Au NPs, on being observed with the bare eye. Several robust and modestly functioning colorimetric biosensors are reported for DNA or oligonucleotides detection.
- Au NPs are also preferred for bioanalysis through SPR transduction and through a change in the dielectric constant of propagating surface plasmon environment of

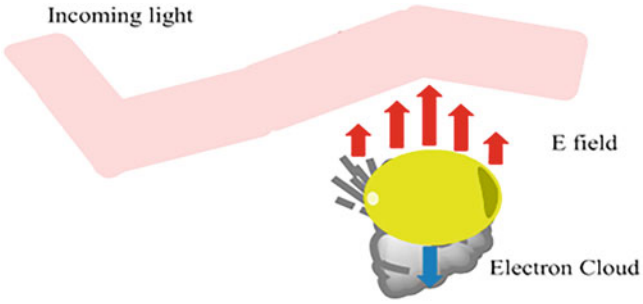


**Fig. 13** Pictorial depiction of polarized electron density corresponding to the resonant excitation wavelength. Excitation with wavelengths lower than the particle dimensions prevented the propagation of surface plasmons along the surface of Au NPs, inducing the polarization of electron cloud in a peculiar periphery of the particle

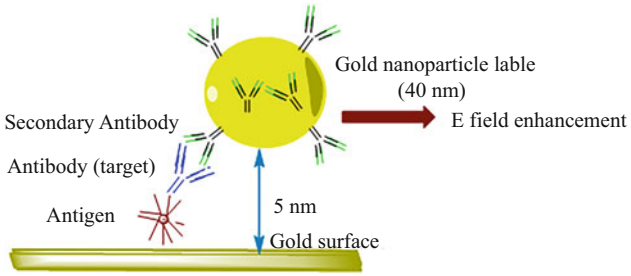


**Fig. 14** Representation of attenuated propagating surface plasmons on Au surfaces provoked by defined size Au NPs, which are at a finite distance, leading to a surplus change of evanescent field and ultimately to an enhanced signal

Au films. This facilitates the detection of analyte(s) in multiple manners such as through changes in the angle, intensity, or reflected light phase.

- A modification in the above technique could be mediated using the Au films and NPs in a sandwich regime. The surface plasmons on Au NPs instigate a disturbance of the native optical field of Au film besides immobilized bioreceptors unit and recognized analyte. Figure 14 pinpoints the optical configuration of this approach for <40 nm Au NPs working at a 5 nm separation from the Au film surface. Here, Au NPs function as labels on being attached to secondary antibodies or DNA strands. Despite further preparative steps being needed for a labelless detection, such an approach facilitates a signal enhancement by several orders of magnitude.
- Au NPs can also aid in the generation of a signal transformation, facilitating discrete single-molecule detection. The working module is activated by a perception of the refractive index of localized surface plasmon resonance (LSPR) conjugated with enzyme-linked immunosorbent assay (ELISA) through 60 nm NPs. Procedurally, horseradish peroxidase (HRP) was immobilized on Au NPs through biotin–streptavidin conjugation. Detection is made using the principle

illustrated by Chen and associates, wherein HRP oxidizes the soluble monomer, 3,3′-diaminobenzidine (DAB), to insoluble and colored polybenzimidazole. This reaction resulted in aggregation in the enzyme surroundings and facilitated the precise detection of even a single HRP molecule bound to Au NPs. In this way, Au NPs spectrum and excitation of energy levels are well suited for sensitive biosensing aided using surface-enhanced Raman scattering (SERS).

Based on surface plasmon-enabled signal amplification of adsorbed or immobilized compounds' vibrational spectrum, it is possible to reach the detection range to an extent of a single molecule. Regarding formal restrictions of the reference inclusion, the studies referred to or recalled for the above facts and accomplishments could be traced to the 2014 *Frontiers in Chemistry* contribution of Holzinger and colleagues (Holzinger et al. 2014).

- Apart from interesting optical properties, Au NPs also exhibit an inherent ability to transfer electrons across a wide range of electronically responsive biological species and electrodes. This attribute of Au NPs is in high demand for redox enzyme-assisted biological sensing having the bioreceptors capable of catalyzing the analyte oxidation or reduction. The distinguishing aspect of such Au NPs-assisted redox signaling from that of conventional electrochemical enzyme biosensors is that in the normal setup the generated species are oxidized or reduced to generate an electrochemical signal. A major issue with this methodology is the diffusion of noticeable molecules to the electrode from where a considerable extent is lost in the solution. This hurdle is resolved by the electron shuttle-like behavior of Au NPs, that is, the NPs could approach the redox center of the enzyme, regenerating the biocatalyst by transferring the electrons (in the redox reaction) to the electrode (Fig. 14).
- A significant attempt to improve the sensitivity of the biosensor using 20 nm colloidal Au NPs improved the DS of an amplitude-sensitive paired surface plasma wave biosensor (PSPWB) from 0.001% sucrose in an aqueous state and subsequent biomolecular interaction of 10 pg•ml$^{-1}$ mouse IgG with anti-mouse IgG. It was noticed that 20 nm colloidal Au NPs conjugated with target molecules enabled a greater mass coverage with a larger resonant angle change of plasmon resonance, resulting in a significant enhancement of DS. The uncoated Au NPs, which are randomly suspended in solution, enabled a distinct recognition of biologically specific binding-induced signal enhancement. The Au NP-conjugated protein A (PA-Au) on interacting with mouse IgG (immobilized over a CM5 sensor chip) was screened with a 330 fg•ml$^{-1}$ sensitivity, thereby enabling nearly sixfold signal amplification compared to similar PA concentrations that are not conjugated with Au NPs (Hsieh-Ting Wu et al. 2007).
- The feasibility of multiple functionalization modes enables Au NPs to function well as combination probes facilitated via distinctive interactions. For instance, hybrid electrodes using Au NPs in combination with silicon oxide, carbon nanosphere, and calcium carbonate have been recently reported to enable synergistic responses in analytical performances (Li et al. 2010). A different study by Cai and colleagues demonstrated a ratiometric electrochemical method using

polythionine-Au as an electrode. The developed immunosensor exhibited an enhanced specificity over a wide linear range with 2.2 pg•ml$^{-1}$ LOD (Cai et al. 2016).

- Thus, the outstanding tunable and optimized properties of Au NPs propel them as promising candidates not merely in bioanalytics through manifold mechanisms. Such abilities of Au NPs are largely due to the shape and size-dependent properties, allowing an accomplishment of desired applications. The performance attributes represent the manifestations of discrete optical, catalytic, and electronic responses of Au NPs.

### 4.2.2 Quantum Dots

- Arguably the most exciting NMs, QDs typically constitute the luminescent semiconducting nanocrystals (NCs) having 3D restricted motion of charge carriers. This restriction is termed "quantum confinement (QC)," a typical determinant of nanoscale influence in the material dimensions. The QDs, with 3D QC, exhibit a restricted motion of charge carriers in all the three dimensions. Owing to this, the fascination toward their biosensing application draws interest from their size-dependent optical and electronic energies. This is the reason for different colors of varying QD sizes. Their use in biosensing revolves around the principle of labeled antibodies to which the test antigen binds and results in the binding intensity proportional to color development. The exhibited color is an indication of perceived binding energy from the antigen–antibody interactions. The native electronic behavior of a QD is semiconducting. Readers are suggested to consult the 2009 review article by Drbohlavova and colleagues to know about the referred articles in this section unless specifically stated otherwise (Drbohlavova et al. 2009).
- Two approaches for QDs' preparation are well demonstrated to date. The first involves a form of semiconductor NPs through colloidal chemistry while the second one involves the epitaxial growth using lithography. The colloidal chemistry mechanism involves the rapid injection of semiconductor precursors into hot and vigorously stirred specific organic solvent containing molecules capable of coordinating with the surface of precipitated QD particles. This mechanism is facile and is referred to as a single-step method in many literature sources. For biological systems, QDs are extensively used in the solution phase. Many studies have documented an urgent need for the deposition of QDs on multiple solid surfaces for biomedical applications. In this context, an alternative promising approach for biological applications is to use QDs labeled biofunctional carrier spheres.
- Optical characterization is generally accomplished using UV-Vis and photoluminescence spectroscopy, offering a rapid, safe, and contactless option. The optical attributes are majorly inferred through fluorescence emission and can be fine-tuned by size variation, a prominent factor that ascertains spectral position and photoluminescence purity extent. The size estimations of QDs are usually made through SEM, transmission electron microscopy (TEM), and dynamic light scattering (DLS). One study by Gu and colleagues reported the size and


**Fig. 15** An illustration of QD sorting in accord with size-emitting light of different colors excited simultaneously by a single-excitation wavelength

composition of optically active CdZnSe/ZnBeSe QDs through photoluminescence, photoluminescence excitation, and Raman scattering spectroscopies combined with photoluminescence and LO phonon energies model (refer Drbohlavova et al. 2009 for discussed studies).

- In general, the QD size ranges from (2–30) nm though some literature sources list the diameter as strictly less than 10 nm. Typical dimensions exclusively depend on the used material for their preparation. Evidence and consensus for calling a nanoparticle QD is the prevalence of QC, present when an NP radius is lower than one of the Bohr electron, hole, or exciton radii. Since the Bohr radius varies from one to another material, it would therefore not be right to coin an NP as QD merely based on its size. Constitutionally, QDs can be metallic (Ni, Co, Pt, or Au) or semiconducting. The reduced dimensions of QDs are the manifestations of significantly distinct characteristics compared to bulk solids, arising from the concomitant quantum confinement effects (Fig. 15).
- Thus, by varying the NC sizes, a large range of emission wavelengths could be detected, thereby supporting efficient multiplexed analysis using conventional optical transduction. The concerns in the detection efficacy might be incurred owing to structural defects in the crystal lattice that trap the excited electrons or holes and ultimately result in nonradiative relaxation.

To counter this, the composite morphology is adopted, wherein wider band gap energy material is composited with the native QD and the surface defects are hindered. The high photochemical stability of such QDs' architecture has emerged as a promising alternative and amicably replaced organic fluorophores (Resch-Genger et al. 2008).

- To date, one of the most studied QDs for biosensing purpose is comprised of cadmium chalcogenides (S, Se, and Te), having a significant absorption spectrum and a size-dependent narrow emission spectrum. Such absorption and emission attributes of QDs are the outcomes of their characteristic valence and conduction band gaps, which in turn are the implicit functions of crystal sizes. This energy gap is a quantitative estimate of electronic excitation from the valence to the conduction band with a smaller crystal size corresponding to a high energy gap, resulting in distinct emission wavelengths arising out of electron–hole recombination (Poznyak et al. 2004). The latest progress in QDs' design provides them with inert or biocompatible coatings, whereby nearly every biomolecule could be attached to these without any undesired effects on photophysical recombination.

- QDs exhibit significant promise in biosensing arising out of their unique physical and optical attributes that facilitate an attachment of multiple biomolecules on their surface. Several assays of QDs are in practice having improved the conventional detection methods of DNA and protein. For instance, the detection of adenosine triphosphate (ATP) using a QD-tagged nucleic acid bound to manifold molecular targets (thrombin, adenosine, or cocaine, to name a few) has been described. Biomolecules can be bound to QDs' surface either directly (via covalent or noncovalent mechanisms) or through an intervening stabilizing layer that acts as a cross-linker between ligand and reactive NP surface. Noncovalent and direct binding can be accomplished through an electrostatically coupled strategy. Compared to the more common covalent mechanisms, the noncovalent self-assembly is simpler and easy to reproduce and accomplish. Using this approach, cysteamine-stabilized CdTe QDs have been reported to bind the single-stranded DNA via electrostatic attraction between positively charged $–NH_2$ groups on QDs' surface and the negatively charged phosphate backbone of DNA.
- The covalent bioconjugation mechanism works via the replacement of thiol acids on QDs' surface with thiolated biomolecules. One study using this binding mechanism has reported covalent linkage of streptavidin maleimide or to conjugated transferrin and mouse anti-human CD71 MAb to CdSe/ZnS QDs.

The use of hydrophilic 1-ethyl-3(3-dimethylaminopropyl) carbodiimide hydrochloride (EDC) and N-hydroxysulfosuccinimide (NHS) for forming QD–protein covalent conjugates is a familiar coupling method. The coupling aims toward the use of the hydrophilic compound as a carboxyl activating agent for coupling primary amines to form amide bonds (Scheme 1).

Using the EDC–NHS coupling probe, Wang and the group reported the conjugation of hydrophilic 3-mercaptopropyl acid-stabilized CdTe NPs with the peptides or proteins mediated by NHS.

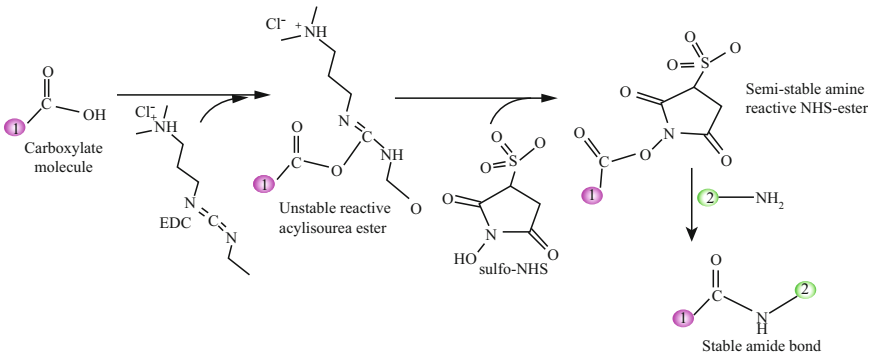


**Scheme 1** The EDC–NHS coupling reaction for manifesting carboxylic group as stable amide linkage. The method utilizes a hydrophilic probe to manifest its –COOH functional group as $–NH_2$ linkage of the product

- The coupling of biomolecules through QDs is more easily accomplished by the core–shell configuration, typically characterized by a CdSe core enclosure in a ZnS shell. Under these configurations, the core is a typical identifier of the band gap and the consequent emission pattern. Since the red shift in the optical spectrum is well known for high particle size, emission characteristics of a QD are modulated via an appropriate selection of material whose core size can be altered. Likewise, the emission spectra could also be changed through varying the Cd to Zn proportion but not the overall NC size at all. Based on such traits, multiple core–shell configurations of QDs are known, having the core comprising an emissive semiconductor (CdSe, CdTe, etc.), which is capped with a thin shell of higher band energy gap material (ZnS, CdS, ZnSe, etc.).
- There are multiple ways in which one can use QDs for biological cell/tissue labeling and cellular imaging, both in vitro and in vivo. Hybrid nanostructures comprising the QDs–liposomal assemblies are being swiftly developed and are studied for efficient uptake ability by the living cells in case of defective apoptotic controls. Such structural assemblies are best suited as fluorescent probes for ex vivo labeling using hydrophilic QDs with no other changes. In a related study, Kerman and colleagues demonstrated a sandwich immunoassay made up of QD-labeled assemblies for detection of total prostate-specific antigen (TPSA), a prominent tumor marker on a screen-printed carbon substrate.
- Modifications are also well known for the use of QDs in molecular tracking via immunohistochemistry, affably substituting the fluorescent beads used to ascertain the motion of neurotransmitters. The (10–20) nm dimensions of molecular detection-suited QDs contrary to that of 500 nm for the latex beads, allowing an in-depth analysis of an individual receptor's lateral movement. The use of QDs has also been illustrated for the detection of genetic diseases via combined imaging with stage-specific scanning confocal microscopy (SCM), which traces the QDs not exhibiting any chromatin aberration, with a resolution of $>10$ nm.

Infrared QDs have also been studied as handy probes for noninvasive in vivo detection, largely within small animals, substituting the poorly stable and low quantum yield of conventional IR-sensitive organic fluorophores (Fig. 16).

**Fig. 16** Mouse embryonic stem cells labeled with six distinct QDs were subcutaneously injected on the back of a thymic nude mice on immediate injection. (Adapted from Drbohlavova et al. 2009)

Likewise, Lin and colleagues studied the in vivo multiplex imaging of mouse embryonic stem cells labeled with peptide-based Qtracker (a dye)-delivered QDs and noticed that QD labeling of mouse ES cells did not adversely affect the viability, proliferation, and differentiation.

- QDs have also been used in the nucleus labeling within the live cells. The studies of Chen and Gerion deserve a mention here, wherein it was noticed that nuclear localization signals (called viral peptides) conjugated with CdSe/ZnS QDs did not exhibit any toxic response within the HeLa cells. Similarly, Lieleg and colleagues developed a specific method of labeling membrane integrins in living osteoblasts using functionalized QDs. The investigators used cyclic Arg-Gly-Asp (RGD) tripeptide sequence and a biotin–streptavidin linkage to specifically couple individual QDs with integrin. Interestingly, even though observations revealed a significant decline in the number of blinking QDs but simulations inferred no harm of blinking QDs to quantitative screening of integrin trajectories.
- Erstwhile studies have demonstrated the luminescent cell marker-equivalent functioning of QDs, having an ability to discretely identify the specific molecular structures. The use of multicolor cellular labeling with QDs is already well-established, involving receptor-mediated uptake or via random endocytosis that employs the passive transport strategies to transport NPs across the cellular membranes. Such incentives eliminated the risk-prone external material cellular transfer methods of microcapillary injection and electroporation (using cell membrane mechanical defects to penetrate across cell membranes), in turn creating awareness about the comparatively safer endocytosis approach.
- Thus, the sensing capability of QDs is substantially mediated by optoelectronic and medicinal applications. Swift efforts are in progress to enhance the biosensing applications of QDs by reducing their toxicity. The attempts in this regard include a coating of QDs surface with a protective and stabilizing shell so that they could be safely used for bioconjugation with proteins, peptides, or other chemical moieties. An important observation has been the high stability of the round shape of QDs for their biosensing applications using them in the solution/colloidal phase.

### 4.2.3 Magnetic Nanoparticles

- Among the most promising alternatives to fluorescent labels in biosensors, MNPs are unique entities exhibiting characteristically distinct magnetic behavior compared to bulk material due to a reduced number of magnetic domains. Magnetic domains refer to regions of parallel magnetic moments caused by the unpaired interacting electrons in an atom. The fundamental source of magnetic force is the movement of electrically charged particles.

So, the magnetic behavior of a material is a direct function of its atomic structure. Electrons in an atom exhibit two kinds of motions, one a planetary motion around the nucleus while another is a motion about their spin. Both these motions manifest

**Table 6** The different configurations of magnetically sensitive materials used for biological sensing

| Type of magnetism | Atomic/magnetic behavior | Examples |
|---|---|---|
| Diamagnetism | Constituent atoms have no magnetic moment<br>Susceptibility is small and negative($-10^{-6}$ to $-10^{-5}$) | Inert gases; metals such as Au, Hg, Cu; nonmetallic elements, e.g., B, Si, P, S; many ions such as $Na^{+}$, $Cl^{-}$, and their salts; diatomic molecules like $H_2$, $N_2$, $H_2O$, most organic compounds |
| Paramagnetism | Constituent atoms have randomly oriented magnetic moments<br>Susceptibility is small and positive ($10^{-5}$ to $10^{-3}$) | Certain metals, e.g., Al, some diatomic gases, e.g., $O_2$, NO, ions of transition metals and rare earth metals and their salts, rare earth oxides |
| Ferromagnetism | Atoms have parallel aligned magnetic moments<br>Susceptibility is large (below $T_c$) | Transition metals Fe, H, Co, Ni, rare earth with (64–69) ranged mass number, alloys of ferromagnetic elements, some Mn alloys, e.g., MnBi, $Cu_2MnAl$ |
| Antiferromagnetism | Atoms have antiparallel aligned magnetic moments<br>Susceptibility is small and positive ($10^{-5}$ to $10^{-3}$) | Transition metals like Mn, Cr, and several of their compounds, e.g., MnO, CoO, NiO, MnS, MnSe, $Cr_2O_3$ |
| Ferrimagnetism | Atoms have mixed parallel and antiparallel aligned magnetic moments, below $T = T_c$, magnetic susceptibility is high | $Fe_3O_4$ (magnetite), $Fe_2O_3$ (maghemite), mixed oxides of Fe, and other elements such as Sr |

distinctive magnetic moments, together contributing to the magnetic behavior of a material.

- Based on magnetic behavior, all materials can be classified into five distinct categories depending on their bulk magnetic susceptibility. The two most common variations of magnetism are diamagnetism and paramagnetism, accounting for the magnetic properties of most of the periodic table elements at room temperature (RT). The magnetic effect in materials is also understood by its prevalence in isolated elements or compounds. Going by this logic, the magnetically sensitive elements are included under the category ferromagnetic. Antiferromagnetism is another form of magnetic behavior noticed in pure elements at RT. Another magnetic effect is ferromagnetic, which is not at all observed in any pure element but is found only in pure compounds such as mixed oxides. Table 6 lists the different kinds of magnetic behavior in elements with suitable examples of each category
- In a diamagnetic material, the magnetic moments of constituent atoms are aligned to nullify each other's contribution in the absence of an applied magnetic field. However, as soon as an external magnetic field (H) is applied, the electrons undergo spinning motions, which generate an electrical current and ultimately

an oppositely directed magnetization concerning that of the applied magnetic field. Readers must note here that all magnetically responsive materials exhibit a diamagnetic effect, but it often remains masked by greater paramagnetic or ferromagnetic sensitivities, which inevitably remain unaffected by the temperature.

- Multiple explanations and justifications are known for paramagnetism, holding distinctive validity for different kinds of materials. For instance, the behavior of materials characterized by noninteracting localized electrons is explained by ***Langevin model***, which works under the assumption that each atom has a randomly oriented magnetic moment due to thermal agitation. The application of a magnetic field modulates these randomly oriented magnetic moments, resulting in a gradual generation of low magnetization in a direction similar to that of the applied magnetic field. With a temperature rise, it becomes tedious to align these magnetic moments, resulting in decreased susceptibility. This kind of response is recognized by "Curie's law" (Eq. 4), C being a material constant, also termed as "Curie's constant."

$$\chi = \frac{C}{T} \tag{4}$$

Materials obeying this law have their magnetic moments localized at the atomic or ionic sites with no interaction between neighboring magnetic moments. Equation 4 is a special case of generalized Curie–Weiss law (Eq. 5) having a temperature constant θ, which refers to the inclination at which a material is placed concerning the applied magnetic field.

$$\chi = \frac{C}{T - \theta} \tag{5}$$

It is important to note here that for a nonzero value of θ in Eq. 5 interaction happens between neighboring magnetic moments and the material is paramagnetic only above a certain transition temperature. The discussion here is restricted to diamagnetic and paramagnetic materials, and for other materials, readers are advised to refer the more specific literature sources (Issa et al. 2013).

- Pauli's model for paramagnetic behavior is deemed fit for materials having free electrons, deemed helpful in the interaction-driven formation of the conduction band. As per this model, conduction electrons are fundamentally free electrons that manifest an imbalance between the electrons with oppositely directed spin, generating a low magnetization in the direction of the applied magnetic field. The corresponding susceptibility of the material is not affected by the temperature until the electronic band structure is altered.

### 4.2.4 Biosensor Utilities of Magnetic Nanoparticles

- Utility attributes of MNPs for improved biosensing could be via their integration into transducer materials or dispersion within the sample followed by their control using an external magnetic field onto the active detection surface. Sensing mechanisms based on MNPs offer benefits in terms of analytical figures of merit such as enhanced sensitivity, low LOD, high SNR, and shorter analysis time compared to those for non-MNP-based strategies. Biosensors employing MNPs have been reported significantly for the detection of several analytes, distinguished via a linear range of detection and extremely low LOD extents. Table 7 provides a list of such biosensors working through distinctive transduction mechanisms such as electrochemical, optical, piezoelectric, and magnetic fields (Rocha-Santos 2014). The subsequent discussion of biosensor configurations of MNPs is exclusively compiled from the 2014 contribution by Rocha-Santos TAP, which was featured in *Trends in Analytical Chemistry*. So, readers are suggested to refer to this literature source unless the reference is otherwise stated.

### 4.2.5 Electrochemical Biosensors

- Electrochemical devises work through measuring the electric current variations (potential difference and impedance) in terms of interactions between electrode and analytes. The electrodes herein could be coated with thin layers of biochemical or biological materials for improved surface activity (Michalet et al. 2005). The sensors working on this principle exhibit the benefits of rapidity, high sensitivity, relatively less expenditure, and lot much simpler methods of miniaturization and operations. Owing to such performance and automation distinctions, these biosensors find significant utilities in clinical, environmental, biological, and pharmaceutical domains. Improvements in the working of EC devices by the use of MNPs have manifolded their application potential via remarkable signal amplification abilities. To make this possible, MNPs can be used in EC devices via contact mode configurations with electrode surfaces, enabling the transport of redox-sensitive species apart from thin film formation, on the electrode surface.
- To date, $Fe_3O_4$ is the most preferred material in use for EC biosensors, attributed majorly to its superparamagnetic behavior, compatibility with antibodies, and enzymes, along with preparation simplicity. A potential constraint with $Fe_3O_4$ is due to its magnetic dipole-conferred attraction and a large aspect ratio, causing its aggregation on being exposed to bioactive fluids. This concern could be resolved by functionalization, which improves its interaction behavior and can make it biocompatible also. The salient functionalized architecture of MNPs in use for biosensors is core–shell Au–$Fe_3O_4$, core–shell Au–$Fe_3O_4$@$SiO_2$, Au–$Fe_3O_4$ composite NPs, $Fe_3O_4$ anchored on reduced graphene oxide, and $Fe_3O_4$@Au–MWCNT–chitosan (Dembski et al. 2008). Of these, core–shell $Fe_3O_4$@$SiO_2$ finds extensive use in biosensors as it allows MNPs' stabilization in the solution phase besides enhanced ligand binding on the MNPs' surface.

**Table 7** Salient performance aspects of MNPs-based biosensors, where the maximum utility of $Fe_3O_4$ in different configurations indicates its functional robustness with an ability of interaction-based modulated biological responses

| Sensor distinction | Configuration of magnetic nanoparticles | Detection limit | Detection range | Analyte |
|---|---|---|---|---|
| **Transduction principle: electrochemical** | | | | |
| Voltammetric immunosensor | Core–shell Au–$Fe_3O_4$ | 0.01 ng•$mL^{-1}$ | (0.005–50) ng•$mL^{-1}$ | Carcinoembryonic antigen |
| Voltammetric immunosensor | $Fe_3O_4$ Au NPs | 0.22 ng•$mL^{-1}$ | ($10^{-3}$- 10) ng•$mL^{-1}$ | Clenbuterol (pork) |
| Voltammetric enzyme-based sensor | Au–$Fe_3O_4$ composite NPs | 5.6 •$10^{-4}$ ng•$mL^{-1}$ | ($10^{-3}$ to 10) ng•$mL^{-1}$ | Organochloride pesticides (cabbage) |
| Voltammetric enzyme-based sensor | $Fe_3O_4$ Au NPs | 2 •$10^{-5}$ M | (2•$10^{-5}$ to 2.5•$10^{-3}$)M | $H_2O_2$ (contact lens care solution) |
| Voltammetric sensor | Core–shell $Fe_3O_4$@$SiO_2$ | 1.8•$10^{-8}$ M | (5•$10^{-8}$to $10^{-6}$) M | Metronidazole (milk, honey) |
| Voltammetric sensor | $Fe_3O_4$ anchored on reduced GO | ND | (0.2–0.6) nM | Cr (III) |
| Voltammetric sensor | $Fe_3O_4$@Au–MWCNT–chitosan | 1.5 •$10^{-9}$ mol•$L^{-1}$ | ($10^{-6}$ to $10^{-3}$) mol•$L^{-1}$ | Streptomycin |
| Voltammetric sensor | Core–shell $Fe_3O_4$@$SiO_2$/MWCNT | 0.13 μM | (0.60–100) μM | Uric acid (blood serum, urine) |
| Amperometric enzyme biosensor | Core–shell Au–$Fe_3O_4$@$SiO_2$ | 0.001 mM | (0.05–1) mM/(1–8) mm | Glucose (human serum) |
| Amperometric enzyme biosensor | $Fe_3O_4$@$SiO_2$/MWCNT | 800 nM | 1 μM to 30 mM | Glucose (glucose solution) |
| Potentiometric immunosensor | Magnetic beads Dynabeads Protein G | 0.007 μg•$mL^{-1}$ | ND | Zearalenone (maize-certified baby food cereal, wheat, rice, maize, barley, oats, sorghum, rye, soya flour) |

| | | | | |
|---|---|---|---|---|
| Potentiometric enzyme biosensor | Core–shell $Fe_3O_4$ | 0.5 μM | 0.5 μM to 34 mM | Glucose (human serum) |
| Electrochemoluminescent immunosensor | Core–shell $Fe_3O_4$ @ Au NPs | 0.2 pg•mL$^{-1}$ | (0.0005–5) ng•mL$^{-1}$ | α-Fetoprotein |
| Electrochemoluminescent immunosensor | Core–shell $Fe_3O_4$ @ Au | 0.25 ng•mL$^{-1}$ | (0–6) ng•mL$^{-1}$ | CrylAc (N/A) |
| Electrochemical impedance immunosensor | FeO carboxyl-modified MNPs | 0.01 ng•mL$^{-1}$ | (0.01–5) ng•mL$^{-1}$ | Ochratoxin A (wine) |
| Electrochemical impedance biosensor | Fe@Au nanoparticles-2-aminoethanethiol functionalized graphene NPs | 2•10$^{-15}$ M | ($10^{-4}$ to $10^{-8}$) M | DNA (N/A) |
| **Transduction principle: optical** | | | | |
| SPR immunosensor | MNPs (fluid MAG-ARA) with FeO core | 0.45 pM | ND | β-Human chronic gonadotropin (N/A) |
| SPR immunosensor | $Fe_3O_4$ @ Au MNPs | 0.65 ng•mL$^{-1}$ | (1–200) ng•mL$^{-1}$ | α-Fetoprotein |
| SPR immunosensor | $Fe_3O_4$ MNPs | 0.017 nM | (0.27–27) nM | Thrombin (N/A) |
| SPR immunosensor | $Fe_3O_4$/Ag/Au MNPs | ND | (0.15–40) μg•mL$^{-1}$ | Dog IgG |
| SPR immunosensor | $Fe_3O_4$–Au nanorods | ND | (0.15–40) μg•mL$^{-1}$ | Goat IgM |
| SPR immunosensor | Core/shell $Fe_3O_4/SiO_2$ | ND | (0.15–40) μg•mL$^{-1}$ | Rabbit IgG |
| SPR immunosensor | Core/shell $Fe_3O_4$/Ag/$SiO_2$ | ND | (1.25–20) μg•mL$^{-1}$ | Rabbit IgG |
| SPR immunosensor | FeO–carboxyl-modified MNPs | 0.94 ng•mL$^{-1}$ | (0.30–20) μg•mL$^{-1}$ | Ochratoxin A (wine) |
| Fluorescence immunosensor | $Fe_3O_4$ | ND | (1–50) ng•mL$^{-1}$ | *Escherichia coli* (N/A) |

(continued)

**Table 7** (continued)

| Sensor distinction | Configuration of magnetic nanoparticles | Detection limit | Detection range | Analyte |
|---|---|---|---|---|
| **Transduction principle: piezoelectric** | | | | |
| QCM immunosensor | FeO magnetic nanobeads | 0.0128 | ($10^3$ to $10^8$) cfu•mL$^{-1}$ | Avian influenza virus H5n1 (chicken tracheal swab) |
| QCM biosensor | FeO MNPs | ND | (0.001–100) ng•mL$^{-1}$ | *D. desulfotomaculum* (N/A) |
| QCM immunosensor | $Fe_3O_4$@$SiO_2$ | 0.3 | (0.001–5) ng•mL$^{-1}$ | C-reactive protein (human serum) |
| Electrochemical QCM immunosensor | Core–shell $Fe_3O_4$@Au–MWCNT composites | 0.3 | ND | Myoglobin (human serum) |
| QCM immunosensor | FeO MNPs | 53 | ND | *E. coli* O157:H7 (milk) |
| **Transduction principle: magnetic field** | | | | |
| Giant magnetoresistive immunosensor | Cubic FeCo NPs | 83 | | Endoglin (human urine) (human serum) |
| Giant magnetoresistive immunosensor | Cubic FeCo NPs | ND | 125 fM to 41.5 pM | Interleukin-6 |

| | | | | |
|---|---|---|---|---|
| Giant magnetoresistive sensor | FeO with PEG coating | 8 Oe | ND | N/A |
| Magneto-optical fiber sensor | $Fe_3O_4$ NPs | 592.8 pm•$Oe^{-1}$ | ND | N/A |
| Magneto-optical fiber sensor | $Fe_3O_4$ in magnetic fluid | 162.06 pm•$mT^{-1}$ | ND | N/A |
| Superconducting quantum interference sensor | Carboxy-functionalized FeO NPs | 1.3•$10^6$ cells | ND | MCF7/Her2-18 breast cancer cells (mice cells) |
| Hall sensor | Mn-doped ferrite ($MnFe_2O_4$) | ND | 10 to $10^5$ cells | Rare cells: MDA-MB-468 cancer cells (whole blood) |
| Hall sensor | Mn-doped ferrite ($MnFe_2O_4$) | ND | 10 to $10^6$ cells | *Staphylococcus aureus*, *Enterococcus faecalis*, and *Micrococcus luteus* (spiking cultured bacteria in liquid media) |

Next in line are the Au–$Fe_3O_4$-composite NPs, with their well-suited morphological, interactive, and surface attributes.

- In yet another worthwhile attempt, Gan and associates engineered a screen-printed carbon electrode (SPCE)-MNPs comprising composite. The working module of the sensor employed acetylcholinesterase (AchE)-coated Au–$Fe_3O_4$-composite NPs, which were adsorbed on the surface of CNT/nano-$ZrO_2$/Prussian blue/Nafion-modified SPCE (Fig. 17). Application of as-designed sensing probe for dimethoate detection in the cabbage produced an output equivalent to the gas chromatography coupled with flame photometer. The use of conducting $Fe_3O_4$/Au MNPs as sensing probes provided a faster response, adequate linear range performance, and sensitive detection of organophosphorus pesticides. Analysis with control combinations inferred a high electrode surface area and manifested a large current response for ultrasensitive thiocholine detection.
- A distinctive advantage of $Fe_3O_4$/Au MNPs-manifested thiocholine detection was the renewability of biosensor surface via removal of $Fe_3O_4$/Au/AChE through superparamagnetism of applied external magnetic field. Easier immobilization of enzyme/MNPs/($Fe_3O_4$/Au/AChE) on SPCE helped in reducing manufacturing costs via inherent advantages of electrode integration, simple manipulation, low sample consumption, reduced use of expensive reagents, and simple experimental design. One exclusive attempt for MNPs-driven electrode regeneration along with reduced impedance using iron oxide carboxyl modified MNPs for anti-ochratoxin-A MAb immobilization. Using this advantage, Zamfir and colleagues fabricated an electrochemical-impedance immunosensor for ochratoxin-A detection using anti-ochratoxin-A MAb-iron oxide carboxyl-modified MNPs at the Au-constituted working electrode surface.
- Thus, MNPs can be easily gathered together as electrode surface entities to confer increased precision and adjustability of working, besides exhibiting the

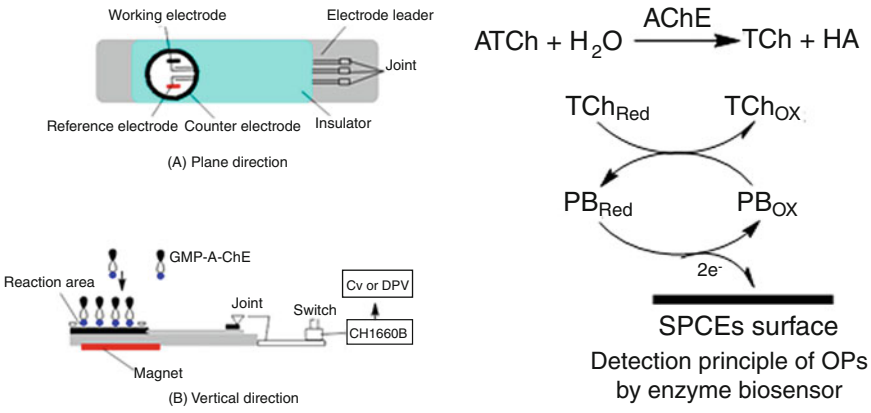


**Fig. 17** Representative illustration of an electrochemical biosensor, apparatus view from (**a**) plane and (**b**) vertical directions. Adjacent is the detection principle for organophosphorus pesticide recognition

renewability of electrodes by releasing the MNPs and their reciprocated replacement. So, the currently used electrochemiluminescent (ECL) biosensors used in functionalized mode with MNPs use the MNPs either as labeling agents or immobilization supports. The generated ECL signal is an amalgamation of sequential stages via chemical (radical combine) and ECL quanta (quantization of emitted energy). The ECL assays represent the workable arrangements of direct interaction, competition, and sandwich mode assays. Multiple QDs such as those of CdSe, CdS, or core–shell-type ZnS/CdSe have been the pillars of immense interest concerning ECL applications owing to the QC-aided optoelectronic applications. All these attributes make the QDs' efficient labels of ECL-based biosensors possessing improved sensitivity on being coated with MNPs and erstwhile capture probes.

- A significant 2012 attempt by Zhou and colleagues demonstrated the workability of a sandwich assay-based ECL immunosensor. The sensor detected α-fetoprotein using MNPs as capture probes and QDs as signal tags. Figure 18 illustrates the optimized process for making the magnetically sensitive capture probes, having $Fe_3O_4$–Au/primary α-fetoprotein (AFP) antibody (Ab1) and signal tag of CdS-Au/secondary AFP antibody (Ab2). The working configuration of the designed biosensor involved anchoring of Ab1 on the surface of Ab2, initiated by anchoring of Ab1 on the surface of $Fe_3O_4$–Au nanospheres through the Au–S linkage. As-formed products with Ab1 were immobilized on the $Fe_3O_4$–Au surface through which AFP was captured from the solution phase. Finally, protein-conjugated CdS–Au NPs were subjected to immunoreactions with the exposed AFP domain. The $Fe_3O_4$–Au/Ab1/AFP/Ab2/CdS–Au was used to fabricate the ECL immunosensor, which functioned via no signal response from the $Fe_3O_4$ MNP-modified electrode in the solution phase. However, $Fe_3O_4$–Au MNP-modified electrode surface generated a slightly enhanced ECL response.

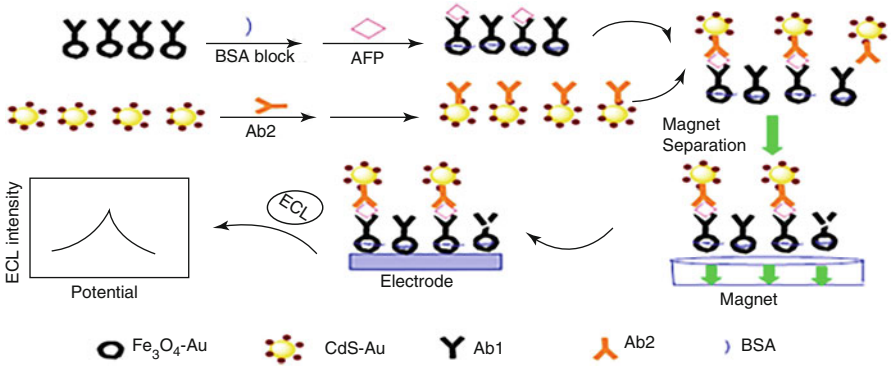


**Fig. 18** Preparation procedure of an electrochemiluminescent (ECL) immunosensor. BSA, bovine serum albumin; AFP, α-fetoprotein; Ab1, primary antibody of AFP; Ab2, CdS–Au-labeled secondary antibody

- The introduction of CdS–Au as a label enhanced the immunosensor signal even further compared to that of the unlabeled system ($Fe_3O_4$–Au/Ab1/AFP). Additionally, 2.5 times enhanced ECL signal was noticed when the CdS–Au composite film was used instead of CdS NPs. This improved response with composite film could be attributed to the catalytic activity of Au NPs, which manifested in enhanced electrical conductivity and sensitivity. The immunosensor revealed a performance comparable with that of ELISA for the detection of AFP in human serum as a potential clinical application.

### 4.2.6 Optical Biosensors

- Optically sensitive biosensors have been used for the detection of multiple analytes of clinical, environment, and food background, attributed to their virtues of low SNR, reduced interferences, and moderate manufacturing costs. Optically modulated biosensors can be classified based on specific optical characterization, including fluorescence spectroscopy, interferometry, reflectance, chemoluminescence (CL), light scattering, and refractive index.
- The assays based on CL sensitivity require optimization concerning emission intensity and better selectivity for quantitative screening of biological and environmental stimuli. These constraints could be overcome using MNPs, wherein significant improvements could be accomplished in catalysis, biomolecules carrier, and separation accessory. Readers are suggested to go through the recent review article by Iranifam for a specific idea about analytical applications of CL detection in assistance with MNPs.
- The extensively primed detection mechanisms in the MNPs-based optical devices are SPR and fluorescence spectroscopy. Figure 19 depicts the functioning of the immunosensor in combination with SPR technology using MNPs assays equipped for the detection and manipulation of β-human chorionic gonadotropin (β-HCG).
- The underlying principle of this screening relies on a grafting-coupled SPR sensor chip that is functionalized with Abs recognizing β-HCG. The MNPs conjugated with Abs endowed dual advantages of labels intended to manifest enhanced refractive index changes after analyte capture as well as prompt analyte delivery carriers at the sensor surface.
- Capturing of MNPs-conjugated antibody and analyte was ensured via coupling with a magnetic field on the surface of a sensor. The use of MNPs and their manifested response on the surface of the sensor via the application of a magnetic field enhanced the sensitivity by four orders compared to that of regular SPR amidst the direct detection. The manifested enhancement was the outcome of larger mass and high refractive index of MNPs, producing an LOD of 0.45 pM corresponding to β-HCG detection. Observations of this investigation present a ray of hope for the detection of viral and bacterial pathogens, overcoming the low sensitivity of SPR-driven biosensors due to a formidable mass transfer hindrance on the sensor surface caused due to analyte diffusion.
- MNPs like $Fe_3O_4$ NPs could also enhance the analytical signal of fluorescence intensity. Using this principle, a microfluidic immunosensor chip having circular

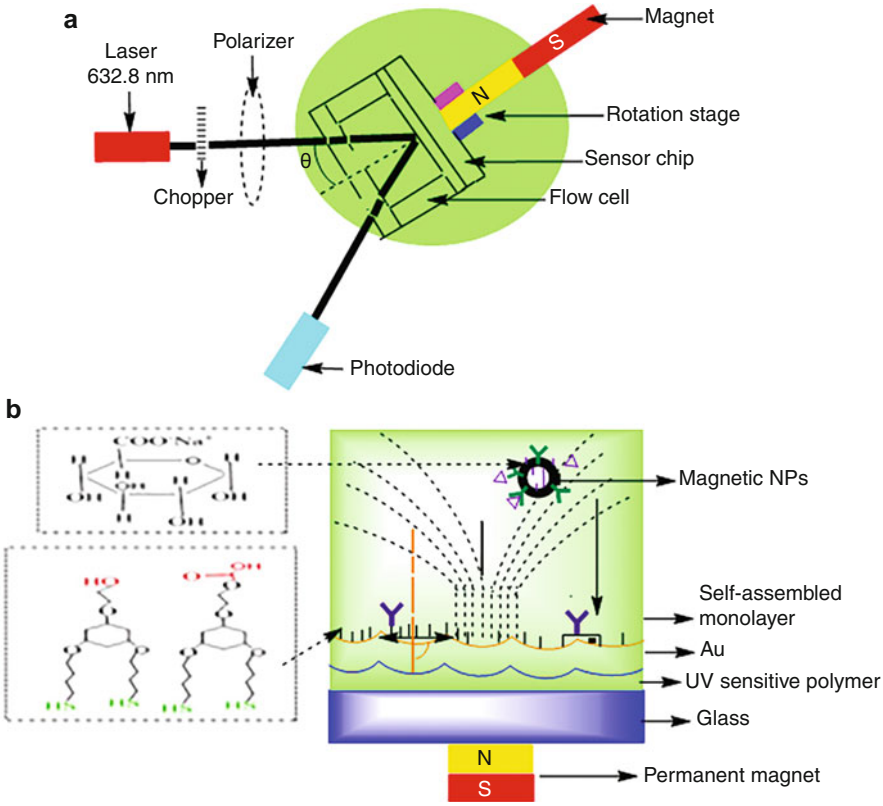


**Fig. 19** Illustration of a surface plasmon resonance (SPR) immunosensor: (**a**) optical sensor setup and (**b**) a sensor chip of the MNP enhanced grafting-coupled SPR sensor

microchannels was developed for *Escherichia coli* detection. The methodology comprised Ab conjugation of $Fe_3O_4$ MNPs followed by in-flow antigen capture in the microchannels. The captured MNPs create a heap-like structure at the detection site under the influence of a reversed magnetic flow. This reversed magnetic flow increased the retention time of antigens at the site of capture and the capture efficacy of antigens, resulting in the enhanced intensity of the fluorescence signal.

### 4.2.7 Piezoelectric Biosensors

- Piezoelectric devices are driven either via quartz-crystal microbalance (QCM) or SAW oscillations. Table 7 depicts that MNPs-based piezoelectric sensors and biosensors work via QCM transduction. QCM is a quartz crystal disk with metal electrodes on each side that vibrates under an electric field influence. The frequency of this vibration depends on disk thickness and cut extent, wherein resonance is attained differently as compound(s) absorb or desorb from a crystal

surface. Reduction in frequency corresponds to the proportional mass of the adsorbed compound.

- QCMs are small, robust, and inexpensive provisions, equipped with producing significantly detectable aftermath corresponding to 1 ng mass change. A significant concern with these devices is the enhanced noise generation as the size reduces erupting from the increase in surface-to-volume ratio. Among other concerns of QCMs are the perturbations from atmospheric humidity along with the challenges for analyte screening within a solution.
- MNPs with piezoelectric attributes could easily overcome the above concerns owing to their incentive offering transduction activities and recognition with an ability of solid-state construction and cost-effectiveness. The mechanisms by which MNPs enable the enhancement in frequency include (1) inherent piezoelectricity of MNPs, (2) MNPs' binding and concentration of analytes at the QCM surface, and (3) actions as matrix carriers for label loading.
- A significant 2013 study demonstrated the working module of a QCM-triggered immunosensor, optimized for the detection of C-reactive protein (CRP). Workable mode involves a sandwich mode immunological reaction between $SiO_2$-coated $Fe_3O_4$ NPs (as capture probes) labeled with MNPs-CRP Ab1 (primary CRP antibody), CRP, and signal tag (HRP) conjugated with HRP-bound secondary antibody. The whole assembly is immobilized on Au NPs, leading to the workable configuration as: (Au NPs-HRP/HRP-CRPAb2). Thereafter, the generated immunological complex is subjected to 3-amino-9-ethylcarbazole (AEC) and hydrogen peroxide ($H_2O_2$).
- Figure 20 depicts the synthesis procedure with the detection principle, wherein the capture probe of MNPs-CRPAb1 enhances the analytical signal due to magnetic separation and immobilization at the electrode surface. The magnetic

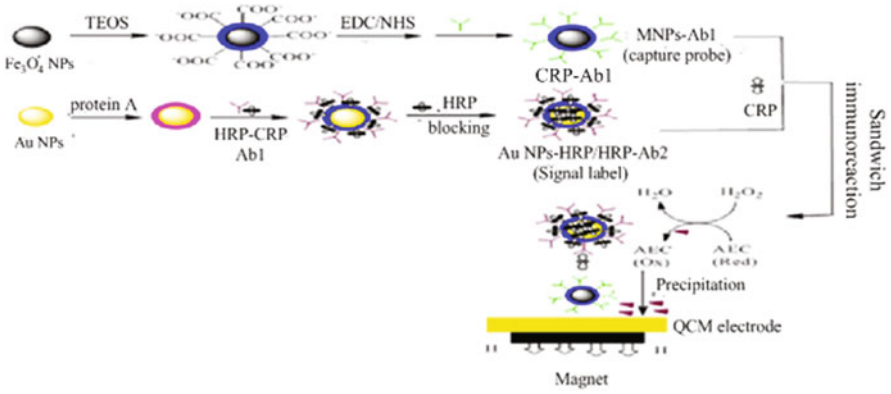


**Fig. 20** Illustration of a quartz-crystal microbalance (QCM) immunosensor (up). Detection principle (down). TEOS, tetraethyl orthosilicate; EDC, 1-ethyl-3-(3-dimethylaminopropyl) carbodiimide; NHS, amine reactive *N*-hydroxysuccinimide; CRP, C-reactive protein; Ab1, primary CRP antibody; Ab2, secondary CRP antibody; Au NPs, gold nanoparticles; HRP, horseradish peroxidase; AEC, 3-amino-9-ethylcarbazole; MNP, $Fe_3O_4@SiO_2$ nanoparticle

beads ($Fe_3O_4$-coupled $SiO_2$) for labeling CRPAb1 facilitated the attainment of uniform size distribution and simplified synthesis of labeled conjugates. In terms of results, the QCM methodology remained comparable with the ELISA, intended for human serum CRP detection. A further benefit is the easier regeneration of the QCM-sensor surface along with repeated usage. The present research aims to know more about the development of magnetic nanostructures along with understanding driven characterization of their piezoelectric behavior as these materials are capable of overseeding the accompanied sensitivity and stability concerns.

### 4.2.8 Magnetic Field-Based Biosensors

- As also reflected in Table 7, magnetically attuned transduction mechanisms involving MNPs' work based on giant magnetoresistance (GMR), Hall effect, magneto-optical, and superconducting quantum interference mechanisms. Magnetoresistive sensors work through magnetoresistance of either a ferromagnetic material or nonmagnetic heterostructures. Varying as per the compositional makeup of thin nanofilm, the MNPs exert their nanoscale effects using GMR or via tunneling magnetoresistance. The response signal generated out of changing electrical resistance regulates the quantitatively triggered analyte binding in the presence of an external magnetic field. Changes in the signaling outputs could be monitored via screening infinitesimal variations in the magnetic field, having an explicit dependence on the applied magnetic field strength (in sensor surroundings).
- Two mechanisms are established for GMR and MNPs' aided interleukin-6 (IL-6) detection, the first characterized by functionalization of GMR sensor using capture antibodies after analyte and capturing antibody binding. The detection is monitored by the binding of MNPs' labeled antibodies with the perceived analyte. The second detection mechanism works via GMR sensor functionalization using capture antibodies, succeeded by GMR biosensor-screened binding of MNP-labeled analyte.
- Both configurations involved the MNPs' dipole field detection generated by sensor surface-captured MNPs, varying sensitively with the distance. The quality of MNPs is highly critical for accurate magnetoresistive detection, mandating the probes to be ideally superparamagnetic with a high magnetic moment and large susceptibility. This is required to ensure magnetization over a small magnetic field and the used MNPs are ideally needed to have uniform size and shape. This is because the magnetic response is decided by these features, which in turn regulate the corresponding stability in physiological solutions along with needful biomolecule coupling.
- Considering the above requirements, the MNPs are selected with high magnetic moment fetching enhanced signal and therefore a high sensitivity. Amidst this consideration for magnetoresistive detection, the preferred materials include metallic Fe, Co, or their alloy-based MNPs. In a study, Li and colleagues have claimed the coupling of a small NP volume with an applied field of 10 Oesterds

(Oe), wherein the net magnetic moment of a single FeCo NP is almost 7- to 11-fold higher than one $Fe_3O_4$ NP.

- Controlling the magnetic moment of a permanent magnet using an externally applied nonhomogeneous magnetic field alongside the detection using magnetosensitive sensors is a potential domain where MNPs are highly useful. The best explanations of such phenomenon are provided by the magnetoresistive, Hall effect through which distinct variations of microscale magnetic field operable devices are controlled. This paved the way for the development of a micro-Hall sensor for ex vivo quantification of rare cells. The chip-based microfluidic sensor determines the magnetic moments of cells in a flowing configuration, labeled with MNPs. The workable sensor module acts via integrated technological breakthroughs, accomplishing biomarker actions on the implicit cells, like, as (1) linear response-mediated performance at $>0.1$ T, facilitating efficient magnetization of MNPs corresponding to maximal signal strength, (2) cell-equivalent dimensions of Hall element fetching an increased working accuracy, (3) an integrated setup of eight sensors consisting of a micro-Hall sensor with a moderated fluidic control than needed to focus the cells over a single sensor, and (4) an array that combines each cell's magnetic flux to facilitate the determination of the total magnetic moment of a single cell. This micro-Hall sensor is capable of high-throughput screening, exhibiting clinical-scale significance using tumor detection from whole blood in 20 ovarian cancer sufferers, presumably at a higher sensitivity compared to that of clinical standards.
- A sensor working through the varied magnetic field was developed via integrating a magnetic fluid ($Fe_3O_4$ NPs) with an optical fiber Loyt–Sagnac interferometer. This sensor works via varied magnified birefringence of a magnetic fluid using an adequately configured optical fiber interferometer design. The sensitivity of this configuration was one to three orders greater than prevailing magnetic fluid sensors.
- Magnetic field-based biosensors are not well-acquainted for sensing the multiple analytes because the corresponding analyte response arises from a singular physical stimulus (the magnetic moment). Thereby, using the varied dimensions of superparamagnetic NPs, analyte responses could be distinguished via explicit magnetization curves, paving the way for simultaneous multiple analyte screening.
- Table 7 comprises the varying sensing configurations using MNPs, distinguished via electrochemical, optical, piezoelectric, and magnetic field-activated transduction mechanisms. It is evident from the compiled configurations that $Fe_3O_4$ NPs find a maximum utility significance owing to their nanoscale-enhancing coupling with Au and $SiO_2$ NPs in distinctive architectures. For instance, core–shell morphology safeguards the magnetic coupling of shell material by conjugating the magnetic effect of the core material. The Fe with an atomic number of 26 forms $Fe_2O_3$ (maghemite) and $Fe_3O_4$ (magnetite) oxides as its major oxidation products. However, in the sensing domain, $Fe_3O_4$ finds exclusively high utility as inferred from its workable combination with Au NPs, doping combinations with

Mn, and immobilized state on multiwalled carbon nanotubes (MWCNTs) and in magnetic fluid too.

- With an outermost electronic configuration of $3d^6 4s^2$, Fe is ferromagnetic but its oxides, magnetite and maghemite, are ferromagnetic. Positioned in the 4th period and 8th group of the periodic table, Fe couples well with its neighbors, Mn and Co, for its magnetic susceptibility. Both Fe (alone) and its oxides exhibit a high magnetic susceptibility at less than critical temperature ($T_c$), arguing well for its structurally compatible combinatorial functioning. With both Mn and Co having an unpaired electron in their outermost shell, their combination with Fe argues for a magnetically coupled response through sustained electromagnetic induction.
- Spin behavior or alignment is the fundamental genesis of magnetic effect, wherein MNPs efficiently couple the magnetic sensitivity owing to dominant quantum effects in a sustained combinatorial regime with minimal adverse impact on native magnetic features of Fe or its oxide. The detection limit in most cases is in the ng•$mL^{-1}$ range or in the order of $10^{-6}$ to even lower extents. Similarly, the detection ranges are in the order of μM, nM, or ng•$mL^{-1}$, together reflecting a high degree of functional sensitivity and suitability.
- The healthcare utility of developed sensing mechanisms is also well-inferred by the diversity of screened analytes, such as uric acid from blood serum or urine, metronidazole from milk or honey, organochloride pesticides (in cabbage), CRP, endoglin (both in human serum), interleukin-6, *E. coli* contamination in milk, and avian influenza virus (H5N1). So, the diversity of these analytes is a strong indication of MNP's enhanced sensing abilities for screening more than one troubling pathological disturbance.
- With the coupling of the external magnetic field, MNPs-driven biosensors exhibit an added incentive in their external control and site-directed activities with greater accuracy. These attributes have been significantly helpful in coupling the localized thermomagnetic influences, enabling efficient eradication of tumor cells through controlled site-directed delivery. The magnetic coupling from an external agency is a handy manifestation in the removal of administered MNPs after their designated in vivo activities.

## 4.3 Reusable Substrate–Analyte Interactive Platforms

Enzymes are the heart of a biosensor working, wherein the usage for large extent commercialization assumes restriction because of high costs, which make the sensing operation highly expensive because of rather the low reusability of enzymes. Although NMs do require a minimum need of enzymes but ideally do not bypass it completely. The structural suitability of most enzymes during any biochemical reaction is very challenging, owing to which immobilization of useful enzymes with functional efficacy and enhanced reproducibility is practically highly desired even though it contributes to additional expenditure. The following are some important aspects regarding the immobilization of enzymes for their biosensing attributes:

- Enzymes, along with whole cells, can be used squarely well for immobilization. To put it more simply, immobilization of enzymes is a technique intended for their confinement over a solid matrix/support distinct from the one possessing any traces of the substrate or product. The simplest way to accomplish this is via attachment of enzymes over a suitable support matrix. Herein, the substrate molecules and the generated products must move in and out of the phase without any restriction. The phase here refers to the one in which enzymes are restrained.
- Multiple materials are suitable for use as matrix or support to aid in immobilizing the enzymes that facilitates a 100% recovery and reuse to aid in their cost-effective use. Usually, inert polymers and inorganic materials are preferred as enzyme support matrices. The major characteristics of an industrially viable carrier matrix are (1) cost-effective, (2) chemically stable, (3) physically compatible for handling and storage, (4) capable of augmenting enzyme specificity, (5) reusability, (6) effective for moderating product inhibition, and (7) forbidding of random adsorption and bacterial adulteration.
- In general, most of the matrices used exhibit only a few of these attributes, owing to which one has to optimize the performance features under the working conditions for the selection of an enzyme immobilization matrix. Typical enzyme immobilization is characterized by continuous economic operations, automatically controlled unit operations, large-scale investment, and viable product recovery.

***The most used enzyme immobilization methods are as follows***:

- Adsorption/carrier binding
- Covalent binding/cross-linking
- Entrapment method
- Membrane confinement

The following points discuss these mechanisms concerning their practical feasibility and conduct. Most of the information is reported after taking inputs from a 2016 literature source by Sirisha and colleagues, featured in *Advances in Food and Nutrition Research*. So, unless otherwise stated, the readers are requested to refer to this article for recalled studies and observations as there is a legal restriction about including fewer references.

### 4.3.1 Adsorption/Carrier-Binding Method

- This method of enzyme immobilization keeps the enzymes adhered to a carrier matrix through a mix of hydrophobic proximities and the multiple salt linkages corresponding to each enzyme molecule. The process uses either matrix suspension with the enzyme or dried enzyme(s) on the electrode surfaces. Commonly used matrix materials are water-soluble carriers like polysaccharide derivatives, glass, synthetic polymers, etc.
- Characteristic interactions of this enzyme immobilization method are mitigated by a strong bond configuration between the enzyme and support milieu. Essential

physiological parameters affecting the explicit interactions are temperature, pH, and substrate inclusion, excess of which can weaken the enzyme-support binding. Adsorbed enzymes are, in general, resistant to proteolysis and aggregation due to interfacial hydrophobic interactions. Certain attributes of suited matrix materials include micro-/mesoporous entities having high surface areas, thiol group functionalization, and microcrystalline cellulose with irreversible chemical binding.

- The prevalence of silanols makes the silanized molecular sieves suitable for enzyme immobilization stabilized via hydrogen bonding. Immobilization efficacy can be improvised by certain chemical modifications of functional support matrices. In this context, a study by Persson and associates screened the efficacy of adsorbed lipase over the polypropylene-grade hydrophobic granules/Accurel EP-100 apart from analysis of lipases–water chemistry. Interestingly, reducing the particle size of Accrual caused a significant increment in the enantiomeric stoichiometry and corresponding reaction pace.
- Physical adsorption-mediated immobilization of *Yarrowiali political* lipase on octyl agarose and octadecyl-sepa beads is a method of high stability, higher yield, and much greater operational regulation with low expenditure contrary to using free lipase. The distinctions in the immobilization-assisted lipase use are attributed to hydrophobic interactions of octadecyl-sepa beads, resulting in enhanced enzyme-support matrix affinity.
- Similarly, adsorption of lipase from *Candida rugosa* over the poly (3-hydroxybutyrate-ω hydroxyvalerate) revealed 94% activity despite 4-h treatment at 50 °C and reusability for 12 cycles. In another significant study, Mishra and colleagues reported enhanced pH stability with 50% retainment for urease by adsorbing over the 1,4-butanediol diglycidyl ether activated by threads, in the dried state. The highlighted aspects elucidate the significance of eco-friendly support materials as a biodegradable, long-lasting, and biocompatible performance, illustrating suitability for steadfast use with no serious ethical concerns.

### 4.3.2 Covalent Binding

- This mode of enzyme immobilization exhaustively depends on the formation of covalent linkages between the enzyme and support matrix, involving the side chain comprising histidine, arginine, and aspartic acid. However, the reactivity is indeed influenced by the orientation of various functional groups like those of ***carboxylic, phenolic, indole, amino, thiol, imidazole, sulfhydryl, and hydroxyl*** functionalities. Enhanced enzymatic actions could be accomplished via ensuring null inactivation of active-site amino acid residues. Some of the widely used enzyme-immobilizing modes based on covalent binding are as follows:
  - Enzyme–matrix covalent interaction in the presence of a substrate or a competitive inhibitor.
  - Formation of the reversible covalently linked enzyme–inhibitor complex.
  - Presence of a zymogen receptor.
- Usually, much greater activity with high stability is noticed corresponding to a characteristic protein orientation *vis-à-vis* involvement of peptide-engineered

faces enzyme conjugation. Observations of a study are quite significant in this regard, whereby greater thermal stability of the enzyme was observed on its covalent linkage with cyanogens bromide (CNBr)-conjugated agarose, CNBr-sepharose, with carbohydrate moiety, and glutaraldehyde as spacer arm. Furthermore, covalently bonded enzymes with modified silica gel carriers (on eliminating nonreactive aldehyde groups with SBA-15 matrix) impart enhanced stability and make them suited to function as hyperactive biocatalysts.

- Other matrix materials popular in use for covalent linkage-driven enzyme immobilization include mesoporous silica and chitosan, well suited to enhance the half-life and improve the thermal labile functioning of enzymes. Using the nanoscale materials (such as nanosheets, NPs, carbon nanotube(s) functionalization) is a revolutionary attempt in improving enzyme functioning. Studies have demonstrated that cross-linking of enzymes with electrospun nanofibers confers a much higher residual chemical activity due to enhanced porosity and surface area (highly important for reducing the activation energy of reactants). Researchers in this context have obtained significant performance improvement using attapulgite nanofibers as support matrices for covalently linked alcohol dehydrogenase, attributed to its thermal flexibility and enhanced quantum effects at the nanoscale.
- Another prominent route to accomplish covalent linkage-driven enzyme immobilization uses magnetic nanoclusters, which operate in multiple directions and are the crux of remarkable improvement in the pharmaceutical industry. The salient attributes of these materials are enhanced operational stability, reuse ability, and longevity of operation. A distinct aspect of this method is the involvement of a cross-linking agent, which is glutaraldehyde. The high aqueous solubility of this material enables the formation of stable intra- and inter-subunit-linked covalent bonds, eminently referred to as bifunctional cross-linkages.

### 4.3.3 Affinity Immobilization

- Affinity-binding-driven enzyme immobilization over a support matrix is stabilized via specific BFs. This method uses the substrate-specific action of an enzyme to engineer the support matrix in varied physiological conditions. The following points discuss the two methods used to accomplish this:
- The first approach is characterized by pyrimidine coupling of the matrix to an affinity-driven ligand corresponding to the target enzyme. The second method uses enzymes in the conjugated phase with another molecule, gradually developing affinity toward the matrix.
- The affinity adsorbents also find significance in enzyme immobilization, wherein immobilized enzymes on complex support matrices like agarose-linked multilayered concanavalin A and alkali-inert chitosan-coated porous silica beads exhibit increased efficacy and stability.
- The bioaffinity-assisted layering of matrices is another potential method used to modulate the reusability of bound enzymes. The inherent benefit of this modulation is due to noncovalent interactive forces, such as van der Waals forces, Columbic interactions, and hydrogen bonding.

### 4.3.4 Entrapment

- The entrapment process relies on enzymatic caging within a polymeric system via covalent or noncovalent bonds, facilitating the substrate and product movement but retaining the enzyme. A distinction from the other methods is the nonbound state of the enzyme to the support matrix.
- Enzymatic caging could be accomplished by (1) inclusion within a highly cross-linked polymer matrix, (2) dissolution in the nonaqueous phase, and (3) semipermeable capsule-driven separation from a bulk solution.
- Various approaches to enzyme entrapment are known like fiber entrapping, gel entrapping, and microencapsulation. Encapsulation with **alginate–gelatin–calcium hybrid carriers** is reported as efficient due to its ability to improve mechanical stability and prevent enzyme leakage. In *C. rugosa*, the entrapping of lipase in chitosan resulted in its enhanced activity besides forbidden leaching.
- Such abilities are chiefly attributed to the biocompatible and nontoxic features of the support matrix, which is receptive to chemical modifications and has hydrophilicity-driven high affinity toward affinity. Chen and colleagues in 2011 reported simultaneous entrapment of lipase and MNPs with biomimetic silica, conferring a significant improvement in enzyme activity under various saline additives.
- Studies have also reported that on being entrapped with K-carrageenan lipases exhibit high tolerance toward organic solvents alongside being highly thermostable. The use of nanostructured supports like electrospun nanofibers and pristine materials for enzyme entrapment is witnessing a persistent encouragement for biomedicine, biofuels, chemistry, and biosensors.

### 4.3.5 Ionic Bonding

- This method binds the enzymatic protein to hydrophobic carriers, containing ion-exchange residues. The typical mechanism is characterized by noncovalent reversible interactions via changes in ionic strength, polarity, and temperature. The working principle herein is similar to the functional protein–ligand interactions in chromatography.
- Support materials used in this enzyme immobilization module include polysaccharides and synthetic polymers, possessing ion-exchange domains. Advantages of this method comprise simpler and easier binding of the enzyme with the carrier unlike that of covalent binding. Usually, ionic binding induces little changes in the confirmation and active-site constitution, enhancing the enzymatic activity on most occasions.
- A cautionary aspect herein is the supposed enzyme leakage from the carrier, particularly if high ionic strength substrate or varied pH solutions are used. This is due to the weak BFs between the enzyme proteins and carrier molecules. The enzyme-carrier BFs are quite strong in this mode contrary to that of physical adsorption, although these are not as strong as in covalent binding.

### 4.3.6 Metal-Linked Immobilization

- This method of enzyme immobilization relies on the precipitation of metal salts over the support matrix. The metals suited for this purpose are capable of binding with nucleophilic functionalities of the carrier matrix. Precipitation of constituent cations over the support matrix surface is attained on heating.
- Studies have demonstrated (30–80)% improved enzymatic activity on immobilization via this method. The mechanism of this process is relatively simple and reversible in its operation. A distinctive benefit of this method is that it allows the regeneration of both enzymes and a matrix.

### 4.3.7 Preferable Materials for Designing Immobilization Supports

The materials employed for the immobilization of enzymes are frequently referred to as a carrier or support matrices. The ideal features of a matrix are of substantial process in accomplishing a requisite extent of enzyme immobilization. Ideal support matrices should have the following attributes for optimal performance:

1. It should not be much costly and must be eco-friendly to get rid of the undesired economic impact of the process.
2. It must be entirely inert after immobilization and should not block the desired reaction.
3. Adequate thermal and mechanical resistance to ensure the use of immobilized enzymes under varied operational conditions.
4. The matrix constituent must be significantly stable.
5. The matrix material should have high renewability after the attainment of the useful lifestyle of the immobilized enzyme.
6. The chosen matrix material must enhance the enzyme specificity.
7. The chosen material should be capable of packing a large amount of enzyme. For this ability, porosity plays a significant role. In general, a large pore size leads to a significant decrement in surface area contrary to a difficult exclusion of the protein with a small pore size. So, the pore diameter must be within the optimal range.
8. To get rid of inhibiting protein adsorption and denaturation, the hydrophobicity of the support matrix must be reduced. Thereby, the support matrix working environment should be amenable to an extent that favors the catalytic activities of immobilized enzymes.
9. The support matrix should be capable of shifting the pH optimum for accomplishing the desired extent of enzyme action.
10. The support matrix should have antimicrobial and nonspecific adsorption characteristics.
11. Rarely ever a matrix is available with an optimum extent of each of the above properties, so caution must be thoroughly exercised in choosing an appropriate support matrix *vis-a-vis* their properties.

Based on their chemical compositions, the support matrices are listed in two major categories, namely, (1) inorganic support material and (2) organic support

**Table 8** Eminent inorganic supports with their characteristic attributes and immobilized enzymes

| Inorganic material | Traits | Immobilized enzyme |
|---|---|---|
| Zeolite (molecular sieves) | Large specific surface area conferring efficient enzyme loading | Glucose oxidase (GO), α-chymotrypsin |
| Ceramics | Both macro- and micropores are efficient in moderating diffusion rate and enhancing the specific surface area | *Candida antarctica* lipase |
| Celite | Inexpensive, less polar, large adhesion area, chemically inert, resistant against pH, temperature, urea, detergents, and solvents | Lipase, polyphenol oxidase, β-galactosidase |
| Silica | Nanosized structures have a high surface area, crystallinity, and high stability to chemical and mechanical forces | Lignin peroxidase, HRP, α-amylase |
| Glass | Highly viscous fluid | α-Amylase, nitrate reductase |
| Activated carbon | Manifold contact sides, high surface area | Acid protease, acidic lipase |
| Charcoal | Splendid adsorbent, least release of fine particulate matter | Papain, amyloglucosidase |

Note: Large surface area, robust handling, and chemical stability are the major distinctions

material (organic supports are further divided into natural and synthetic materials). The following points discuss the salient aspects of these entities with suitable examples.

### 4.3.8 Inorganic Materials as Supports

- The materials included in this class include glass, silica gel, alumina, metal oxides, zirconia, and several other silica-based compounds that are ideal materials and are widely used due to their significant thermal and mechanical resistance. These entities also exhibit significant microbial opposition for inhibited bacterial or fungal growth due to their substrate attributes.
- Rigidity and porosity are the two characteristic features of inorganic support. Besides, these materials exhibit unchanged ore diameter and volume ensuring a fixed volume and shape of the support. Table 8 comprises several inorganic support matrices with their major characteristics and extensively immobilized enzymes.
- **Silica**: Inorganic supports, like $SiO_2$ and $SiO_4$, constituted matrices are highly suited for enzyme immobilization. Both of these prevail as 3D polymers, although $SiO_4$ is rigid while $SiO_2$ is flexible. In both these support matrices, amphiphilic functionalities contribute to the adsorption efficacy. Zeolites comprise another domain of silica-rich microporous matrix surfaces, equipped with enhanced surface area to immobilize the proteins. Though silica carriers are relatively inert materials, these require significant optimization for being used as an enzyme immobilization support matrix. For this purpose, the silica bed

supports are preferentially treated with aminoalkyltriethoxy silane that engineers the matrix surface with $–NH_2$ functionalization. A series of further modifications make these materials befitting for enzyme immobilization. For example, penicillin-G-amidase is initially conjugated with dextran before its immobilization over the amino-activated silica gel that confers its enhanced thermal stability. Similarly, lignin peroxidase and HRP were immobilized on activated silica to get rid of chlorolignins from the eucalyptus kraft effluent. In a significant attempt, Soleimani and colleagues observed an improved cleansing action of detergents after their binding with α-amylase on silica NPs. Another study reported enhanced enzyme carrier bonding after surface engineering of silica, involving amination of –OH and siloxane functionalities apart from absorption of methyl or polyvinyl functionalities.

- **Ceramics**: These entities are solid, insoluble, and nonmetallic and are derived from cooking plastic materials. **Metal oxides such as $Al_2O_3$, $TiO_2$, $ZrO_2$, and $SnO_2$ are referred to as ceramics**. Due to their porous character, ceramics are highly preferred materials for enzyme restriction. A 2004 study by Magnan and colleagues reported lipase immobilization from *Candida antarctica* on a ceramic membrane that modulates hydrolytic and synthetic reactions through curtailing feedback inhibition. Ceramic foams were found effective in enhancing the working surface area and decreasing the diffusion rates.
- **Glass**: The support matrices of glass represent another prominent inorganic enzyme immobilization means. Glass-made matrices are highly viscous and have been successfully recruited as immobilized supports for enzymes like α-amylase. In the process, phthaloyl chloride comprising $–NH_2$ group-functionalized glass beads were screened as strong and sustainable. Likewise, the reason being immobilized over the glass pH electrodes acted as a biosensor for monitoring blood urea extent to as low as 52 $mg•mL^{-1}$.
- **Charcoal**: The use of charcoal as immobilized support is immensely popular for enzymes like amyloglucosidase with no cross-linking agents for starch hydrolysis and accomplishing 90% catalytic activity. Charcoal has been studied as an efficient adsorbent with efficient adsorption ability and a low release of particulate matter.
- **Activated carbon**: Studies have shown reliable evidence for natural as well as HCL-modified activated carbon for enzyme immobilization. Recently, acid proteases and acid lipases were immobilized on mesoporous-activated carbon particles and demonstrated significantly greater catalytic efficacy even after being reused for 21 cycles (Sirisha et al. 2016). A 2010 study by Daoud and associates reported remarkable enzyme immobilization enabled via (600–1000) $m^2.g^{-1}$ surface area and (300–1000) pore volume.

### 4.3.9 Organic Supports

- **Natural polymers**: A wide range of natural materials, such as hydrophobic polysaccharides, viz., chitosan, collagen, carrageenans, alginate, cellulose, starch, agarose, etc., are widely preferred as support matrices for immobilization of enzymes. The structural flexibility of similar materials makes them capable of

**Table 9** The various natural organic polymeric supports used for enzyme immobilization

| Support | Properties | Enzymes immobilized |
|---|---|---|
| Alginate | Used in the form of xanthan-alginate beads, alginate-polyacrylamide gels, and calcium-alginate beads<br>Can be reused and significantly improves enzyme stability | Cellulase, cross-linking with divalent ions and glutaraldehyde stabilizes the enzyme activity |
| Chitosan and Chitin | Used in combination with alginate, less leaching, reliable for enzyme trapping, and can entrap more enzymes as beads | D-Hydantoinase, acid phosphatase, chymotrypsin, glucose isomerize, glucose oxidase, and lactase |
| Collagen | Retains significant activity after multiple reuse cycles | Tannase, catalase, and alkaline phosphatase |
| Carrageenan (linear sulfated polysaccharide) | Improves stability, pseudoplastic sensitivity imparts thinness under shear stress and recovers the corresponding viscosity on stress removal. Cheap, long-lasting, and has greater entrapment | Lipase and α-galactosidase |
| Gelatin (hydrocolloid rich in amino acid content) | High adsorption ability and promotes loading efficacy | Amylase, urease, and galactosidase via cross-linking with glutaraldehyde and formaldehyde |
| Cellulose | Greater storage capacity, better formability, and flexibility | Fungal laccase, penicillin G acylase, glucoamylase, α-amylase, tyrosinase, lipase, and β-galactosidase |
| Starch | Stable | Bitter gourd peroxidase, α-amylase, and glucoamylase |
| Pectin | Used in combination with glycerol as a plasticizer to reduce the brittleness of pectin-chitin and pectin-calcium alginate, have enhanced thermal, denaturant resistance, and catalytic attributes | Papain and pectin lyase |
| Sepharose | Porous, easy adsorption, retain catalytic properties at extremes of pH, temperature, and high salt concentration | Amylase and glucoamylase |

forming inert gels due to easily activated chemical functionalities. Such attributes facilitate a reversible and irreversibly optimized binding of proteins and enzymes over the support matrix. Other significant advantages of these natural-grade materials as immobilization matrices include their cost-effectiveness and thermal and mechanical inertness on being cross-linked with bifunctional chemical agents. Table 9 describes some widely used organic supports as enzyme immobilization support matrices.

- **Alginate**: This is a sulfate-functionalized polysaccharide obtained from the brown algal cell wall. Concerning the usefulness of alginate in enzyme

immobilization, xanthan-alginate beads, calcium alginate beads, and alginate-polysaccharide gels are well known for improved enzyme performance and reusability. Improved enzyme stability via the use of alginate is well reported, involving cross-linking with divalent ions and glutaraldehyde.

- **Chitosan**: It is a polysaccharide that finds usability as a support matrix having manifold optimal carrier suitable characteristics. These attributes include mechanical inertness, rigidity, hydrophilicity, and active reactive groups that can directly interact with enzymes besides having an affinity for protein binding. Studies have reported that chitosan-coated enzymes exhibit less leaching compared to those of alginate due to chitosan's more prompt ionic and physical interactions with enzymes. It has also been demonstrated that a wet composite of chitosan and clay has plentiful –OH and $–NH_2$ groups. This material is thereby more efficient for enzyme immobilization with enhanced hydrophilicity and porosity. It was observed that *Bacillus circulans*, a chitin-binding domain of chitinase, confers a strong affinity for retaining D-hydantoins.
- **Cellulose**: This is perhaps the most commonly used carrier molecule for enzyme immobilization. It has a distinguishingly lower binding capacity besides being inexpensive and available in fibrous as well as globular textures. A notable study for enzyme immobilization using cellulose was reported by Namdeo and Bajpai in 2009, wherein α-amylase was immobilized to cellulose dialdehyde-coated magnetite NPs and enabled a novel starch degrading system. Likewise, enhanced forbearance and viability of the enzyme were obtained following its immobilization over the glutaraldehyde-activated ionic liquid-cellulose film.
- **Collagen**: The attributes of collagen making it an efficient enzyme immobilizing support matrix comprise protein similar nature, significant water-holding capacity, and good porosity. The basis of collagen immobilization is via the formation of a covalent bond between the collagen side chains and that of the enzyme, resulting in a stronger enzyme hold over the support. Using glutaraldehyde as a cross-linking agent, collagen is used for tannase immobilization. Chen and associates 2011 showed that on being immobilized to $Fe^{+3}$-collagen fibers, catalase activity remained significant even on 26 reuses.
- **Carrageenans**: It is a red algal and linear-sulfated polysaccharide. The attributes of carrageenans contributing toward its significance in enzyme immobilization include good gelling and high protein-holding ability with pseudoplastic receptivity, collectively making it thin under shear stress besides enabling a viscosity recovery on being distressed. A 2010 study by Jegannathan and colleagues demonstrated an encapsulation efficacy of 42% during biodiesel generation via the coextrusion method using carrageenans as a support matrix.
- **Starch**: A natural polymer with linear amylase and branched amylopectin units, for significant hydrophilic actions, starch is a renewable and one of the most trusted raw materials used for enzyme immobilization. In this context, a 2019 investigation by Matto and Hussain reported significant immobilization for bitter gourd peroxidase using calcium-alginate and starch comprising hybrid. Analysis revealed comparatively greater stability of the entrapped enzyme in the presence of urea (a denaturant) because of the sustained and coordinated chemical actions

of carbohydrate moieties rather than that for the surface-immobilized enzymes (without the alginate-starch-calcium hybrid).

- **Pectin**: This is a structural polysaccharide of plant origin and is a major constituent of the primary cell wall. In plant tissues, pectin serves as a significant intercellular cementing material. It is a gelling agent with good water-holding capacity. Ceniceros and colleagues 2003 developed advanced materials for the treatment of skin damage through papain immobilization onto pectin along with (0.2–0.7)% glycerol. The ability to form highly stable polyelectrolyte complexes with entrapped enzymes makes pectin–chitin and pectin–calcium-alginate confers them with significant thermal and denaturant resistance for improved catalysis by the immobilized enzyme.
- **Sepharose**: This enzyme-supported matrix finds its commercial significance from its beaded texture and is activated by cyanogens bromide (CNBr). The CNBr-activated Sepharose 4B is used for the immobilization of amylase and glucoamylase, characterized by enhanced porosity with better and greater macromolecule adsorption. Alkylation-engineered sepharose increases its catalytic retainment at extreme pH, high salt concentration, and temperature.
- **Artificial Polymers as Immobilization Support Matrices**.

  Polymers of synthetic grade comprise the ion-exchange resins, with a porous surface and a hydrophobic sensitivity. These characteristics impart a strong enzyme immobilization potential to synthetic polymers, exemplified by their inertness toward a microbial attack. Polystyrene, polyvinylchloride, polyacrylate, polyamide, polypropylene, diethylaminoethyl cellulose (DEAE cellulose), and UV-activated PEG are some prominent synthetic polymers used as enzyme support matrices. Polystyrene was the first-ever synthetic polymer used for enzyme immobilization.

***Some other significant attempts using synthetic polymers for enzyme immobilization are summarized next***:

1. Amberlite and DEAE cellulose for α-amylase immobilization.
2. PVC is used for immobilizing cyclodextrin glucosyltransferase and guards against thermal inactivation.
3. Synthetic polymer polyurethane microparticles were produced by mixing polyvinyl alcohol and hexamethyl diisothiocyanate in 1:3 proportions. The use of polyurethane microparticles for enzyme immobilization improved the loading ability and catalyzing efficiency through the enhanced surface area.
4. Polyethyleneglycol, along with glutaraldehyde, is used for immobilization of white radish peroxidase and forms a protective layer around the active enzyme center to guard against oxidative stress.
5. UV-activated PEG having high porosity has been used for wastewater treatment.
6. Glutaraldehyde-activated nylon is well known for lipase immobilization.

# 5 Early Disease Diagnosis Using a Biosensor

## 5.1 Mechanisms for Improved Detection Sensitivity

The present diagnosis of critically infectious diseases caused by bacterial, viral, or fungal pathogens relies on manifold laboratory-based tests, including microscopy, culture immunoassays, and nucleic acid amplification. Primitive methods for in vitro diagnosis rely on age-old mechanisms that are time-consuming and mandate the analysis in centralized laboratories, skilled manpower, and larger-sized equipment. With the progressive miniaturization and constantly bettered understanding of nanotechnology principles, the point-of-care diagnosis methods have been a boon to faster and more accurate diagnosis without cumbersome, elaborate laboratory testing and the manpower requirement. Biosensor-mediated diagnosis of infectious diseases is characterized by improved DS of pathogen-implicit antigens with the multiplex detection of host-immune response for an overall improved specificity.

The flexibility exhibited by a biosensor functioning augments the development of integrating the detection of pathogen-varied targets as well as typical biomarkers that represent distinctive host-immune responses at variable stages of an infection. Physical distinctions of biosensor-mediated clinical diagnosis of infectious diseases comprise a low requirement of to-be analyzed sample, a robust screening mechanism based on specific interactions, reduced cost, time, and user-friendly operation. Working in labeled or label-free configurations, the modern biosensors imbibe the integrated micro- and nanofabrication technologies, working through optical, electrical, and mechanical transducers. While label-free assays screen the analyte via biochemical reactions on a transducer surface, the labeled assays comprise the analyte sandwiching between capture and detector agents, wherein the latter is conjugated using enzymes, fluorophores, or QDs toward a quantifiable signal output. The following points discuss the two modes with some more illustrations.

- **Labeled assays**: These are the most commonly used biosensing assays, having the analyte sandwiched between the capture and detector agents (CAs and DAs). The CAs are immobilized on a solid surface such as electrodes, glass chips, and nano- or microparticles, whereas the DAs are conjugated to signaling tags that could be fluorophores, enzymes, or NPs.
- **Label-free assays**: These assays couple the optical, electrical, or mechanical transducers with the signaling tag. The sensor–tag interactions diversify the optical sensors equipped for perceiving the fluorescent, colorimetric, or luminescent tags (Sin et al. 2014).
- While electrochemical sensors are capable of detecting the redox reactions from enzyme tags, magnetoresistive sensors detect magnetic tags. Thus, together these systems enable quantitative or semiquantitative analyte detection by relating the generated signal with the captured analyte quantity. In general, capture and detector elements exhibit different binding sites, leading to enhanced specificity with reduced background. Some assays of labeled configuration are as described next.

- Practiced as the most standardized sandwich immunoassay for infectious disease diagnosis in clinical laboratories, enzyme-linked immunosorbent assay (ELISA) typically uses capture and detector antibody modified with an enzyme tag to facilitate the conversion of a chromogenic substrate to colored molecules. The quantitative configuration measures the optical density of the colored product and upon comparing it with a standard serial dilution of a known target molecule (the screened antigen) concentration. For instance, Liao and team developed an electrochemical sensor assay for the specific detection of urinary pathogens in clinical samples. The detection was facilitated by immobilized capture oligonucleotide and labeled detector oligonucleotides for screening for the existence of bacterial 16S rRNA. Signal was generated by a redox current of the conjugated enzyme tag to the detector probe.
- To date, the best-known commercial-grade sandwich assays are the lateral flow immunoassays (also referred to as immunochromatographic test strips), equipped with qualitative measurements of the signal by visual observation and on a semiquantitative mode via engineering interfaces such as low-cost laser photodiode or amperometric detectors.
- Some of the better commercial assays in terms of discrete analysis are the home pregnancy detection kits and urine analysis strips. Likewise, lateral flow assays are also well known for the analysis of saliva, HIV antigens, malaria, and tuberculosis screening using serum inspection. Salient benefits of lateral flow assays include moderate expenditure, almost very minimal sample preparation, and a robust interpretation of results (Sin et al. 2014). Demerits of this configuration involve a poor sensitivity to distinctly recognizing the clinically suited targets and the respective qualitative/semiquantitative results. Recent attempts have worked out the signal amplification through functionalizing the NPs (having a high aspect ratio) with several different kinds of biomolecules, significantly bettering the LOD. As of now, the latest design of labeled biosensors is characterized by the incorporation of bio-barcodes, metal, and magnetic NPs (Table 10).

**Table 10** Working interfaces of labeled biosensors, with corresponding distinctions and possible concerns

| Technology | Benefits | Uncertainties |
|---|---|---|
| Redox electrochemistry (amperometric) | Adjustable detection platform for POC configuration and easier integration with other electric field-driven approaches | No real-time detection and assay involves multiple steps |
| Bio-barcode | POC-compatible detection platform and easy-to-interpret results | No real-time detection, cumbersome probe preparation, and multiple steps in the assay |
| Metal nanoparticles | POC-compatible detection platform, easy-to-interpret results, and multiplex | No real-time detection, temperature fluctuation affected assay results, and multiple steps in the assay |

*POC* point of care

- **Bio-barcode amplification**: This labeling procedure is amicable for detecting proteins and nucleic acids without any essential need for enzymatic reactions. The conventional procedure for bio-barcode amplification (BA) comprises a sandwich assay, with the capturing of targets using micro-/nanoscale particles conjugated with oligonucleotides as proximal signal amplification alternatives. Procedurally, on capturing each target, several barcode DNA strands are generated for the next detection using an energetic impulse (usually electrochemical or optical). A very recent study used BA for the detection of HIV-1 capsid (p24) antigen, an important marker to detect the decreased $CD4^+$ T-cell decreased count, enabling a timid, HIV-1 infection detection. The screening method used the anti-p24-coated microplate for the early detainment of the p24 coat, followed in line by the biotinylated detector Ab. Subsequently, the streptavidin-functionalized NPs-based BA DNA was optimized for likely signal amplification. This is followed by the detection using a chip-based scientometric method. The optimized probe displayed a (0.1–500) pg•$ml^{-1}$ LOD, with ~150-fold higher sensitivity compared to conventional ELISA. The commercial feasibility was screened using clinical blood samples, with 100% negative and positive predictive outcomes in 30 and 45 samples, respectively. Apart from this, the HIV-1 detection consumed 3 days lesser compared to the ELISA for seroconverted samples.
- **Metal nanoparticles**: These entities are also efficient signal amplification labels for biorecognition sensitivity enhancement, imbibed by their quantum mechanically distinguished optical attributes. Several studies have explored Au and Ag NPs as they exhibit the plasmon absorbance bands in the visible light spectrum and are determined in turn by the size of their respective particles. Thereby, the spectral variations arising out of the aggregation and monodispersed states have been the basis of biomaterial-metal NPs-integrated functional systems as the detection amplifiers. One study has, for example, used Au-labeled antibodies as an integrated part of a microfluidics chip for simultaneous diagnosis of HIV and syphilis from 1 μl of whole blood. The reduction of $Ag^+$ on the Au NPs comprises signal amplification within a millimeter-sized channel provision. Thereafter, the OD of silver film is detected and is quantified using low-cost optics or qualitatively through the naked eye. A ccomparative analysis of this sensing configuration with commercial ELISA kits revealed a 100% sensitivity and (98–100)% specificity for HIV and (82–100)% sensitivity, (97–100)% specificity for syphilis.
- **Magnetic nanoparticles**: The signaling amplification using MNPs-coupled detectors in biosensors offers the advantage of compatible utility in solution-phase sandwich assays like that of diagnostic magnetic resonance. The distinction between solution-phase assays is the relatively faster assay times compared to diffusion-dependent surface structure-based assays. The diagnostic magnetic resonance exhibited by MNPs is described by the presence of capture as well as detection moieties in solution, wherein both are linked to MNPs. On screening a potential analyte of interest, magnetic particles cluster as antibodies and bind the analyte. The clusters of magnetic particles are more efficient at dephasing nuclear spins of adjacent water protons, decreasing the spin–spin relaxation time and generating a quantifiable signal. In a significant attempt, Chung and colleagues

developed a magneto-DNA platform targeting bacterial 16S rRNAs, capable of profiling a panel of 13 bacterial species from clinical samples as diverse as urine, pleural fluid, biliary fluid, ascetic fluid, and blood. Concomitantly, reverse transcription-PCR amplification of 16S rRNA, polymeric bead capture conferred target DNA enrichment, and lastly, magnetic amplification via conjugated magnetically labeled beads to the target DNA can collectively enable a single bacterium DS. A single MNP is capable of disturbing the native chemical balance of billions of water molecules residing in the vicinity. Potential drawbacks of the magnetic bead DS comprise the manual sample preparation along with PCR analysis as a separate step from the nuclear magnetic resonance-based sensor.

### 5.1.1 Label-Free Assays in Biological Sensing

These assays of a biosensor functioning monitor the changes that occur when target analytes bind with molecular-capturing elements immobilized on a solid support or exhibit variations in the interfacial capacities or resistance. Such assays require merely a single recognition element, paving the way for a simplified assay configuration, and reduced detection time and reagent cost. This mode of recognition is particularly useful for small molecular targets that can be buried within the binding pocket of capturing element. This leaves a very low chance for a possible interaction with a detector agent that is required for a labeled assay. Yet another advantage of the label-free detection method of biosensing is the steadfast ability to quantitatively assess the molecular interactions in real time, accompanied by continuous data recording. Furthermore, the target agents can be detected in their natural form (without labeling and chemical modification) and can be preserved for further analysis. Label-free sensing for infectious diseases is made feasible through a binding event-generated distinction in optical, electrical, or mechanical signaling (Table 11). Readers are requested to see the details of referred studies in this section in the Sin et al. 2014 literature source as we are subject to the restriction of not including more than 50 references.

- **Optical transducers**: The energy converters of optical sensors are characterized by their precise involvement in optical phenomena such as changes in surface plasmons and interferometry. As also elaborated previously, surface effect in the form of SPR is the excitation of an electromagnetic wave propagating along the interfering direction of two interacting media. It is mandatory herewith that the interacting media should have dielectric constants of different signs, like those in a metal and sample buffer prepared using a specific angle of the incident light beam (Sin et al. 2014). The output signal is generated via total internal reflection (TIR), resulting in a reduced intensity of reflected light. The inclination at which resonance happens is minutely affected by the variations in refractive index, corresponding to the nanoscale-thick film formation on account of surface molecular interactions. The variations could be screened by analyzing the least shift in light intensity over a defined time lapse. A useful attempt herein used SPR-driven biosensor for the detection of *Escherichia coli* (O157:H7) and methicillin-unresponsive *Staphylococcus aureus* using T4 and B14 bacteriophages as

**Table 11** The whereabouts of label-free sensing mechanisms for infectious diseases, underlining the working principle, distinctive prospects, and the lacking aspects

| Assay configuration | Technology | Distinctions | Uncertainties |
|---|---|---|---|
| Optical transducer | Surface plasmon resonance | Real-time detection and high-throughput possibility | Diligent to sample matrix changes, cumbersome sensor surface functionalization, and bulky optical probe |
| Electrical transducer | Redox electrochemistry (amperometric)<br>Impedance spectroscopy<br>Potentiometry<br>Field-effect transistor | Simple sensor design, robust detection platform: flexible for miniaturization<br>Simple electrode design, real-time detection<br>Real-time detection and possibility of consecutive measurements on different samples<br>Real-time detection, stable sensing response, and POC-compatible detection platform | Requires redox species to increase current generation, no real-time detection, and vulnerable to sample matrix effects<br>Sensitive to sample matrix effects, bulky equipment, and no trivial data analysis<br>Bulky equipment, sensitive to sample matrix effects, cumbersome sample preparation, and mandates temperature control<br>Vulnerable to sample matrix effects, complicated sensor configuration, and acute dependence on temperature control |
| Mechanical transducer | Microcantilever<br>Quartz-crystal microbalance | Real-time detection, multiplex, and high-throughput possibility<br>Simple electrode design, real-time detection, and detection platform compatible with POC configuration | Vulnerable to sample matrix effects, mandates diligent temperature control, and bulky equipment<br>Vulnerable to sample matrix effects, diligent temperature control, and stress adjustment |

detaining organisms. This biosensor could screen 1000 cfu•ml$^{-1}$ within 20 min duration.

- Another strategy for bettering the functional accuracy of optical biosensing is backscattering interferometry (BI), working through a singular monochromatic light source (low-power He–Ne or red diode laser), optimized for focusing over a microfluidic channel. The reflected light intensity is monitored via a detector. The typical operation involves a coherent illumination of a fluid-filled channel, from the light source, generating varied interferences due to the sub-wavelength structures of the channel. Processing of output response is made via analysis of fringe pattern using a detector positioned in the backscattered direction through which changes in refractive indices could be monitored to quantify the underlying molecular binding patterns. The working configuration is optimized for screening via free solution or surface-immobilized molecular proximities, which are

generally discrete for microfluidic devices. Detection to the picoliters extent is illustrated via determining the binding constants ranging from micro- to picomoles. A select study (Kussrow & colleagues) herein demonstrated a rapid screening of human IgG from syphilis sufferers, making use of a purified recombinant treponemal antigen r17, explaining the significance for serological diagnosis in a clinical specimen.

- The label-free configurations of optical biosensors usually necessitate an accurate placement of light for coupling with the sensing region, a critical aspect for point-of-care applications. Thereby, optical sensing can be significantly advanced using the BI modulation summed up over the different sample regions. Integrated optical analysis facilitated the positioning of multiple active and passive optical components over the same substrate, allowing the configuration of multiple sensors over a single chip. A recent attempt herein comprised the design of a nanobiosensor working via light transmission in plasmonic nanoscale perforations and explicit classification of specific antibodies for multiple diverse strains of rapidly developing viruses. The optimized configuration involved a direct coupling of perpendicularly incident light using sensing assays that eased the requirements for photocoupling. Analysis of the performance on a clinical scale was estimated via detection of single-enveloped RNA viruses (vesicular stomatitis and pseudotyped Ebola strains) and squarely the largely masked DNA viruses.

### 5.1.2 Electrically Stimulated Transducers

Majorly attributed to their high sensitivity, simplicity of application, and the ability to be coupled with automated, miniaturized processing tools, the sensing mechanisms using electrical and electronic signal modulation are reasonably well demonstrated. To date, the most reported working principles of electrical biosensors for the diagnosis of infectious diseases comprise voltammetric, amperometric, impedance, and potential difference analysis. Both voltammetric and amperometric sensors function via measuring the electrical current passing through an electrolyte in terms of direct current potential difference between the two electrodes in an electrolyte, with time.

- A noted attempt in this regard is the study by Qiu and colleagues, wherein the investigators developed an immunosensor for amperometric detection of hepatitis B surface antigen. The working configuration of the probe involved a glassy carbon electrode modified with a network of cationic poly(allylamine)-fragmented ferrocene and anionic Au NPs. This combination enabled the formation of a biocompatible, stable thin film having a high specific interfacial area that minimized the loss of mediator as well as antibodies through accurate and selective adsorption to hepatitis B surface antigen.
- Electrical biosensors working through monitoring impedance changes function by resisting the current flow on the application of a sinusoidal potential difference over a wide range of frequencies, with a constant DC bias potential difference. Impedance is computed as the ratio of applied sinusoidal potential differences

(generally varies) and the concomitant current output generated across the interface.

- Multiple studies screened infectious disorders using well-characterized impedance-driven biosensors. In one of these noteworthy attempts, α-mannose carbohydrate was recognized to screen the presence of *E. coli* ORN 178, a surrogate for pathogenic strain O157:H7. The optimized configuration exhibited an LOD of $10^{-2}$ CFU (colony-forming units) per ml as its LOD. Another rigorous study by *Shafiee and accomplices* screened enriched HIV-1 and its multiple subtypes having magnetic beads functionalized with anti-Gp120 (HIV core protein) antibodies. Viral lysates were screened using impedance measurement to the ultra-low extents of (10–6 to 10–8) units at ml extents on an electrode having simplistic geometry. Both of these studies pinpointed discrete and specific recognition of a small molecular target that was possible due to nearly null interaction with the detecting probe, a major feature of labeled assay configuration. A prominent need highlighted in both cases, however, mandates that capturing elements should be capable of accommodating the analyte within a restricted binding domain.
- Another method for the detection of analytes using the potential difference measurement based on the measurement of accumulated charge using a high-impedance voltmeter with the trifling current flow is "potentiometry." A significant attempt herein demonstrated an immunosensor that worked through the potentiometric transduction ability of single-walled CNTs in combination with protein-explicit RNA aptamers. The net aim centered on the identification of variable surface glycoproteins (VSGs) of African Trypanosomes. Aptamers are fundamentally the small and synthetically made RNA/DNA segments that are capable of forming secondary or tertiary structures for binding to specific molecular targets. A major limitation curtailing the functioning of such assays is the short half-life of RNA aptamers, characterized by the receptiveness of phosphodiester backbone alongside the ribonuclease and exonuclease-bound 5′ and 3′ termini. Keeping this in mind, the study focused on the synthesis of nuclease-resistant RNA aptamer sensors having 2' F substituted cysteine and uracil nucleotides. To summarize, the functional sensing domain (VSG-specific, nuclease-resistant RNA aptamers hybridized with SWCNTs) worked well for attomolar extent detection of VSG protein in the blood.
- A fairly similar sensing mechanism involves FET, making use of a moderate current passage of a semiconductor via an externally applied electric field due to the charged particles in the vicinity. In general, the response of this sensing mechanism is accomplished in terms of threshold potential shift of field-effect structure, owing to the binding at the gate electrode. The optimized sensing assay was used for the detection of the pathogenic yeast strain, *C. albicans*, through a network of SWCNTs functionalized with monoclonal anti-*Candida* antibodies, integrated functioning as a conductor channel. The specific detection of yeast membrane antigens was conceptualized through this sensor at an LOD of 50 cfu•$ml^{-1}$.
- The explicit probes working through assessing the FET dynamics exhibited stability over a wide pH range and electrolyte concentrations, besides being

generated in large concentrations at a relatively low cost. These accurate sensitivities for the nucleocapsid protein detection by the FET platform comprising biosensor, in a complex media, equated the functioning with an ELISA protocol.

- **Mechanical transducers**: Recent advances in microelectromechanical systems (MEMS) and nanoelectromechanical systems (NEMS) have added a new realm in the working sensitivity of transducers capable of perceiving physical stimulus changes such as those in forces, motions, mechanical properties, and mass accompanied by molecular recognition. Among the different mechanical biosensors, cantilever and QCM comprise one of the most accurate probes. Mechanical bending of micro- or nanocantilever is screened through an optical readout mechanism optimized for accurate detection of stress/strain profile of the cantilever promptly after an analyte binds the probe. A notable attempt by Mader and colleagues herein functionalized a cantilever array with carbohydrate molecules to capture *E. coli*. The probe used by investigators involved Au coating of the top edges of the cantilever array functionalized with self-assembled layers of distinct mannosidase. The assembly facilitated a real-time reproducible detection of diverse *E. coli* strains including ORN 208, 178, and 206, with a sensitivity ranging well above four orders. Structural similarity of galactose with mannose paved the way for accommodating an internal reference cantilever with galactose to screen the nonspecific binding and concurrent nonspecific reactions, such as changes in pH, refractive index, or the reactions occurring on the cantilever underside.
- In a closely related study, Liu and colleagues used cantilever-driven biosensing to ascertain real-time cellular growth via monitoring the drug–cell interactions. The detected stimulus comprised the real-time growth of *S. cerevisiae* strains, YN94-1 and YN94-19, using the polymer cantilevers. The static mode of cantilever scanning exhibited an enhanced sensitivity, distinguishing the impacts of energizing the interactions between essential nutrients (completely synthetic uracil) and 5′-fluoroorotic acid in the yeast cells. In place of preferred silicon nitride cantilever probes, polymer-based probes were designed at a moderate expenditure with much lesser micromachining, encompassing a high sensitivity by tough polyimide modulus.
- The detection using piezoelectric mechanisms, involving QCM, works through assessing the dynamics of resonant frequency for oscillating quartz-crystal, in response to the alterations of surface-adsorbed mass, following the biorecognition. The discrete analyte identification was based on the internal mechanical stress generated in a piezoelectric responsive substrate, being coupled with an external potential. This stress gives rise to a varying electric field that in turn generates an acoustic wave throughout a crystal in a perpendicular orientation concerning the plate surfaces. A change in the QCM resonance frequency depends on multiple aspects, among which changes in mass, viscosity, the dielectric constant of the solution, and ionic status of the crystal–buffer solution interface are prominent. A noteworthy effort herein from Hewa and accomplices reports a QCM-based immunosensor for screening influenza A and B viral strains via conjugating Au NPs to anti-influenza A or B MAbs. The optimized configuration exhibited an

LOD of $10^3$ pfu•ml$^{-1}$ for laboratory culture preparations and clinical-grade analysis (nasal cleansers). Screening for clinical grade revealed a significant comparison of as-prepared biosensor with standard shell vial and cell culture assays, analyzed for 67 clinical specimens, overall possessing higher sensitivity and specificity than ELISA.

- Still another way to enhance the sensitivity and specificity of QCM biosensors involved the imprinting of a molecular-grade film over a QCm chip. Polymers imprinted molecularly have emerged as vital accessories in the fabrication of synthetic recognition elements. This is very well illustrated by the work of Lu and group, who demonstrated a biomimetic sensor generation via epitope imprinting for the detection of HIV-1 glycoprotein, Gp41. This glycoprotein has been demonstrated as an explicit marker for HIV infection progression and the therapeutic response *vis-a-vis* administered therapies (antibodies). Better affinity-minimized random (nonspecific) interactions and cost-effectiveness are the major benefits of epitope-driven imprinting over the traditional approach involving proteins. In another significant attempt, dopamine was employed as a functional monomer for the Gp41 detection, comprising polymerization on the QCM chip surface in the presence of a synthetic peptide analogous to 579–613 residues of Gp41. The optimized configuration enabled quantitative Gp41 sensing with 2 ng•ml$^{-1}$ LOD, an extent comparable with that of ELISA. The sensor also functioned well in the screening of Gp41 spiked human urine samples, exhibiting feasibility for point-of-care use.
- Another closely matching probe was reported by Tokonami and colleagues, wherein a molecularly imprinted polymer film comprising excessively oxidized polypyrrole (OPPy) in combination with QCM was used for direct bacterial detection. The optimized setup enabled an LOD of $10^{-3}$ CFU per ml or lesser extents within 3 min. Bacterial cavities created in OPPy film exhibited a high selectivity, enabling the distinctive recognition of the target bacterium, *Pseudomonas aeruginosa*, in a mixture containing uniformly similar morphology bacteria, comprising *Acinetobacter calcoaceticus*, *E. coli*, and *Serratia marcescens*.

As label-free sensing configurations generally do not rely on signal amplification, enhancing the detection specificity and sensitivity is majorly accomplished via an optimum selection of sensing probes and transducers. Recent advances in bioanalytical methods and characterization assays are highly aimed to design and implement improved sensing probes having significantly high sensitivity, specificity, and long-term stability. A formidable challenge limiting the clinical utility of label-free biosensors is the replication of the identification principles from laboratory-scale to commercial-grade clinical samples, such as blood, serum, and urine. This is substantially attributed to the complex matrices of clinical samples, which may result in nonspecific, random binding and generation of aberrant signals. For instance, charge-driven label-free biosensors are highly affected by even minute changes in pH, ionic strength, and vicinity temperature. Likewise, nanowires generally mandate sample desalination before the detection while microcantilevers need precise temperature regulators. The random binding-driven interactions are the

common causes of loose control, leading to a measurable signal that is not much distinct from the one generated by the targeted analyte. Several alternative methodologies are documented to moderate the matrix interference of samples. The most common of these involves the design of hydrophilic antifouling surfaces such as PEG, whose surface modification is reported as a befitting biomarker for screening the clinically significant sensitivity in the native blood serum using EIS. Another strategy uses zwitterionic polymers with a hydrophilic receptiveness and electrically neutral character, being of significant use as antifouling interfaces. It is important to recall here the observation of multiple investigations, wherein coating the probe surface with poly carboxy betaine methacrylate (a zwitterionic polymer) inhibits the random and nonspecific protein adsorption from the blood serum. This significantly improves the antibody–target-binding affinity, making it possible to screen clinical samples through a label-free detection (Sin et al. 2014).

## 6 Case Studies on Biosensor-Diagnosed Cancers

Cancers are perhaps one of the worst mortalities affecting mankind at present. Even though consistent progress in molecular characterization and diagnostic assays has collectively improvised their pathological know-how, timely treatment is badly recognized as the need of the hour. Irrespective of the organ concerned, hereditary factors and mutational onsets are the major manifestation factors of all cancers. Of late, the treatment methodologies have though bettered but only in terms of curative aspects and not much with a preventive outlook. Persistent trouble with the efficient treatment of cancers pertains to their metastasis and changing mutational consequences in the aftermath of environmental variations. For instance, lung cancer (LC) has a particular higher probability to affect smokers, whereby more rigorous information on stage-specific biomarkers is inferred. Although such events are less observed in nonsmokers, manifold reasons, including genetic factors and a higher risk of passive smoking, may accumulate viciously. Similarly, the geographical specifications affected by unprecedented mining activities are more vulnerable to deteriorating soil quality (deposition of heavy metals and radioactive elements), wherein the chances of ophthalmological and throat tumors are aggravated. Likewise, Asian and African females are more susceptible to breast cancers (BCs) than European females. For the treatment of cancers, early diagnosis is a must so that the spread to nonoriginating locations is minimized. To ensure this, it is highly urgent to screen the initial stage biomarkers through which the efficacy of treatment protocols could be modified as per the severity. Since this chapter is not attributed to cancers and their molecular aspects, a description of the emerging biosensor-mediated fastened treatment of more threatening, LC and BC is described in detail with others being briefly summarized.

## 6.1 Lung Cancer

- Prevailing as a molecular heterogeneous disorder, LC mandates a need for robust and accurate therapy for adjudging its pathological manifestation. On a histological basis, LC prevails as small-cell (SCLC) and non-small cell (NSCLC) subtypes, with ~85% of sufferers being affected by NSCLC. Notable NSCLC subtypes include lung adenocarcinoma (LAD) and lung squamous cell carcinoma (LSC). The latest research analysis predicts tobacco smoking as the leading LC cause, contributing to >80% of the global cases. Despite all forms of LC exhibiting some sort of association with tobacco smoking, the LSC and SCLC are more dependent on smoking than LAD. LAD affects nonsmokers more commonly, facing a higher vulnerability of having LC from sources other than tobacco smoke (Hackshaw et al. 1997).
- However, despite smoking being a major cause of increasing LC mortality, present treatment options are the outcomes of a paradigm shift from generalized cytotoxic therapy to personalized medicine. Indeed, treatments do assume a specific regime in light of swift genetic modifications and varying programmed death ligand-1 (PD-L1), the latter being vitally involved in escaping the targeted therapies through immune checkpoint blockers (ICBs). Table 12 pinpoints the overexpressed cell surface receptor proteins in LC, giving rise to significant intratumoral heterogeneity with distinct molecular characteristics. These proteins are authentic biomarkers of LC manifestation, with Kirsten rat sarcoma (KRAS) and epidermal growth factor receptor (EGFR) being the genes undergoing rapid mutations, noticed with greater frequency in LAD and LSC. Several serum tumor markers have been studied in LC, including carcinoembryonic antigen (CEA), CA-125, CYFR A21-21, chromogranin A, neuron-specific enolase (NSE), retinol-binding protein (RBP), α1-antitrypsin, and LSC carcinoma antigen.
- No single blood test is known for LC, and CEA is a widely studied tumor marker, reported as elevated in (0–38)% of SCLC patients and (30–65)% of those having the extensive disease. Studies estimate elevated CEA in (30–65)% of NSCLC sufferers, with a retrospective investigation of 153 NSCLC patients (entirely resected tumors) by Muley and colleagues reported lower overall survival rates for elevated CEA expressions contrary to those of normal. Both CEA and CA-125 are expressed to a lower extent in patients having the early-stage disease compared to that with metastatic manifestation. Aggressive pathology, coupled with an advanced stage at diagnosis and a high relapse propensity, is the major cause for a below-par SCLC prognosis to date. The data regarding the identification of potential biomarkers against LC are substantially retrospective with a dearth of larger prospective trials. A significant role of post-translational modifications has made proteomics an emerging platform (superseding genomics) to screen the corresponding effect on carcinogenesis.
- To date, however, 2D-gel electrophoresis is extensively used to screen the potential SCLC and NSCLC biomarkers, but the overall process is cumbersome with low sensitivity. The limited extent of available tissue is another factor

**Table 12** Overexpressed cell surface receptor proteins of lung cancer cells

| Sr. no. | Receptor noticed in specified LC cell line | Associated cellular function and possible clinical application |
|---|---|---|
| 1. | EGFR studied in A549 LC cells | Cell surface tyrosine kinase protein receptor involved in growth, division, and proliferation, and EGFR targeting chitosan NP silenced the mitotic checkpoint, Mad2, and induced cell death |
| 2. | CD44, acutely expressed in NSCLC tumors and hyaluronic acid, noticed in A549 and SK-LU-1 LC cells | Targeted for (30–60)% tumor growth inhibition, promotes macrophage repolarization and activates p53-mediated apoptosis |
| 3. | Transferrin, type II transmembrane glycoprotein involved in cellular Fe transport and growth regulation, noted in H460 human LC cells, and expressed in 76% LAD and 96% SCLC cases | Low use and limited therapeutic success, but acts significantly in the blood–brain barrier (BBB) |
| 4. | Folate receptor alpha (FRA) | 74% LADC and 13% SCLC overexpress FRA, targeted via polyspermine NPs conjugated with folic acid, FA-conjugated chitosan graft PEI-mediated small hairpin delivery to cancer cells, induced stable shRNA condensation, and DNAse protection |
| 5. | Integrins noted in H1299 cells | α5, β1, and αvβ3 are common in all LCs, and αvβ3 is used for improved diagnosis involving PEG-grafted nanoparticle surfaces<br>Induces EGFP gene silencing in H1299 cells, and PLGA NP promoted VEGF inhibition in a mouse model |

Note: These entities are the crucial riders of implicit identification of tumor cells and their characteristic expression is used as a diagnostic measure for tumor cells

affecting the identification of potential LC. Thereby, screening the optimum serum biomarkers could be of much clinical significance, so plasma proteome analysis is a complex undertaking, having witnessed significant advances. Using multidimensional chromatography and mass spectrometry (MS) analysis, as many as 1175 LC implicit plasma proteins have been identified. Besides electrophoresis and MS, other notable methods for LC detection developed in the last decade include computed tomography (CT), chest radiograph (CRG), magnetic resonance imaging (MRI), positron emission tomography (PET), and biopsy. Quite disappointedly, all these methods suffer from poor sensitivity besides being expensive and inducing physical/chemical risks. As a result, they could not enable early-stage LC diagnosis. Although subsequent methodologies of ELISA and PCR did exhibit high sensitivity besides having less invasive procedures, the detection progress is slow, along with an expensive consumption of reagents.

- Of late, several robust mechanisms have emerged to steadfast the LC diagnosis using the fluid mechanics dynamics; visible as electrochemical, optical, microfluidics, and microarray-based biosensors (refer Yang et al. 2019 for details). Compared to the conventional methods, the novel sensing mechanisms in these biosensors have better sensitivity, selectivity, and stability besides being a moderate cost and relatively simpler operational modes. A common factor in the emerging progress of these biosensors has been the emergence of multifunctional and size-varied energy possessing NMs. The functional diversity of NMs manifested from their high SA, multiple interactions at the same instant, and size-driven energy modulation is the reason for improved detection limits and reduced detection times in these biosensors. For accurate screening of LC, it is pertinent to have a sound knowledge of various early-stage LC biomarkers that are described next.
- In most general words, markers are the biochemical parameters that can be measured in the plasma or other body fluids isolated from suspected cancer patients, commonly exhibiting a susceptibility of being the prerequisite for serological tumor marker diagnosis. The typical expression of tumor markers at a given instant is determined by several tumor parameters such as size, mass, expression extent, synthesis ability, and catabolic and excretion rates besides the tumor blood supply. Variation in any of these factors is likely to aggravate the complexity, leading to enhanced sensitivity of tumor marker detection. In the last decade, DNA methylation has emerged as a prominent sensitive and specific epigenetic event that has been reported for accurate screening of LC pathological changes. It is significant to mention here that the expression of the abovementioned LC markers may have an association with smoking history, ethnicity, and genetic factors but such dependence is merely quantitative. So, the desired need is to have accurate and sensitive molecular characterization tools that can screen even a minute expression of these. The following points shed light on some prominent markers among these. For cited literature in the subsequent subsections, readers are suggested to refer a 2019 review article by Yang and associates, featured in the *Journal of Biosensors and Bioelectronics*.
- **Neuron-specific enolase**: With a 39 kDa molecular weight, neuron-specific enolase (NSA) comprises two matching polypeptide chains (α/γ or γ/γ). NSE is essentially glycolytic enzyme enolase that substantially prevails in peripheral neurons besides central and neuroendocrine tissues. The occurrence of NSE in SCLC was reported first in the 1980s, with all sufferers showing a high NSE expression. NSE release may occur in erythrocytes and blood platelets with a concentration variation that is independent of age, sex, and smoking history. In 2003, it was reported that NSE also served as an important NSCLC marker, being recognized as a survival indicator irrespective of erstwhile prognostic factors.
- **Cytokeratin 19 fragment**: A 36 kD cytokeratin 19 fragment, **cytokeratin 19 fragment** (CYFRA 21-1) reside in the epithelial cell (including bronchus epithelium) cytoskeleton and is the only source of CYFRA 21-1. CYFRA 21-1 has been screened as exclusively expressed in lung tissues and is the most sensitive NSCLC marker (exclusively in LSC). Studies based on multivariate

analyses unanimously reveal CYFRA 21-1 as an important marker for screening the NSCLC prognosis, treatment efficacy, and recurrence.

- **Carcinoembryonic antigen**: With a molecular weight of ~180 kDa, carcinoembryonic antigen (CEA) is a cell-membrane-associated glycoprotein group, expressing to the highest extent in the fetus serum of 22nd pregnancy week (not in a healthy adult). The importance of CEA as a tumor biomarker is not limited to LC, and it is also a keen identifier in the colon, gastric, pancreatic, breast, and ovarian cancers. The normal CEA range for adult nonsmokers and smokers is $<2.5$ ng•ml$^{-1}$ and 5 ng•ml$^{-1}$, respectively. A rise above these concentrations signifies the recurrence or progression of LC. A high CEA concentration in the exhaled air condensate is perhaps the best predictive aspect of early NSCLC. The screening of lung malignancies is usually made via combined detection of CEA and CYFRA (a 21-1 extent).
- **Squamous cell carcinoma antigen**: This is a 48 kDa protein, associated with the serine protease inhibitor family. The squamous cell carcinoma antigen (SCCA) prevails in squamous cells and is referred to as a structural protein, indicating a differentiation cancer stage. Variations in SCCA extents are the familiar indicators of lung squamous carcinomas, cervix, uteri, head and neck regions, and esophagus. Varied SCCA expression levels inferred different LC stages; an NSCLC monitoring by SCCA mandates its screening in combination with CYFRA21-1.
- **Carcinoma antigen 125 (CA125)**: This is a 200 kDa membrane mucin-like glycoprotein and prevails as a prominent BC, ovarian cancer, and LC biomarker. Among the different LC forms, adenocarcinoma and large cell LC exhibit significantly high carcinoma antigen 125 expressions. Thus, CA125 can be used as a predictive marker for evaluating the prognosis, treatment accuracy, and early treatment response in NSCLC.
- **Tissue polypeptide antigen (TPA)**: This is a cytoskeleton protein having 20 kDa, first noticed as being released from proliferating cells originating from ER and cell membrane. TPA can independently exhibit a significant LC prognosis.
- **Others**: Besides the abovementioned LC markers, some other markers used to screen the LC include carbohydrate antigen 19-9, tumor M2-pyruvate kinase (M2-PK), progastrin-releasing peptide (ProGRP), vascular endothelial growth factor (VEGF), serum human epididymis protein-4 (HE4), cancer-testis antigen (NY-ESO-1), clinical application markers such as CRP and lactate dehydrogenase (LDH). Besides these, a range of newly discovered markers for LC includes exosomal microRNA, navitoclax, TFIIB-related factor 2, DR-70, Glasgow prognostic source, serum microRNA 21, and serum-microRNA 204, serum microRNA-100, apurinic/apyrimidinic endonuclease 1, and urokinase plasminogen activator.
- Erstwhile of the above serum markers, those belonging to bronchoalveolar lavage fluid (e.g., ubiquitin-specific peptidase 8, chitinase 3-like 1, glutathione-s-transferase P1) and breath markers (e.g., 2,4-dimethylheptane, 2-methyl-1-pentene and 4-methyloctane) are also the prominent LC markers.

### 6.1.1 Biosensors for Lung Tumor Biomarker Detection

Updates corresponding to this section are almost summarized from the 2019 review article by Yang and associates, featured in the *Journal of Biosensors and Bioelectronics*. Thereby, readers are suggested to refer to the details of non-listed references from this literature source.

1. **Neuron-specific enolase detection**: Possessing a significant specificity toward NSCLC, the NSE screening has been made using electrochemical, optical, and surface-enhanced Raman scattering (SERS)-driven biosensors. A high sensitivity, rapidity, and simplicity of operation are responsible for a wider application of electrochemical and optical analytical methods. Several NMs and biocompatible polymers are being applied to design biosensors to achieve stable and greater signal amplification. The following sections describe the recently reported NSE sensing configurations using electrochemical, optical, and feasible NMs.

### 6.1.2 Electrochemical Biosensors

The biosensors working on an electrochemical basis for NSE detection can be labeled or label-free in configurations and may use NMs or polymers for functioning through a sensitive platform. The labeled configurations usually amplify the detection signal as per the modified platform and labeled tag. Contrary to this, the label-free version merely requires a modified platform for signal amplification. In a 2017 attempt, Wei and his team configured the electrochemical biosensors for NSE detection using Au NPs and reduced graphene oxide composites-driven signal intensification. The Au NPs-reduced GO enabled the enhanced binding sites for modified Ab, thereby enhancing the detection signal sensitivity. The designed sensor configuration exhibited a linear relationship from (0.1 to 2000) ng•ml$^{-1}$ with 0.05 ng•ml$^{-1}$ LOD. To further enhance the DS, the investigators used porous 3D graphene–starch architecture as a sensing platform with Au NPs-coated ordered mesoporous carbon–silica (OMCSi–Au) as a target. The introduced modifications enabled a higher surface area to capture the target proteins alongside accelerated electron transfer, resulting in a 0.008 pg•ml$^{-1}$ LOD.

The simplified configurations of the label-free assay have been the reason for their greater use in NSE detection with comparatively higher stability. In a 2018 attempt, Zhang and his team used a 3D macroporous reduced GO-polyaniline film-engineered Au electrode for NSE detection. The rGO-PANI composite exhibited a larger specific surface and high electron conductivity with manifold electroactive sites. To overcome the vulnerable stability of sensing interactions, the molecular imprint (MIP) served as artificial receptors for implicit target molecule recognition. Another configuration was reported by Wang and colleagues, who used a 3D structured Au nanoarray as amplification moiety and 1-(3-mercaptopropyl)-3-vinyl-imidazolium tetrafluoroborate as the molecularly imprinted film, on the removal of NSE templates. The NSE detection response exhibited a linear range from (0.01 to 1) ng•ml$^{-1}$ with an LOD of 2.6 pg•ml$^{-1}$ and $<5\%$ relative standard deviations (RSDs). Another study aimed at NSE detection in serum samples used a wireless POC testing system constituted of Au NPs nanocomposites, thionine, and

amino-functional graphene as a microfluidic paper-based analytical device and a smartphone as a signal receiver for NSE detection. The sensor exhibited a low LOD along with a wide detection assortment in serum samples that argued well for clinical applications.

### 6.1.3 Optical Biosensors

As opposed to electrochemical mechanisms, the optical biosensors exhibit a low interference with the detection system, commonly used to detect biological targets. Amalgamating electrochemical and optical detection mechanisms, the photo-electrochemical (PEC) analytical methods are well compatible with a more sensitive NSE detection. To elucidate this, Lin and colleagues designed an enzyme-free multicolor immunosensor for NSE detection. The sensor utilized $Cu^{+2}$-modified carbon nitride nanosheets as catalytic substrate with Au nanobiopyramid as a chromogenic substrate for multicolor display when $TMB^{2+}$ etches Au nano-biopyramid and develops multicolor patterns.

### 6.1.4 Other Biosensor Configurations

The SERS has been viciously reported for immunosensing purposes, with a modifiable surface for biomolecule conjugation. A potential attempt in this regard by Gao and colleagues prepared nanostar Au morphology that was then conjugated with malachite green isothiocyanate (MGI) after being functionalized with silica NPs (Si NPs). The assembly was used as SERS probes via applying disposable paper-based lateral flow strip as a platform and Au nanostars coupled with MGI-Si NPs as detection probes. The biosensor exhibited a wide detection range of (1–50,000) ng•ml$^{-1}$ and 0.86 ng•ml$^{-1}$ LOD in diluted blood plasma samples.

2. **Cytokeratin 19 fragment 21-1 detection**: Recognized as the most effective NSCLC biomarker, CYFRA21-1 exhibits high sensitivity and specificity. Disappointingly, very few studies are reported on CYFRA21-1 detection, and the necessary aspects of electrochemical and optical biosensors are discussed next.

### 6.1.5 Electrochemical Biosensors

The labeled configurations are rather more common for CYFRA21-1 detection. In one such attempt, Zeng and colleagues developed a labeled biosensor using 3D graphene oxide, chitosan, and glutaraldehyde as platform and Ab-modified nanocomposites (prepared using $-NH_2$ functionalization of MWCNTs), thionine, Au NPs, and HRP-labeled Abs as a label. Another attempt by Gao and associates reported an immunosensor using Si nanowire tunneling FET (optimized by CMOS compatibility). The bottom-up approach of tunneling FET immunoassay can detect CYFRA21-1 extent as low as 0.65 fg•ml$^{-1}$. Other than frequently used NMs, studies have used rare earth metal hydroxides and hydrogel assemblies for CYFRA21-1 detection. A study by Tiwari and colleagues has shown that lanthanum hydroxide ($La(OH)_3$) NPs were immobilized on an indium-tin-oxide glass substrate as a signal amplification platform due to a larger number of bioactive sites, high electron transfer mobility, and electrocatalytic response. The developed immunosensor

exhibited high sensitivity for CYFRA21-1 detection with 5 min response time. Another study by Wang and Ma reported enhanced DS of amperometric biosensors using a conductive hydrogel. The probe involved functionalized cross-linked phytic acid (containing Au NPs) for CYFRA21-1 detection, resulting in unmatchable redox activity and electron transfer ability, developing a linear response within (50 fg•ml$^{-1}$ to 100 ng•ml$^{-1}$, with an LOD of 38 fg•ml$^{-1}$). Readers are requested to find the details of the above-referred studies in the 2019 *Journal of Biosensors and Bioelectronics* contribution by Yang and associates.

### 6.1.6 Optical Biosensors

Low interference, weak background nature, and high sensitivity are the features of an optical immunoassay for CYFRA21-1 detection. For instance, Yu and colleagues, through their 2019 research attempt, developed a novel PEC biosensor having biofunctional polydopamine/tungsten oxide NPs as a sensing platform. Besides these, the SPR-based biosensors relied on light-stimulated electronic oscillations at the changeable metal film surface, which can be as such used for CYFRA21-1 detection. Another advantage of SPR biosensors is their high stability and sensitivity for plasma screening. As a paradigm shift, Chiu and colleagues in 2018 fabricated an ultrasensitive SPR immunosensor based on cystamine as a linker on a GO sheet immobilized on the chip surface. The biosensor exhibited significant stability and sensitivity and revealed kinetically fitted values in the human plasma. Owing to legal restrictions, the referred studies could be traced to the 2019 *Journal of Biosensors and Bioelectronics* contribution of Yang and associates.

3. **Carcinoembryonic antigen detection**: Noted as a broad-spectrum tumor marker, screening the CEA expression is viciously recognized as an implicit signature for diagnosis, prognosis, and monitoring the different cancers. Compared to other biomarkers, a higher molecular weight of CEA enables a larger number of functional groups for immobilization and modification. This has been the reason for a range of biosensors being available for CEA detection, including electrochemical, optical, SPR based, SERS-based, aptasensors, and others. The following sections discuss the recent progress in biosensors design for CEA detection.

### 6.1.7 Electrochemical Biosensors

The recent surge in electrochemical biosensor development for CEA detection is substantially due to their fast response, stability, high sensitivity, and specificity. Apart from this, the attainment of high signal amplification has been made possible by the incorporation of different NMs, including noble metal NMs, carbon NMs, and polymeric NMs. Among the electrochemical options, much interest has been in labeled configurations, wherein Lee and colleagues 2017 designed a sandwich biosensor using Ag NPs in combination with rGO (AgNPs-rGO) for modifying the SPCE as sensing matrix and HRP-labeled Ab as a tag for CEA detection. The sensor exhibited a (0.05–0.50) μg•ml$^{-1}$ calibration with 35 ng•ml$^{-1}$ as LOD. The preferential benefits of using NMs in place of enzymes comprise remarkable stability, better sensitivity, and improved modification. As per Feng and colleagues, the

Au NPs dotted thionine-functionalized CNTs and Au NPs-doped PAN-coated CNTs are used as sensing platforms and signal labels, respectively. The configuration exhibited significant sensitivity toward CEA detection due to CNTs' and Au NPs' dual-signal amplification. In another study, Wang and colleagues attempted the CEA detection using Ag NPs modified with molybdenum disulfide-coated $Fe_3O_4$ NPs ($Ag/MoS_2@Fe_3O_4$) as a label and similar to the ELISA method. The investigators selected Ab-conjugated $Ag/MoS_2@Fe_3O_4$ via ELISA, which resulted in the conduct of detection on magnetic GCE with the assistance of a chosen label. The configuration exhibited a 0.03 pg•ml$^{-1}$ as LOD, much lower than contemporary attempts of similar times. The emergence of systematic ligand evolution through exponential enrichment paved the way for choosing aptamers to specifically recognize the high-affinity targets, leading to enhanced specificity and stability besides simpler synthesis and modification. An exclusive attempt in this reference used aptasensor based on sandwich tactics for a sensitive CEA detection. The CEA aptamer 2 (CEAapt2), dendritic Pt@Au nanowires (Pt@AuNWs), and toluidine blue together formed Pt@AuNWs-CEAapt2-Tb bioconjugate as a signal tag while Au-functionalized GCE immobilized with CEAapt1 was used as sensing probe for capturing the CEA in a sandwich-type configuration. The configuration demonstrated a good linear response to the (0.001–80) ng•ml$^{-1}$ CEA range with 0.31 pg•ml$^{-1}$ LOD.

Among the notable attempts toward CEA detecting label-free electrochemical biosensors, the one by Shao and associates used a label-free immunoassay based on Prussian blue nanocubes-loaded molybdenum-disulfide nanocomposites ($MoS_2$-PBNCs) as a sensing platform. This platform displayed splendid electrocatalytic ability that could be applied for CEA recognition in human serum with a good resolution. The advantages offered by polymeric NMs have been incentives to improve the CEA detection resolution, wherein significant redox activity, easier modification, adequate biocompatibility, and stability are some prominent traits. Making use of these characteristics, Ji and colleagues in their 2015 work used Au NPs-doped polydopamine to modify carbon-encapsulated $Fe_3O_4$ NPs embedded in porous graphitic carbon NCs ($Fe_3O_4$@C@PGC) as CEA detection probe, with $<$0.33 pg•ml$^{-1}$ LOD and $<$3% RSD. A detailed description could be traced to the 2017 contributions of Ji and Shao research groups. Based on relative polymers doping, Li and colleagues used Au-F127 nanospheres as an electrochemical interface for CEA detection and observed 0.5 pg•ml$^{-1}$ LOD over a (0.001–10) ng•ml$^{-1}$ calibration range. Owing to legal restrictions, the referred studies could be traced to the 2019 *Journal of Biosensors and Bioelectronics* contribution of Yang and associates.

### 6.1.8 Optical Biosensors

Among the noted attempts of optically activated biosensors for CEA detection, the 2018 study by Danesh and group used a fluorescent aptasensor based on 5,6,7-trimethyl-1,8-napthyridin-2-amine (ATMND) as a dye and a three-way junction pocket as fluorescent quenching probe. The CEA aptamer conjugate of the three-way junction pocket was stripped in CEA presence. The sensor was very effective in CEA detection with significant recovery from human serum. In another potential

effort, Wang and colleagues aimed for high sensitivity and used upconversion NPs (UNPs) to fabricate a FRET-driven immunosensor using fluorescein isothiocyanate (FITC)-labeled primary Ab ($Ab_1$) and Au NPs-labeled secondary Ab ($Ab_2$) to form Au NPs-CEA-FITC-Ab complex in the presence of CEA. The sensor displayed a comparatively more universal and easy-to-use analytical view due to manifested colored and fluorescence-sensitive dual readout. More recently, black phosphorous as an emerging 2D-layered material has been studied for thickness-dependent direct band gap, high-charge carrier mobility, characteristic current on/off ratios, and, most significantly, angle-dependent transport anisotropy for an accurate CEA detection. Another worthwhile attempt by Peng and colleagues used Au NPs doped with a few layers of black phosphorous (BP-Au) as a platform for CEA detection inspired by splendid catalytic activity and low activation energy of BP-Au. On initial optimization, the SERS as a spectroscopic tool for CEA detection maximized the benefits of high sensitivity, characteristic spectroscopic fingerprint, along with nondestructive data acquisition. Using such incentives, Lin and colleagues developed a simple method for CEA detection in human serum based on Ab-adsorbed Au and γ-$Fe_2O_3$@Au NPs as a probe for a (1–50) ng•$ml^{-1}$ linear range with 0.1 ng•$ml^{-1}$ LOD. The designed configuration exhibited efficient photoirradiation conversion to an electrical signal, high sensitivity, low cost, and simple instrumentation. In this reference, one study by Wu and colleagues used $Zn_{0.1}$ $Cd_{0.9}S$-hybridized g-$C_3N_4$ functionalized indium-tin-oxide slices as a photoactive matrix for CEA detection. The synergistic influence of g-$C_3N_4$ and NCs resulted in a high-intensity response and ultralow LOD. A 2015 attempt by Peng and colleagues reasoned the high sensitivity and wide dynamic signal response range for developing electrochemiluminescence biosensors. The developed biosensors comprised GO/carboxylated MWCNTs/Au/CeO NPs as sensing matrix for CEA detection. This platform manifested a good electron transfer, stability, and high specific surface area NCs, ensuring accurate CEA detection to ultralow LOD extent. Owing to legal restrictions, the referred studies could be traced to the 2019 *Journal of Biosensors and Bioelectronics* contribution of Yang and associates.

### 6.1.9 Other Biosensors

Other than electrochemical and optical mechanisms, several biosensors have been reported for CEA detection. For instance, Chu and colleagues demonstrated a FET-driven rapid and movable probe, having Ab-coated AlGaN/GaN high electron mobility transistors as detection matrix. The configuration exhibited good stability and selectivity in human serum. In another potential effort, Liu and colleagues used an ultrasensitive lateral flow immunoassay accommodating MNPs as a CEA determination probe. Yet another significant attempt toward POC CEA detection in human serum by Jiang and colleagues used glucose oxidase (GOx)-entrapped Au hollow microspheres (AuHMs) as a signal label, working through a quantitative pH determination. With the GOx-AuHM labeling, the sensor accurately tracked the CEA over a wide linear range, with 0.062 ng•$ml^{-1}$ LOD.

4. **Squamous cell carcinoma antigen screening**: Aggravated SCCA activity remains a noted hallmark of LC, cervical squamous cell carcinoma, and hepatocellular carcinoma, making it hereby very urgent to develop sensitive and robust recognition assays. The advances in electrochemical and optical biosensors along with the emerging use of NMs are briefed next.

### 6.1.10 Electrochemical Biosensors

The shape and size-dependent physical and chemical properties of NMs have been the authentic assets for their enzyme equivalent functioning in the efficient design of electrochemical biosensors for SCCA detection. Making use of such attributes, Wang and colleagues prepared the composites of Au@Ag@Au NPs as enzyme mimetic tags in an attempt to attain better stability and replace the $H_2O_2$ catalytic response. After the immune response, the biosensor exhibited 0.18 pg•ml$^{-1}$ LOD and a 0.5 pg•ml$^{-1}$ to 40 ng•ml$^{-1}$ wide detection range for SCCA. With an intent to maximize the stability and sensitivity, Liu and colleagues made a range of NCs using graphene having β-cyclodextrin-loaded graphene sheet (CD-GS) as a sensing platform owing to high supramolecular recognition of CD with GS (prevents GS stacking besides improving its biocompatibility) and the ternary hollow Pt/Pd-Cu nanocube-fastened 3D graphene scaffold as a receptive label. Using this sensing platform and sensitive label, the investigators fabricated a controlled release system-driven labeled biosensor to detect SCCA. In furtherance, Ma and colleagues fabricated a sandwich-like biosensor having β-cyclodextrin-functionalized Au-anchored $SiO_2$ (CD-Au@$SiO_2$) as a label and primary antibody, $Ab_1$ restricted Au electrode as a sensing probe for an ultrasensitive SCCA screening. The investigators used 1-methyl-1H-benzimidazole-functionalized mesoporous $SiO_2$ to encapsulate methylene blue (MB) with CD-Au@$SiO_2$ as a regulator and finally entrap the arbitrarily modified secondary antibody, $Ab_2$. MB was released from MBI-MS at $<7$ pH, wherein the SCCA and functional $Ab_2$ participated in an immunological reaction. The detection was pursued distinctly within (0.001–20) ng•ml$^{-1}$ with 0.25 pg•ml$^{-1}$ LOD. Owing to legal restrictions, the referred studies could be traced to the 2019 *Journal of Biosensors and Bioelectronics* contribution of Yang and associates.

For label-free electrochemical sensing of SCCA, a 2016 study by Li and group used icosahedral Au NCs as carriers for rapid SCCA detection that were subsequently integrated to Au NPs-anchored GCE through 1,3-di-(3-mercaptopropyl)-imidazolium bromide (DMIB). The sensor exhibited a good response with 12.6 pg•ml$^{-1}$ as LOD. A further significant attempt by Gao and associates toward fabricating a label-free electrochemical biosensor for screening SCCA used $Fe_3O_4$ as a nanocontainer and aminated polystyrene microspheres (APSM) as a molecular gate to achieve toluidine blue encapsulation. The optimized configuration exhibited an amplified signal as inferred through square wave voltammetry analysis for released TB, giving a correlated SCCA quantity.

### 6.1.11 Optical Biosensors

The recent past has witnessed significant developments in the development of photoelectric immunosensors using composite-grade NPs owing to their exceptional

chemical inertness and robust action mechanism. In one such noted attempt, Wu and colleagues designed magnetic GO ($Fe_3O_4$@GO) as a sensing matrix and Au NPs/carbon nitride ($C_3N_4$) as a signal label to form an "in-electrode"-type electrochemical biosensor for SCCA detection. The $Fe_3O_4$@GO enabled an effective capture of the primary antibody, $Ab_1$, to amplify the recognition signal while Au NPs/carbon nitride ($C_3N_4$) enhanced the secondary antibody, $Ab_2$, loading capacity besides providing a high conductivity for an improved ECL intensity. The (0.001–10) ng•ml$^{-1}$ detection range and 0.4 pg•ml$^{-1}$ LOD argued well for efficient SCCA detection by the prepared immunosensor. Using the label-free PEC approach, Ye and colleagues used $MoSe_2$ nanosheets with photocurrent intensity and hollow Au nanospheres (HGNs) as a sensing platform for latent SCCA detection. Because of the HGNs-$MoSe_2$, NC-enhanced photocurrent intensity and improved binding site activity, the fabricated sensor exhibited a 0.21 pg•ml$^{-1}$ LOD for SCCA. Moving on to POC devices, Lin and colleagues 2018 fabricated a naked eye colorimetric immunoassay for SCCA detection using Au nanobiopyramid-functionalized Ag nanorods (Au NBP@Ag) as carriers. The carriers were designed to modify the secondary antibody, $Ab_2$, and amplify the detection signal. The sensor exhibited a good linear relationship (2.5–105) ng•ml$^{-1}$ with 2.5 ng•ml$^{-1}$ LOD (for naked eye) and 0.85 ng•ml$^{-1}$ (for spectrometer). Owing to legal restrictions, the referred studies could be traced to the 2019 *Journal of Biosensors and Bioelectronics* contribution of Yang and associates.

### 6.1.12 Carcinoma Antigen 125 Detection

A shift or change in carcinoma antigen 125 (CA 125) concentration reveals the stage of LC, the reason for which investigators are interested to detect <35 U•ml$^{-1}$ extent of this biomarker. The progress regarding sensing attempts made for CA 125 detection is described next.

### 6.1.13 Electrochemical Biosensors

The simple, easy-to-operate, highly sensitive, and rapid detection procedures of electrochemical immunoassays have been the basis for manifold electrochemical biosensors being reported for CA125 detection. In one of these past decade attempts, Torati and colleagues reported one-step electrochemical CA125 detection using layered Au nanostructures as a platform that on being coupled to CA125 binding sites generated a significant electron transfer to amplify the detection signal. The analysis of this sensor using differential pulse voltammetry revealed a splendid linear response with 5.5 U•ml$^{-1}$ LOD. A modification in the sensing platform via incorporating polymer–metal complex, PANI in conjugation with Au NPs and catalytic NMs was attempted by Zheng and colleagues, who developed an amperometric immunosensor for CA125 detection. The analytical response was obtained in the (0.01–5000) U•ml$^{-1}$ range with 4.4 mU•ml$^{-1}$ LOD. Still another study developed a microflow biosensor using thin film-modified Au array microelectrodes prepared by electrocatalyzed polymerization of anthranilic acid to IDAs as a sensing platform. The platform was used to ascertain the progress of immunoreactions through

electrochemical impedance spectroscopy (EIS), whereby the complex detection transformation was simplified.

### 6.1.14 Optical Biosensors

The first major last decade attempt using optical biosensors-mediated CA125 detection was the investigation of Al-ogaidi and colleagues, who designed a CL resonance energy transfer biosensor using graphene quantum dots (GQDs) as a detection platform and HRP-labeled secondary Ab as the probe. The immunosensor retrieved an energy transfer between reactive oxygen species (generation of HRP-$Ab_2$ catalyzed $H_2O_2$) and luminal on the formation of CA125-immobilized $Ab_1$ and HRP-$Ab_2$ complex. The designed configuration exhibited a (0.1–600) U•$ml^{-1}$ detection range and a 0.05 U•$ml^{-1}$ LOD. In fluorescence immunoassays, GQDs and carbon dots are preferred as immune tags for enhanced DS, resulting from the adequate and uniform surface modification, biocompatibility, and photobleaching stability. A potential attempt by Tsai and colleagues focused on the fabrication of GQDs labeled with $Ab_1$ as a sensing platform and fluorescent NPs conjugated with $Ab_2$ as a detection probe. Another significant attempt by Hosu and accomplices proposed a colorimetric smartphone-driven immunoassay working through detection of the grayscale index of ($Ab_1$-Ca125-$Ab_2$@Au)-sandwiched immunocomplex, stained by Ag, for robust CA125 detection. Owing to legal restrictions, the referred studies could be traced to the 2019 *Journal of Biosensors and Bioelectronics* contribution of Yang and associates.

### 6.1.15 Other Biosensors

Among the noted attempts based on lab-on-a-chip and POC, CA125 detection is the study by Nunna and colleagues, who fabricated a biosensor working via microfluidic flow conditions for monitoring the capacitive sensor. Another effort in this direction was made by Mansouri and associates, who introduced a flexible FET-type aptasensor using MWCNTs/rGO as a CA125 sensing platform. Another significant contribution was the study of Ju and colleagues, who reported an EDFM-DM sensor using Ag NPs as a fluorescent-devoid CA125 detection probe. Both (this and previous) biosensors exhibited a good linear range of response with ultralow LOD toward CA125 detection in clinical samples and biological fluids. Referred studies could be traced to the 2019 review article by Yang and associates featured in the *Journal of Biosensors and Bioelectronics* since the references as per legal bindings for the present compilation cannot exceed 50.

5. **Tissue polypeptide antigen**: TPA shows abnormal activity in rapid increments in malignant tumors as there is a rise in TPA expression amidst mitosis (cell division of increasing cell populations). This is the reason for considering TPA as an important factor in the auxiliary diagnosis, the basis on which TPA sensing is done to monitor LC prevalence. The first notable effort in this regard is the study of Wang and colleagues, who reported a sandwich configuration of the biosensor using graphene sheets as a signal transfer platform and Pd–Pt bimetallic NCs-labeled Ab as a probe for $H_2O_2$ catalysis. The developed sensor showed a

DS in the range of pg•ml$^{-1}$. Interestingly, Pd–Pt combines exhibited superior catalytic efficacy compared with any single NC besides exhibiting higher stability than enzyme-tagged $Ab_2$. Another study by Wang and colleagues used multifunctional graphene NCs (Au@MGN) through Au NPs absorption as nano-$Fe_3O_4$@GO with significant electrochemical property and biocompatibility. Subsequently, the investigators fabricated an electrochemical immunosensor using Au NPs-modified GCE as a platform and Au@MGN as a TPA detection probe. The sensor exhibited a wide calibration range (from 10 fg•ml$^{-1}$ to 100 ng•ml$^{-1}$) and 7.5 fg•ml$^{-1}$ as LOD. The same research group of 2016 fabricated an immunoassay using 3D-ordered macroporous Au films as matrix and bifunctional, nano-raspberries as labels for TPA detection. It was ascertained that these bifunctional, nano-raspberries exhibited a higher peak current reduction (compared with Au and Pt NPs) due to remarkable electron transfer ability and intense catalytic activity toward $H_2O_2$. Referred studies could be traced to the 2019 review article by Yang and associates featured in the *Journal of Biosensors and Bioelectronics*.

### 6.1.16 Breast Cancer

Recognized as the most fatal disorder among females, BC contributes to ~23% of global cancer cases globally, typically accounting for the second largest extent deaths among all cancer-related deaths (DeSantis et al. 2014). The scenario is more precarious in developing and underdeveloping economies, where lacking clinical facilities and missing awareness aggravate the treatment recourses. The involvement of various factors in BC onset is the reason for diversified symptoms depending on the specific size and type of tumor. Accordingly, the treatment varies and requires timid diagnosis, efficient remedial procedures, and post-medication cautions to nullify a recurrence. Predicted as being carried by every one in eight US women with staggering 39,620 deaths reported in 2013 itself, the BC menace has been dreadful (DeSantis et al. 2014). Over the last few decades, BC treatments have seen consistent progress, facilitating prompt recognition with reduced mortality. It is pertinent to mention here that BC classification can be made using morphological or immunohistochemical markers.

Conventional procedures for BC diagnosis include mammography, biopsy, MRI, sonography, molecular breast imaging, thermography, etc. (Table 13). These methods are steadfast and can screen (80–90)% tumors. Besides these methods, biomarker expressions are also screened such as ELISA, radioimmunoassay, and immunohistochemistry. Despite being efficient and enjoying a majority level of patient confidence, all these methods are associated with certain limitations, presumably due to unpredictable mutational reasons that remain nonprogrammed in the diagnostic probes. False-positive (negative) results obscure the situation through error-prone analysis and needless biopsies. So, present research attempts to counter BC mortality are dedicated to the expansion of detection methods that are highly sensitive, noninvasive, and amenable for POC diagnosis. The salient attributes of biosensors include their sensitivity, specificity, and cost-effectiveness besides a quick response for the shortest appraisal of physiological fluids (including blood,

**Table 13** Conventional techniques for breast cancer diagnosis with concurrent concerns

| Technique | Limitations |
|---|---|
| Mammography | Low sensitivity and specificity<br>Sensitivity falls on rising tissue density<br>Unable to ascertain tumor in dense and rigid tissue at the initial stage<br>Frequent false-positive outcomes<br>Low-energy X-rays could cause mutations<br>Disintegration of tumor tissue amidst analysis may result in metastasis |
| Biopsy | May untrace the tumor cells<br>Needless and elaborate surgery<br>May result in metastasis<br>Needs talented expertise<br>Suited as a later-stage confirmation<br>Expensive |
| MRI | Unable to detect ductal and lobular carcinoma<br>Costly |
| Sonography | Requires expertise for real-time monitoring<br>Less sensitive and relatively expensive |
| Fluorescence in situ hybridization (FISH) | Provides semiquantitative results<br>Separates the sufferers as biomarker positive or negative groups |
| ELISA | Elaborate<br>Costly<br>Unresponsive to low-level expression markers<br>Intrinsic analyte color may give false results |
| Radioimmunoassay (RIA) | Radioactivity risk<br>Complex procedure<br>Elaborate<br>Needs skilled manpower |
| Immunohistochemistry (IHC) | Complicated technique<br>Time-consuming<br>Requires skilled manpower |

serum, urine, saliva, milk, etc.) in a non-patient-sensitizing manner. For the subsequent sections about BC, readers are suggested to refer the 2017 *Biosensors and Bioelectronics* contribution of Mittal and colleagues and the 2019 Elsevier book Chapter 3 by Pereira and accomplices.

### 6.1.17 Need for Biosensor-Facilitated Breast Cancer Diagnosis

The biosensor for BC diagnosis works through a distinctive screening of biomarkers (to be screened target molecule) using the coordinative functioning of bioreceptors (recognizing element) and a compatible biotransducer. The biomarkers corresponding to BC are depicted in Fig. 21, distinguished into stage and biomolecules based. Typical biomarkers prevailing on cell surface gradually shed off extracellular domains (ECDs) in the serum are usual analytes. It is pertinent to mention here that the biomarkers vary in their specificity concerning the tumor

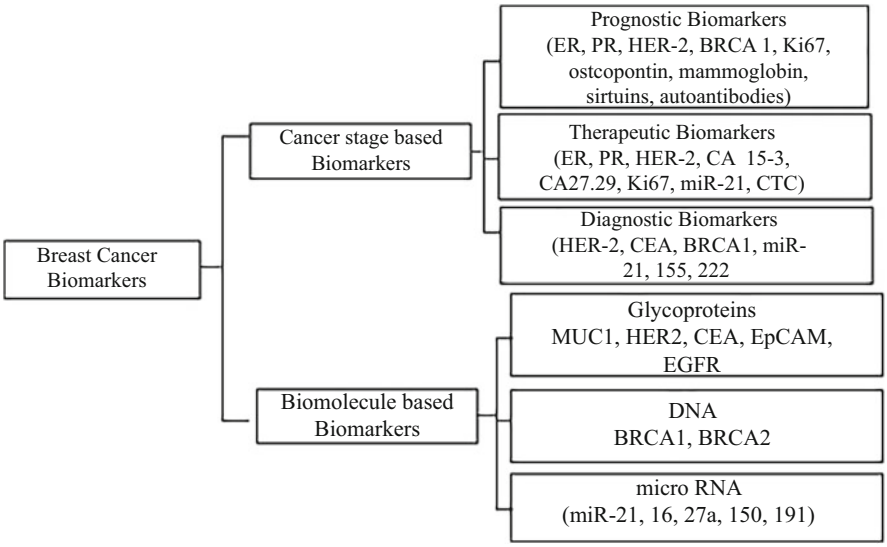


**Fig. 21** Classification of breast cancer biomarkers

concerned and may exhibit varied expression levels corresponding to different tumor stages.

So, multiplexing the biomarkers at a uniform screening platform is likely to provide better inference. Studies identifying these indications (individual or in combinative mode) illustrate a simplification via classifying the tumor cells that ultimately provides the prognosis information. For distinct recognition of a biomarker, selecting a specific biotransducer regime is a prerequisite, which in turn depends on the biochemical signal generated by implicit biomarker–bioreceptor interaction. For instance, change in $H^+$ concentration is ascertained through potentiometric biotransducer, gain or loss of electrons is made through the amperometric transducer, light emission/absorption/fluorescence/reflectance is made via optical screening, and a mass variation is perceived by the piezoelectric biosensor. Finally, some enhancers (usually NMs or high adsorptive properties harboring reagents) are needed to intercept a lower extent of bioreceptor–biomarker interaction.

There are several biomolecules such as cell surface proteins, mutated genes, and microRNAs that vary in the expressed in/on tumor cells and are implicit indicators of tumor progression. Such biologically pertinent entities are known as biomarkers, which are typically required to be easily extractable from the physiological fluids of the sufferers in a nonsensitizing procedure. Like all other cancer biomarkers, those for BC also exhibit dual-classification modes as stage-dependent and overexpressed biomolecules (Fig. 21). From a diagnostic viewpoint, biomolecules-based biomarkers have a greater significance, although there always remains a definitive correlation between diagnostic and prognostic significance of a biomarker. For instance, human epidermal growth factor receptor 2 (HER-2), and estrogen and progesterone receptors are recognized as diagnostic as well as prognostic

biomarkers. The following sections discuss the biomolecules-based biomarkers that are recognized as target molecules in biosensing.

1. **Glycoproteins**: These biomarkers mainly comprise the surface-bound carbohydrate–protein combinative molecules, such as HER-2, Mucin1 (MUC1), and CEA, epithelial cell adhesion molecule (EpCAM), and EGFR. In general, these are unregulated and result in cancer cell proliferation via growth factor generation, which alters the MAPK, PI3K/Akt pathways besides inducing metastasis. Among the several BC-sensitive glycoproteins, HER-2 and MUC1 are the most standardized diagnostic and prognostic biomarkers. HER-2 is a proto-oncogene encoding trans-membrane glycoprotein, the overexpression of which is detected in (20–30)% of BC cases. HER2-positive BC is the most aggressive of all known BC forms. The HER-2 receptors comprise extracellular ligand-binding domain that undergoes dimerization on ligand binding and an intracellular tyrosine kinase domain that undergoes phosphorylation in response to dimerization. This phosphorylation henceforth activates the manifold receptors to pave the way for downstream signaling cascade pathways, viz., APK, PI3/Akt, etc. MUC1 is a glycoprotein that guards against pathogenic infections and is encoded by the MUC-1 gene. It is generally expressed at the apical surface of epithelial cells in several organs including the breast. However, in BC cells, MUC1 is overexpressed over the whole cell surface.
2. **DNA biomarkers**: Mutations in oncogene result in tumor aggravation contrary to those of tumor suppressor genes that fail in their functions and are usually associated with tumor incidence and are widely used as recognition biomarkers. Epigenetic alterations in nuclear and mitochondrial DNA are also recognized as indicators of BC progression. For BC diagnosis, BRCA1 and BRCA2 genes are the typical and largest probability exhibiting DNA biomarkers, which are the tumor suppressor genes articulated in normal cells and help in repairing the double-stranded DNA breaks or induce death, if these are beyond repairable extent. They also regulate the cell cycle checkpoints and cell division. Thus, these collectively play a decisive role in maintaining genome integrity. Mutations in BRCA1 and BRCA2 genes are usually associated with an aggravated BC threat that is noticed in nearly (21–40)% of inherited BC cases. Expression of BRCA1 protein is reported as reduced in 30% of sporadic BC cases. The relative extent of BRCA1 protein downregulation depends on the BC severity and is inversely related to BRCA2 protein expression, a characteristic that is used for the diagnosis of sporadic BC. Thus, BRCA2 protein can be screened as a prognostic and diagnostic BC biomarker.
3. **MicroRNAs**: MicroRNAs (miRNAs or miRs) are small noncoding RNA fragments regulating a characteristic gene expression. These fragments act by masking the actual function of the underlying genome region, whereby their upregulation and downregulation both are considered pertinent diagnostic markers. Several miRs are up- and downregulated in cancers, but miR-21 is exclusively screened for in BC diagnosis owing to its higher (87.6%) sensitivity and specificity (87.3%) in the initial stage compared to other biomarkers (CEA

and CA15-3). The miR-21 is overexpressed in blood plasma and cancerous tissue compared to normal breast tissue due to which it is significant as a diagnostic and therapeutic biomarker. The aggravated expression of miR-21 is associated with increased metastasis of BC via MAPK pathway stimulated HER-2 activity. Despite being established as a stable and noninvasive biomarker in BC diagnosis, it exhibits certain limitations, including sequence homology with related RNAs, the prevalence in other (except BC) cancers, and low serum occurrence. Such issues, therefore, limit the miR use as biomarkers. To overcome these arbitrary hurdles, usually northern blotting and in situ hybridization are practiced for miR screening, but here also, a low sensitivity along with more time and sophisticated conduct setup curtail the biomarker suitability of miR.

Quantitative reverse transcription polymerase chain reaction (qRT-PCR) is a highly responsive and broad-spectrum procedure for miR analysis, but it also exhibits certain limitations concerning erstwhile laboratory-bound assays. In this reference, electrochemical biosensors have emerged as breakthrough POC devices. Initiating attempts dedicated to miR detection exclusively relied on hybridization and guanine oxidation. Thereby, miR-21 is detected through its hybridization by monitoring its hybridization with a complementary probe and has been investigated. Of late, a consensus about miR expression levels revealed decreased miR-21 expression (to femtomolar extents) using iridium (III) complex with miR-21 recognizing G-quadruplex.

4. **Circulatory tumor cells (CTCs)**: The characteristic morphological traits of cancer cells are highly different from their normal counterparts, which also augment their screening. CTC analysis is an inference of tumor metastatic activity, the separation, and quantification of which could assist the cancer screening. Instinctive information conveyed by CTC includes the invasive extent of a particular tumor, through antitumor drug response along with the mechanism of personalized anticancer therapy. The prominent distinguished phenotypic features of cancer cells aiding in their isolation from normal cells include size, morphological prospects, and magnetic sensitivity. The quantification is rendered difficult due to their low bloodstream (0–10 per ml of whole blood) count compared to healthier and physiological constituents (e.g., $10^9$ erythrocytes and $10^6$ leucocytes per ml blood). Studies predict with certainty that a high tumor population could be a decisive factor as a clinically imperative phase in BC.
5. **Other biomarkers**: Certain biomarkers are specifically targeted for BC diagnoses, such as cell-free DNA, autoantibodies, and antigens such as urokinase-dependent plasminogen activator system (UPA), the plasminogen activator inhibitor (PAI), and the Thomsen–Friedenreich (TF). A brief description of such biomarkers is appended later.

### 6.1.18 Cell-Free DNA

Circulating cell-free tumor DNA (cfDNA) is a significant cancer biomarker, with the BC having an implicit association with excessive DNA damage caused by the apoptotic and necrotic cells. These cells prevail within (0–2000) $ng \bullet ml^{-1}$ (as DNA content) in plasma, serum, and urine. Quantitative profiling of cfDNA provides

ample scope to develop noninvasive methods of BC diagnosis besides therapeutic information. Studies focused on exploring cfDNA as a BC biomarker infer a direct correlation between BC progression and cfDNA concentration. However, their use in biosensor-mediated BC detection is still in a progressive state and requires an authentic analysis of underlying mechanisms.

### 6.1.19 Autoantibodies

A potential role of autoantibodies in early-stage BC diagnosis has been made much later than other biomarkers. It was noticed that the malignant potency of a cancer results in Abs circulation against the cancer antigens in the serum, which can be easily used as a biomarker to ascertain the instantaneous tumor status. Autoantibodies against tumor-associated antigens (TAA) can be ascertained in the serum and saliva of the sufferers, listed as effective biomarkers for an early diagnosis. The autoantibodies reported in the BC patients against the corresponding antigens include p53, heat shock proteins (HSP- 27, 60, and 90), GIPC-1, c-myc, c-myb, cyclin D1, cyclin B1, RS/DJ-1, etc. The expressions of these have been reported as a positive correlation between the extent and cancer progression. For instance, an autoantibody-based microarray has been reported for 10 respective BC tumor antigens and successfully applied to investigate the BC samples. Although detection of autoantibodies in serum is a noninvasive approach, the heterogeneous nature of BC, along with poorly understood humoral immune response, limits their frequent clinical application.

#### Urokinase-Dependent Plasminogen Activator, Plasminogen Activator Inhibitor (PAI), and Thomsen–Friedenreich antigens

Besides the above biomarkers, a combinatory prevalence of independent molecules is also proposed to augment the diagnostic efficacy. Urokinase-dependent plasminogen activator, PAI, and TF antigens are also reported as disease signals in pre- and postmenopausal women. However, the detection of these markers in real samples through biosensors is awaited based on which multiple novel avenues against BC diagnosis could be opened.

### 6.1.20 Screened Breast Cancer Biomarkers in Biosensors Accomplished Diagnosis

Tables 14, 15, 16, 17, and 18 comprise the different biosensor configurations for prompt detection of BC biomarkers. With progress in electron microscopy and sharper precision tools, robust and faster principles are being swiftly undertaken to develop devices for affordable, portable, and time-scale robust analysis without any compromise in sensitivity and specificity. Although most of the developed systems are not yet feasible for clinical or market applications, the explored analyte–probe configuration could steadfast the BC diagnosis in near future. The following sections discuss the marker-specific studies and advances chronologically.

**BRCA1**: Manifold configurations of biosensors have been proposed and reported for early BRCA1 detection (Table 14). To begin with, Tiwari and colleagues demonstrated an electrochemical biosensor using chitosan-co-polyaniline as a

**Table 14** Summary of biosensors aimed at BRCA1 detection in the human serum

| Transducer | Principle | LOD and linear range | Response time and shelf life |
|---|---|---|---|
| Electrochemical | Restriction of complementary DNA probe | 2.104 μA•fmol$^{-1}$; (0.05 to 25) fmol | 16 s and 6 months |
| Electrochemical | Complementary sequence immobilized on Au NPs inside a highly cross-linked amine-modified PEG film | 1.72 fM; 50.0 fM to 1 nM | Undisclosed |
| Electrochemical | DNA probes conjugated to PANI/PEG nanofibers | 0.0038 pM; 0.01pM to 1 nM | 30 min and >10 days |
| Electrochemical | Zwitterionic peptides anchored to citrate doped PEDOT conducting polymer | 0.03 fM | Undisclosed |
| Fluorescence | Carbon dots-based fluorescent passage and Au NPs for recognizing nucleotide BRCA1 sequences | (4–120) nM | Undisclosed |
| Colorimetric | Three spots labeled with digoxin for each detected target to amplify the typical enzymatic reading | 10 fM and 10 fM to 10 nM | Undisclosed |

sustainable support platform while being applied on an indium-tin-oxide support. The study involved designing a probe with BRCA1-associated cDNA sequences that were immobilized over a surface and produced an electrochemical response in the presence of a single-stranded DNA. The configuration revealed 0.05 fmol as LOD with splendid sensitivity and reproducibility to facilitate early-stage BC detection. In another attempt, Wang and colleagues also demonstrated an electrochemical biosensor aimed to screen the BRCA1 in the serum to an extent as low as 1.72 FM. The configuration comprised a label-free DNA sensor made via GCE modification carrying highly cross-linked PEG film containing $–NH_2$ groups. This sensor was further tailored using Au NPs, conferring an outstanding sensitivity.

Another significant attempt was made by Hui and associates, who used PAN/PEG nanofibers as probe materials to detect BRCA1. The fabricated configuration facilitated BRCA1 detection in the human serum without getting affected by nonspecific adsorption in the complex media with nanofibers and conferred antifouling abilities for a significant immobilization-driven probe capture.

Through another attempt, Wang and associates used zwitterionic peptides modified with a citrate polymer-doped poly(3,4-ethylenedioxythiophene (PEDOT), which imparted an antifouling ability along with enhanced electrical conductivity to make way for the binding of a suitable DNA probe. This configuration exhibited a much lower LOD (0.03 fM) compared to the earlier one (1.72 M) demonstrated by the same research group. Henceforth, another notable attempt by Zhong and colleagues comprised a fluorescent, dual-channel biosensor configuration based on carbon dots and Au NPs, working through a hairpin structure. The working involved a specific binding of BRCA1 RNA/DNA targets to its complementary sequence on

**Table 15** ERα, PR, and CEA bioreceptor targeting biosensors for BC diagnosis

| Biomarker | Transducer | Principle | LOD and linear range | Response time and shelf life |
|---|---|---|---|---|
| Erα | Optical | The hollow core of photonic crystal fiber with anti-ER-labeled primary and secondary Abs | 0.4 μg•ml$^{-1}$ | Undisclosed |
| PR | Electrochemical | Aptamer on Au electrode and iron redox probe settings | 0.90 μg•ml$^{-1}$, 10–60 ng•ml$^{-1}$ | 40 min and undisclosed |
| CEA | Colorimetric | Au NPs and a few layers of black phosphorous hybrid | 0.20 pg•ml$^{-1}$, 1–10$^{4}$ pg•ml$^{-1}$ | Undisclosed |
| CEA | Chemiluminescence | CEA aptamer conjugates with hemin aptamer through 1,1′-oxalyldiimidazole | 0.58 ng•ml$^{-1}$<br>0–200 ng•ml$^{-1}$ | 30 min and undisclosed |
| CEA | Colorimetric | Au NPs as anti-CEA Ab carriers labeled with biotin | 48 pg•ml$^{-1}$;<br>0.05–50 ng•ml$^{-1}$ | 15 min and undisclosed |
| CEA | Electrochemical | Paper-based microfluidics immunodevice | 0.01 ng•ml$^{-1}$ | Undisclosed |
| CEA | Fluorescence | FRET between upconverting NPs and Pd NPs | 1.7 pg•ml$^{-1}$/(4–100) pg•ml$^{-1}$ | Undisclosed |

Note: Attainment of nano- and microscale detection range through different probe configurations define the diversity of biosensor functioning

**Table 16** HER2 bioreceptor targeting biosensors for breast cancer detection

| Transducer | Principle | LOD and linear range | Response time and shelf life |
|---|---|---|---|
| Electrochemical (amperometric) | Sandwich immunoassay working through nanobodies | Undisclosed and (1–200) $\mu g \cdot ml^{-1}$ | (2–20) min and >3 weeks |
| Electrochemical | DNA-derived electric current with DNA self-assembly for signal intensification | 0.047 $pg \cdot ml^{-1}$ and (1–100) $pg \cdot ml^{-1}$ | Undisclosed |
| Colorimetric | HER2 Abs anchored Au NPs-loaded liposomes | 5 Sk-Br-3 cells and undisclosed | 2 h and undisclosed |
| Electrochemical (amperometric) | Modified Au NPs and graphene oxide loaded on GCEs | 0.16 nM, (0.37–10) nM | Undisclosed |
| Electrochemical | Sandwich aptasensor using molybdate to generate an electrochemical current | Undisclosed and (0.01–5) $ng \cdot ml^{-1}$ | Undisclosed |
| Electrochemical | Organic-electrochemical transistor | Undisclosed and ($10^{-14}$ to $10^{-7}$) $g \cdot ml^{-1}$ | Undisclosed |
| Electrochemical (voltammetry) | Reduced graphene oxide-chitosan film as an electrode with MB as a redox probe | 0.21 $ng \cdot ml^{-1}$, (0.5–2) $ng \cdot ml^{-1}$ | Undisclosed |
| Electrochemical | Immunosensor with hydrazine and aptamer-conjugated Au NPs | 37 $pg \cdot ml^{-1}$, 1 $ng \cdot ml^{-1}$ to 10 $\mu g \cdot L^{-1}$ | Undisclosed |
| Electrochemical (voltammetry) | Anti-HER2 Abs conjugated with FeO NPs on Au electrode | 0.995 $pg \cdot ml^{-1}$, 10 $ng \cdot L^{-1}$ to 10 $\mu g \cdot ml^{-1}$ | Undisclosed |
| Photoelectrochemical | ZnO/graphene composite and S6 aptamer on a portable indium-tin-oxide microdevice | 58 $cells \cdot ml^{-1}$, ($10^2$ to $10^6$) $cells \cdot ml^{-1}$ | 20 min and >2 weeks |
| Electrochemical (EIS) | Charge transfer resistance of an Fe redox probe changes with Ab-bound protein extent | 7.4 $ng \cdot ml^{-1}$, (10–110) $ng \cdot ml^{-1}$ | 35 min and undisclosed |
| Electrochemical | The immobilized polycytosine DNA sequence in an Au NPs matrix | 0.5 $pg \cdot ml^{-1}$, (1–1000) $pg \cdot ml^{-1}$ | Undisclosed |
| Electrochemical | Aptamer-modified interdigitated Au electrodes | 1 pM; 1 pM to 100 nM | Undisclosed |
| Electrochemical | Inkjet-printed 8-electrode array, needing biotinylated Ab and polymerized HRP labels | 12 $pg \cdot ml^{-1}$ and undisclosed | 15 min and undisclosed |

Au NPs followed by a subsequent release from carbon dots, resulting in a positive fluorescent signal with a linear response, ranging within (4–120) nm. Another attempt by Yang and associates demonstrated a sandwich-like biosensor that worked through a magnetic bead platform. The configuration involved a tetrahedral probe, having its three vertices labeled with digoxin while the fourth was labeled with a

**Table 17** The different biosensor configurations used for screening the characteristic BC biomarkers

| Biomarker | Transducer | Principle | LOD and linear range | Response time and shelf life |
|---|---|---|---|---|
| Mucin 1 | Electrochemical | Aptamer//cell/aptamer sandwich array on an electrode surface | 100 cells•ml$^{-1}$ ($10^2$ to $10^7$) cells•ml$^{-1}$ | Undisclosed |
| Mucin 1 | Electromagnetic | Aptamer-functionalized Au nanorods | 100 cells•ml$^{-1}$ ($10^2$ to $10^5$) cells•ml$^{-1}$ | 30 min and undisclosed |
| Mucin 1 | Electrochemical (voltammetry) | Polyadenine-aptamer-functionalized Au NPs/graphene oxide hybrid | 8 cells•ml$^{-1}$ and (10–$10^5$) cells•ml$^{-1}$ | 40 min and undisclosed |
| Mucin 1 | Electrochemical | Biotinylated aptamer immobilized on Au NPs-graphene oxide-PEDOT composite | 0.031 fM, 3.13–31.25 nM | 15 min and 14 days |
| CA 15-3 | Optical | Abs immobilized via surface standard amine coupling on an optofluidic ring resonator | 1 unit•ml$^{-1}$ and undisclosed | 20 min and undisclosed |
| CA 15-3 | Optical | Cysteamine-capped cadmium sulfide QDs | 0.002 kU•L$^{-1}$ and undisclosed | 15 min and undisclosed |
| CA 15-3 | Electrochemical (voltammetry) | Detection of seven tumor markers using alkaline phosphatase-based competitive immunoassay for hydroquinone screening | 0.7 U•ml$^{-1}$ and (1.2–3.7) U•ml$^{-1}$ | Undisclosed |
| CA 15-3 | Electrochemical | Nanoporous Au/graphene hybrid platform combined with HRP | 5•$10^{-6}$ U•ml$^{-1}$, (2•$10^{-5}$-40) U•ml$^{-1}$ | Undisclosed |
| CA 15-3 | Electrochemical | Label-free highly conductive N-doped graphene sheets modified electrode | 0.012 U•ml$^{-1}$ and (0.1–20) U•ml$^{-1}$ | Undisclosed |
| CA 15-3 | Electrochemical | Functionalized graphene with 1-pyrenecarboxylic acid sensing probe and MWCNTs with ferritin labels | 0.009 U•ml$^{-1}$ and (0.05–100) U•ml$^{-1}$ | Undisclosed |
| CA 15-3 | Electrochemical | Electrically conducting poly (toluidine blue) as synthetic receptor film | 0.10 U•ml$^{-1}$ and (0.10–100) U•ml$^{-1}$ | Undisclosed |

Note: LOD, working range, response time, and probe shelf life are the decisive performance defining criteria

**Table 18** miR-21 and miR-155 target attempts toward a prompt breast cancer diagnosis

| Biomarker | Transducer | Principle | LOD and linear range | Response time and shelf life |
|---|---|---|---|---|
| miR-21 | Electrochemical | Probes conjugated to a pencil graphite electrode | 1.0 mg•ml$^{-1}$ | Undisclosed |
| miR-21 | Electrochemical | Two supplementary probes that self-assemble to form 1D DNA concatemers | 100 aM; 100 to $10^5$aM | Undisclosed |
| miR-21 | Electrochemical | MB as a redox indicator | 84.3 fM; 0.1–500 pM | 60 min and undisclosed |
| miR-21 | Electrochemical | Hybridization to a specific biotinylated DNA probe restricted on magnetic beads | 0.04 pM; 0.1–500 pM | 30 min and undisclosed |
| miR-21 | Fluorescence | 2-Aminopurine probe in conjunction with a G-quadruplex structure | 1.48 pM; undisclosed | Undisclosed |
| miR-21 | Electrochemical | Probe engineered with a pyrrolidinyl peptide nucleic acid/PPy/Ag nanofoam | 0.20 fM and (0.20–$10^6$) fM | Undisclosed |
| miR-21 | Electrochemical | Target stimulated glucose release from propylamine-functionalized mesoporous silica NPs | 19 pM; (50–5000) pM | Undisclosed |
| miR-155 | Electrochemical | Graphene oxide sheet on GCE surface with thiolated probe-functionalized Au nanorods | 0.60 fM; (20–8000) fM | Undisclosed |
| miR-155 | Electrochemical | Immobilization of anti-mi-R-155 on Au SPE | 5.7 aM; (10–$10^9$) aM | Undisclosed |
| miR-155 | Colorimetric | Covalent conjugation of a DNA probe to negatively charged Au NPs | 100 aM; (100 to $10^5$) aM | Undisclosed |

detection probe. The enzyme-labeled antidigoxin Ab thereby possessed three distinct regions for binding each detection probe, which together facilitated signal amplification. The configuration distinguished the DNA sequences with only one base mismatch and provided PCR-grade products.

**ERα**: The sole attempt toward ERα detection-mediated BC screening was made by Padmanabhan and colleagues, who used an optical transducer for a volumetric detection of proteins, to the extent as low as 50 nL (Table 15). The configuration used a hollow core-photonic crystal fiber working via TIR mode, allowing a fluorescence-driven green and red response on being recognized by secondary Ab.

**Progesterone (PR)**: The summary of studies dedicated to using PR detection-enabled BC screening is described in Table 15. The first notable effort was made by Jimenez and colleagues, who selected a PR aptamer through systematic ligand evolution via significant enrichment (SELE) to develop a label-free aptasensor having an enhanced signal gain, monitored using EIS. The conformational change

of aptamer immobilized on Au electrode on PR binding revealed an enhanced resistance to electron transfer on an iron standard redox probe with (10–60) ng•ml$^{-1}$ linear PR detection and 0.90 ng•ml$^{-1}$ LOD.

Developments toward CEA detection-enabled BC diagnosis are summarized in Table 15, wherein the first notable attempt by Peng and colleagues used the catalytic attributes of a few layers of black phosphorous modified through a concurrent generation of Au NPs toward 4-nitrophenol that was screened using colorimetric assays. This catalytic activity was reversibly suppressed in an Ab's presence but was reactivated on CEA inclusion. The 0.20 pg•ml$^{-1}$ as LOD and 1 pg•ml$^{-1}$ to 10 μg•ml$^{-1}$ as linear detection range argued well for distinguished sample analysis. In another significant attempt, Khang and associates fabricated a chemiluminescence aptasensor having dual DNA aptamer for competitive CEA and hemin binding within 30 min at RT. Subsequently, Amplex Red and $H_2O_2$ were added to generate resorufin, which depended on the HRP concentration equivalent for mimicking G-quadruplex DNAzyme formed on hemin and dual DNA-binding interaction. The detection was made through the development of red light on 1,-1′-oxalyldiimidazole addition to the analysis cell, decreasing the intensity with enhanced CEA concentrations.

Yet another significant attempt by Liu and colleagues demonstrated a colorimetric enzyme immunoassay having Au NPs as carriers for HRP-labeled anti-CEA detection Ab and magnetic microparticles as sustaining substrates. The generated complex resulted in an optical signal for an improved sensitivity compared to ELISA-detected CEA. A subsequent attempt by Wu and associates demonstrated a sandwich immunoassay having a secondary Ab facilitated the growth of the long-chain polymeric material to provide adequate HRP-binding sites. The growth of polymeric material played a key role in signal amplification, with a direct positive correlation of secondary Abs bound to the support and the generated electrochemical signal by the HRP-O-phenylenediamine-$H_2O_2$ system. The support was formed by a carbon electrode printed on a paper-based microfluidics electrochemical immune device. Another attempt by Li and associates demonstrated a FRET-based biosensor using UNPs and Pd NPs. With aptamer bound to UNPs, the proximity of Pd NPs to the aptamer quenched the UNPs fluorescence. In the presence of CEA, the aptamer preferentially combined with CEA and yielded conformational changes to weaken its interaction with Pd NPs, facilitating recovery of fluorescence signals. The configuration enabled an ultrasensitive CEA detection from the diluted human serum within (4–100) pg•ml$^{-1}$ linear range and 1.7 pg•ml$^{-1}$ LOD.

**HER2**: Among the most targeted BC biomarker, HER2 has been extensively screened as a BC progression indicator, and these attempts have most actively used the electrochemical configurations (Table 16). In one of the earliest attempts of the last decade, Patris and colleagues designed a sandwich immunoassay based on nanobodies aimed to recognize another HER2 epitope on SPEs. The capture nanobody was immobilized on the carbon-working electrode while the detection of Ab was HRP-conjugated. Upon detection, the signal corresponded to p-quinone electroreduction, generated by the HRP at SPE in the presence of hydroquinone and $H_2O_2$. In another experimental setting, Shen and associates developed a self-assembly-

driven DNA intensification biosensor capable of generating electric current. The HER2 aptamer served the purpose of both ligand (for recognition) and signal-generating reporter on a sandwich format. The sensor LOD was 0.047 pg•ml$^{-1}$ with a (1–100) pg•ml$^{-1}$ detection range. In the next major attempt, Tao and associates designed a colorimetric biosensor having a probe with HER2 Abs anchored on liposomes loaded with Au nanoclusters. The specific intent of using Au nanoclusters was their intrinsic peroxidase ability that resulted in the color change of solution on reacting with 3,3′,5,5′-tetramethylbenzimide in the presence of $H_2O_2$. The configuration enabled the screening of HER2-positive BC cells in human serum and BC tissue with an LOD of even five cells.

- Yet another significant attempt by Saeed and colleagues utilized Au NPs with a short harmonizing HER2 sequence, being covalently bonded to graphene oxide-modified GCE. Binding of HER2 to Au NPs with the involvement of an additional short stretch of DNA modified via HRP-hybridized-free HER2 sequence generated the corresponding electrochemical signal (binding of TMb with $H_2O_2$). Another elegant attempt by Hu and accomplices used a HER2-specific aptamer as a ligand to capture HER2 by generating a redox-modulated current signal. The intensity of this current varied with the progress of the aptamer–molybdate phosphate moieties reaction, producing a current that varied directly with HER2 concentration in the (0.01–5) ng•ml$^{-1}$ range. A separate study by Fu and colleagues reported an organic electrochemical transistor-based biosensor for intercepting the electrochemical actions on gate electrodes to an extent of $10^{-14}$ g•ml$^{-1}$. The Au GATE electrode was engineered with a capture-specific polyclonal anti-HER2 Ab, enabling the detection via HRP-bound secondary Ab. The current was generated as a response to the $H_2O_2$ and HER2 interactions.
- A subsequent attempt line is the effort of Tabasi and colleagues, who fabricated an ultrasensitive electrochemical aptasensor using graphene and chitosan film as a compatible electrode material for aptamer binding. Readers must note here that graphene and chitosan combination has been investigated significantly for a thin film formation, along with negligible nonspecific reaction and accompanied biocompatibility of chitosan. The HER2 interaction with the aptamer resulted in conformational variations that were attributed to a concentration-dependent higher signal being generated by the electrochemical probe MB. Henceforth, Zhu and colleagues fabricated a sandwiched configuration of biosensor, wherein a probe comprised of an immobilized Ab on a nanocomposite having Au NPs capped with 2,5-bis(2-thienyl)-1H-pyrrole-1-(p-benzoic acid) unswervingly on a bare electrode surface. The detection was accomplished using a hydrazine-Au NP–aptamer bioconjugate, having hydrazine as reactant bound to the Au NPs that contained Ag for the moderation of signal intensification. A turning point aspect of this study was the silver staining of target cells that exhibited a black appearance that could be easily viewed through a microscope, thereby making the clinical analysis of tumor cells a robust task.
- In furtherance, Emami and accomplices demonstrated a label-free immunosensor, wherein anti-HER2 Abs are conjugated with FeO NPs, which were further spread over an Au electrode surface. The sensor exhibited a significant response to

screen as low as 0.995 ng•ml$^{-1}$ HER-2 with 5.921 μA ml•ng$^{-1}$ sensitivity. A succeeding attempt is the effort of Liu and associates, who demonstrated a PEC biosensor for screening SK-Br-3, an HER2-positive cell line. The investigators used a high photoelectric signal of ZnO along with graphene's splendid charge transportation and separation and S6 aptamer's specificity to target SK-Br-3 cells. Next in line is the study of Akran and coworkers, who developed an electrochemical immunosensor for HER2 screening via the preparation of carbon paste electrodes using graphite powder, multiwalled CNTs, an ionic liquid, paraffin, and the entire assembly functionalization with Au NPs (through electrodeposition). The optimized configuration exhibited a charge transfer resistance that increased linearly with increasing HER2 antigen concentration for 35 min of optimum incubation, exhibiting a linear dependency within (10–110) ng•ml$^{-1}$.

- A subsequent significant study is an attempt by Li and accomplices, who used an immobilized polycytosine DNA sequence housed in an Au NP matrix as the sensing probe to capture HER2. The response was quantified as the electrochemical current intensity generated at the electrode surface, corresponding to the reaction between polycytosine DNA phosphate backbone and molybdate. The optimized configuration exhibited a linear response from 1 pg•ml$^{-1}$ to 1 ng•ml$^{-1}$, having 0.5 pg•ml$^{-1}$ as LOD, ruling out the nonspecific activity entirely among the human IgG, IgA, p53, and CEA. The next crucial attempt is the study of Arya and colleagues, who used thiol-terminated DNA aptamer-engineered interdigitated microelectrodes (IMEs) for HER2 detection, making use of Au electrodes as sensing detectors. The optimized configuration exhibited a significant selectivity in working, detecting the multiple serum proteins within the 1 pM to 100 nM linear range. A more recent attempt by Carvajal and colleagues worked out to make an inkjet printer-configured electrochemical sensor, having the analysis platform comprising an inkjet Au 8-electrode array, a counter electrode, and an inkjet-printed Ag electrode, which has been bleach chlorinated to form an Ag/AgCl quasireference electrode. The working assay was based on the detection of an immunological response, sing the microfluidic device labeled with streptavidin/HRP composite. Designed sensor configuration responded well with 15 min assay time and an LOD of 12 pg•ml$^{-1}$.
- The above studies illustrate a significant diagnostic accuracy with multifunctional probe designs for HER2 identification. Much has been accomplished due to a high surface area of NMs through which their functionalization potential and interactive sites are greater. It is important to understand that though broad-working mode classifications list all developed configurations in the electrochemical regime, the exact mechanism and probe sensitivity may differ. Thereby, a particular sensor configuration suitable for HER2 detection in advanced stages may not be that much efficient in the initial cycles, whereby the corresponding HER2 expression is well below the desired threshold.

**Mucin 1**: Attempts to monitor mucin 1 protein expression for possible progress in BC manifestation are described in Table 17. The first notable effort in this direction was made by Zhu and colleagues, who used aptamer–cell–aptamer sandwich

architecture to detect MUC1 in MCF-7 BC cells. The developed sandwich-configured biosensor worked well only in the presence of targeted cells. The electrochemical response is generated from HRP labeling on MUC1 aptamer, the subsequent monitoring of electron mediator thionine with an enhanced specificity on doubling the aptamer recognition ability.

- Next in line is the study by Li and associates, who used an electromagnetic approach based on SPR as the MUC1 detection method on MCF-7 cells. The aptamer-functionalized Au nanorods sensed MUC1 within (100–$10^5$) cells•$ml^{-1}$ range and an LOD of 100 cells•$ml^{-1}$ in 30 min on the whole. The following attempt is the study by Wang and associates, who designed a sandwich-configured electrochemical biosensor working through a polyadenine-aptamer-modified Au electrode and a polyadenine-aptamer-functionalized Au NPs-graphene oxide hybrid for a label-free sensitive MUC1 detection in MCF-7 BC cells. The sensor detected as low as 8 cells•$ml^{-1}$ with a (10–$10^5$) cells•$ml^{-1}$ linear range.
- The latest effort toward MUC1 screening is the study from Gupta and associates, who used conducting attributes of a polymer nanocomposite to develop an electrochemical aptasensor. The nanocomposite Au NPs film and graphene oxide-doped PEDOT were developed over the surface of fluorine tin-oxide glass. The configuration enabled MUC1 detection to as low as 0.31 fM with eight times apta-electrode reusability.

**CA 15-3**: Cancer antigen 15-3 (CA 15-3) is a carbohydrate-containing protein antigen and a member of a mucin protein family. Although the exact role of Ca 15-3 in BC progression is not completely known, it reduces cell–cell interaction alongside inhibiting cell lysis. To date, the major involvement of CA 15-3 protein in BC patients has been from the diagnosis aid, in particular for BC recurrence and metastasis screening during active, therapy resulting from allowing organ specificity.

- The first notable effort toward screening CA 15-3 expression in BC pathogenesis is the study by Zhu and colleagues, who reported a label-free optofluidic ring resonator for a rapid CA 15-3 detection. The optimized configuration functioned well in diluted human serum with a least detection extent of 1 U•$ml^{-1}$ in nearly 30 min. Subsequently, Elakkiya and associates used optics as transducer technology using a cadmium sulfide QD surface capped with cysteamine. The optimal configuration was evaluated in saline and antigen-spiked serum samples and was able to detect 0.002 KU•$l^{-1}$ extent of CA 15-3 with an unchanged response time of 15 min. In furtherance, Marques and accomplices developed the first multiplexed electrochemical immunosensor for a simultaneous CA 15-3 and HER2 screening. The configuration was made using a personalized dual SPCE with electrodeposited Au NPs-modified surfaces on an in situ scale. The electrodes were thereafter coated with monoclonal antihuman CA 15-3 and HER2 Ab. The detection was controlled by voltammetric analysis with 5 U• $ml^{-1}$ LOD.

- Chronological efforts comprise the studies of Ge, Li, and Akter research groups, wherein graphene-based electrochemical immunobiosensors were developed. The attempt by Ge and the group used a nanoporous/graphene hybrid as a platform, having liposomes with encapsulated HRP as labels. A CA 15-3 presence triggered the HRP release from liposome, alongside reducing $H_2O_2$ with thionine as an electron control agent. The encapsulation significantly aided in the signal amplification facilitating a 5 μU•ml$^{-1}$ as LOD. In the study, Li and colleagues applied graphene to an electrochemical immunosensor in an N-doped graphene sheet configuration. The approach conferred a high conductivity to graphene-engineered electrode, resulting in adequate electron transfer and high sensitivity without any labeling requirement. The optimized configuration revealed an LOD as low as 0.012 U• ml$^{-1}$ within (0.1–20) U•ml$^{-1}$ linear response range. The attempt of Akter and colleagues employed noncovalent functionalized graphene oxide as sensing probes and multiwalled CNT-supported ferritin linkages as labels, both conjugated to CA 15-3 Abs. The detection of CA 15-3 was facilitated by the amide bond between –$NH_2$ groups of secondary Ab, ferritin, and –COOH groups of multiwalled CNTs, through an enhanced bioelectrocatalytic reduction of $H_2O_2$, mediated via hydroquinone probe on the functionalized graphene surface.
- The latest effort in CA 15-3 detection is the study of Riberiro and colleagues, who developed an electrochemical biosensor having a synthetic receptor film working through molecular imprinting. The methodology involved CA 15-3 imprinting on a poly(toluidine blue) film following which the assays were performed in buffer and artificial sera, enabling a selective CA 15-3 adsorption onto the MIP film on 30-min incubation. The analysis of calibration plots revealed a linear dependence of CA 15-3 within (0.10–100) U• ml$^{-1}$ range with 0.10 U•ml$^{-1}$ LOD.

**miRNA21**: Fundamentally, miRNAs are the small, highly preserved noncoding RNA fragments implicated in gene expression regulation. These RNAs are transcribed by RNA polymerases II and III generating precursors that undergo a series of cleavages to form mature microRNA. Figure 22 depicts the molecular functioning of miRNA, wherein binding mediates with 3′-untranslated regions of target mRNA. The bound sequence of miRNA could be oncogenes or tumor suppressor genes, the targeting of which respectively results in tumor arrest and aggravation following the suppression of oncogenes and tumor suppressor genes. The following sections discuss the research attempts toward screening the miRNA 21 expression for ascertaining the BC presence (Table 18).

- The very first attempt in this regard was the study of Kilic and associates, who fabricated an electrochemical biosensor using enzyme-amplified miR21 biosensing from a cell lysate of total RNA. The detection was accomplished through capture probes and covalently attached cell lysates over the pencil-grade graphite electrodes by EDC–NHS coupling chemistry. The optimized configuration operated sensitively with 1 μg•ml$^{-1}$ LOD. A subsequent attempt involved a study by Hong and associates, who designed an electrochemical ultrasensitive

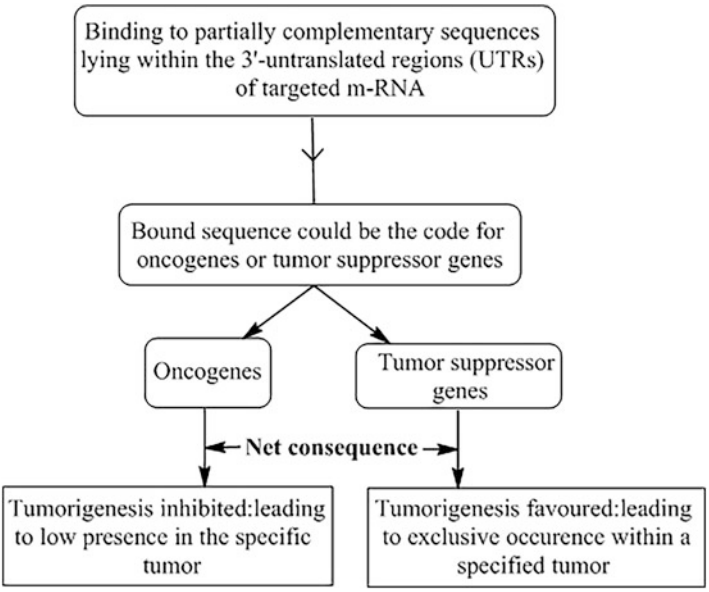


**Fig. 22** An overview of the molecular functional controls exercised by miRNA as an antitumor targeting agent, coordinated through the functional activities of oncogenes and tumor suppressor genes

biosensor for screening the BC-associated miR-21. The probe involved a self-assembled DNA concatamer, wherein a long DNA chain of multiple copies of identical DNA sequences linked end to end, facilitated the miR-21 detection in complex biological samples (enzymes or labels) with 100 aM LOD.

- Next in line is the attempt by Vargas and associates, who fabricated a sensitive amperometric magnetobiosensor for prompt miRNA detection. The detection mechanism involved direct target hybridization through a specified biotinylated DNA probe immobilized on magnetic beads, conjugated with streptavidin. The label comprised a specific DNA–RNA Ab and the bacterial protein A conjugated with an HRP homopolymer for signal amplification. The single-step configuration attained a (1–100) pM linear range and an LOD of 10 aM in a 25 μl sample, devoid of any target miRNA intensification within 30 min. Yet another promising attempt toward miRNA-21 detection is the study of Raffiee-Pour and associates, who used MB as a redox indicator with no label use. The kinetic mode of assays revealed a higher MB stability in binding with miRNA/DNA compared to ss-DNA, generating an LOD of 84.3 fM.

- In furtherance, Li and associates amalgamated a 2-aminopurine probe with a G-quadruplex structure to design a biosensor for overexpressed miR-21 detection from human BC cell lysate without quenchers or enzymes. The optimized configuration comprised two DNA hairpins that considerably elevated the

hairpin's fluorescence for a 1.48 pM LOD. Thereby, the fluorescent sensitivity of G-quadruplex-bound 2-aminopurine compensated the requirement of coupling enzymes or reaction quenchers with the probe and simplified the probe interaction. The next attempt in the direction of biosensor-mitigated BC diagnosis is the study of Kangkamano and colleagues, who used a modified electrode to detect miR-21 using a label-free electrochemical biosensor. The designed probe was engineered with pyrrolidinyl peptide nucleic acid/polypyrrole/Ag nanofoam with generated signal exhibiting a direct correlation to the detected miR-21 extents within (0.20 to $10^6$) fM. The latest attempt in this regard is the study by Deng and associates, who fabricated an electrochemical biosensor involving a target-induced glucose release from propylamine-engineered mesoporous silica NPs. The optimized configuration used glucose as the signal generating a tag for glucometer readout, wherein labeling and time-consuming repeated washing steps were bypassed. The sensor worked well with 19 pM LOD. Attempts made toward screening miR-155 as the BC biomarker were relatively fewer and could be traced in Table 18, with two of the three studies using electrochemical transducers.

## 7 Handheld Devices: Glucometer and Extensions

**Glucometer**: A glucose meter, more famously a glucometer, is a handheld device for knowing the approximate blood glucose concentration. The alternative version could be a strip of glucose paper dipped into a substance (the concerned medium/environment) after which the developed color is matched with the database of glucose chart. The features comprise the essentials of household blood glucose monitoring (HBGM) for persons suffering from diabetes mellitus or hypoglycemia. The conventional methodology involves extracting a small blood drop via pricking the skin using a lancet before placing it on a disposable test strip that is read by the meter for knowing the blood glucose extent, in $mg \bullet dL^{-1}$ or $mmol \bullet L^{-1}$.

Ever since the 1980s, a major goal of type 1 and type 2 diabetes mellitus treatment had been to attain close to normal blood glucose extents for a longer duration, which is then screened using HBGM. The major incentives of this approach include a reduced occurrence frequency and severity of long-lasting hyperglycemia complications as well as moderating the short-term hypoglycemic life-threatening troubles.

### 7.1 Working Principle

Multiple configurations of glucometers are known, which invariably rely on the oxidation of glucose to gluconolactone catalyzed via glucose oxidase (GOx), although some of the modules also rely on the oxidation mediated via glucose dehydrogenase (GDH). In general, GDH has a weaker sensitivity over GOx, with a higher susceptibility to interfering reactions involving related moieties.

- The development of glucose biosensors is documented in terms of generation chronology, with the first-generation devices working via colorimetric reactions. These devices are presently in use in the glucose test strips for urinal detection of glucose. Other than GOx, the test kit comprises benzidine derivative that is oxidized to a blue polymer using the $H_2O_2$ produced amidst oxidation. A significant hurdle herein mandates the periodic development of test strips for the removal of a blood sample, resulting in the requirement of frequent instrumental calibration. The instrument is a handheld device working through a digital model using the transduction of screened glucose excess. Having a changeable ability, present-day glucometers work on the electrochemical principle, with the test strip housing a capillary that is equipped to suck in a reproducible blood quantity. The glucose in sucked blood reacts with GOx or GDH coated on the electrode surface.
- The enzyme is reoxidized in an excess amount of intervening moieties, such as the ferricyanide ion, ferrocene derivative, or osmium bipyridyl complex. The intervening agent hereby undergoes oxidation via electrochemical reaction at the anode surface, generating an equivalent electric current. By Faraday's law, the net charge flowing through an electrode varies directly with the blood glucose amount that has reacted with the enzyme.
- Measurements using the colorimetric method rely on the quantification of the net charge generated by the glucose oxidation over some time while those made using the amperometric method use some meters and quantify the electrical current generated at a specific time instant by the intended glucose reaction. The assessment works through Newton's second law of motion, wherein the progress of glucose reaction is estimated analogous to assessing the rate of change of momentum after an object has been in motion. The analyzed time scales are variable for the colorimetric method but the amperometric mode has the time scales as fixed, although inevitably both methods predict the blood glucose concentration in an analyzed sample.
- A similar principle works in test strips designed to screen the presence of diabetic ketoacidosis. Such test strips use a β-hydroxybutyrate dehydrogenase rather than GOx and have been used to detect and treat certain complications resulting from prolonged hyperglycemia. The sensors for estimating blood alcohol extents have been developed using the same approach, even patented but not yet commercially developed.

## 7.2 Working Features of a Glucometer

Model-specific working specifications of glucometers regulating their functioning and user acceptability are as discussed next.

- **Size**: In general, the average size of a typical glucometer is equivalent to the hand palm though hospital meters could be the size of remote control. The devices are battery regulated.

- **Test strips**: Test strips inherently provide a sensitive and engineered surface, comprising chemicals that react with the glucose quantity in the blood drop (sample being examined). The strip can be plastic grade, having a small spot impregnated with GOx and other constituents. In general, the strips are fabricated for one-time use although some configurations do employ disks, drums, or cartridges equipped with a consumable amount of being examined material for multiple analyses.
- **Coding**: As test strips vary on batch-to-batch basis, certain models mandate the user to manually enter a code that is written on a particular vial of test strips or on a chip that comes with a test strip. Upon entering the coding or chip into the meter, the device is optimally (through in-built programming) calibrated to that batch of test strips. In case of wrong proceeding, the meter reading may go up to 4 mmol•$L^{-1}$ (72 mg•$dL^{-1}$), which is quite inaccurate. Such outcomes of inappropriately coded meters could be serious for patients who are actively managing their diabetes extent and may place them at an enhanced risk of hypoglycemia. Some test strip configurations carry the code information imprinted in the strip while others have a microchip in the vial of strips that can be inserted into the meter. Such design variations minimize the user error likelihood. In some yester designs, a single touch standardizes the test strips around a single code number, wherein the need for a code change is eliminated after it is once set. In some relatively recent models, there is no provision to change the code after it is once set.
- **Volume and time requirement for sample analysis**: Quite often, the typical size of blood drop required for analysis in the differently optimized configurations lies within (0.3–1) μL. The primitive configurations require a large sample quantity (referred to as hanging drop from the fingertip); a smaller volume, however, indeed minimizes the operational fluctuations. The normal time taken to read a test strip ranges from (3–60) s for different model configurations.
- **Alternate site screening**: A smaller drop volume needs pricking of the forearms or other lowly sensitive areas contrary to the fingertips. This testing mode is suited only for stable blood glucose quantities, such as before having meals, amidst fasting, or just before going to bed at night time.
- **Display**: The digital versions of the instrument provide the glucose values in mg•$dL^{-1}$ or mmol•$L^{-1}$. The preferred measurement units vary on a countrywide basis like mg•$dL^{-1}$ is preferred in the United States, France, Japan, Israel, and India. However, in Canada, Australia, and China, mmol•$L^{-1}$ is used. Germany is the only country to date where both units are accepted for measurement. There have been many confusions regarding the measurement units by the instruments, with the patient being misled by the fact that a mmol•$L^{-1}$ reading is a very low reading in mg/dL or the converse. In general, a mmol•$L^{-1}$ value is presented as a decimal point, whereas without a decimal value is in mg•$dL^{-1}$.
- **Glucose versus plasma glucose measurements**: The glucose extent in plasma (one of the blood constituents) is higher than in whole blood, and the difference tends to be ~11% with a normal hematocrit. The understanding of such distinction is significant as household blood glucose meters estimate glucose in whole blood

contrary to the plasma extents estimated in most laboratory tests. At present, several meter configurations occupy the market, wherein the result is processed as "plasma equivalent" even though actual measurements pertain to whole blood glucose. The conversion to whole glucose from that of plasma equivalent is facilitated by an inbuilt equation formatted into each glucose meter. Such a facility enables the patients to compare their glucose determinations with the lab test.

- **Provision for yester records**: Many meter configurations at present include a clock that is set by the user for date and time along with a memory for recording past test results. Such a provision is an important step in diabetes care as it aids in keeping a record of management and the gradual shifts (over days and weeks) in blood glucose trends and patterns. In general, most memory chips display an average of recent glucose readings. A common lacuna of all configurations equipped with clock facility pertains to inappropriate time settings of the clock (due to time changes, static electricity, etc.), whereby the timing of past measurements could be misrepresented, making the management cumbersome.
- **Information transfer**: Several meter configurations, at present, are equipped with sophisticated data-handling ability *vis-à-vis* downloading via cable to a computer having diabetes management software for displaying the test results. Apart from this, some configurations also allow an entry of additional parameters such as insulin dose, the quantity of carbohydrates eaten, and the optimum extent of exercise. Several meters are configured along with insulin injection devices and cellular transmitters. A radio link to an insulin pump allows automatic transfer of glucose measurements to a calculator that assists the wearer in deciding the apt insulin dose.
- **Economy**: Typical expense of a household-used glucose meter is presently high due to the sophisticated needs of test strips used. The 2006 expenses of a glucose meter strip ranged within (0.35–1) $. Very often, manufacturers provide meters at a negligible cost to enable the use of profit-incurring test strips. While type I diabetics may require testing 4–10 times per 24 h (due to insulin modulation extents), type 2 diabetics need a less frequent analysis, particularly in the absence of insulin therapy as a treatment recourse. A recent study funded by the National Health Service, UK, focused on analyzing the cost-effectiveness of self-monitoring of blood glucose and reported significant variations in the customer price not being accountable to the improved working aspects of detecting instruments. The study estimated ~12 million as the spent amount for the 42 million self-monitored glucose tests, which lacked the acceptable accuracy norms. Additionally, accomplishing £23.2 m per annum efficiency savings seemed well within reach, subject to the disinvestment of the National Health Service from the lowly functional technologies compared to the available alternatives (albeit at a higher cost). Inspection revealed some meters as being assembled with counterfeit test strip batches, which substantially contributed to error-prone outcomes.

## 7.3 Configured Variations

Based on the analyzing ability and the working specifications, the most well-known configurations for glucose meters include hospital glucose meters, noninvasive meters, and continuous glucose monitors. A brief profile of each of these variations is described next.

- **Hospital glucose meters**: Such configurations include special glucose monitors that are now used in multipatient hospitals. These are optimized to provide a more rigorous quality control summary. The data-handling provisions in these systems are optimized to transfer glucose results into electronic medical records and the laboratory computer systems for billing requirements.
- **Noninvasive meters**: Due to a possible risk emanating from continuous skin contact, such glucometer configuration has eluded the users for a long time. The quest for its exclusive search began in 1975 but has not met any success even to date, with no clinical- or commercial-scale viable product. The maximum progress in this direction relates to a 1999 approval of a sole product for selling, relying on a technique that requires electrical pulling of glucose through intact skin. This product was withdrawn after a short time in light of its poor performance and occasional damage to the user's skin.
- **Continuous glucose meters**: This configuration comprises a disposable sensor positioned beneath the skin, a transmitter connected to the sensor assembly, and a reader for receiving and displaying the measurements. Such sensor types can be used for several days before a possible replacement. These configurations allow real-time measurements and eliminate the need for fingerprick-driven testing of glucose levels. A pressing limitation is an inaccuracy of working as these instruments read the interstitial fluid glucose levels that are much lower than the corresponding blood extents.

## 7.4 Accuracy Concerns of Glucose Meters

Despite significant technological advances and a periodic review of met accuracy standards for glucose, and ace meters by the International Organization for Standardization (ISO), the accuracy of glucose meters remains a challenging issue. As per ISO15197 Instructions Manual, blood glucose meters must provide results that are within 15% of laboratory standard concentrations above 100 $mg \bullet dL^{-1}$ on a minimal of 95% measurements.

- Disappointingly, several factors could affect the testing accuracy such as proper and upright calibration of meter, optimum temperature and pressure changes for wiping off the strip, size, and quality of blood sample being screened, humidity, aging of test strips, and high levels of certain materials (such as ascorbic acid) in the blood. The model configurations vary in their implicit vulnerability to these

factors along with their inbuilt settings to either prevent or warn of the display of the inaccurate results with error messages.

- Recently, an improvised design of conventional Clarke Error Grid (a benchmark standard for analyzing and displaying the reading accuracy), Consensus Error Grid, has been introduced. The older glucometer models still mandate a coding with the used test strip lot failing that the accuracy of reading may tamper on a possible lacking calibration.
- Another pressing issue is the error in the displayed readings for hypoglycemic and hyperglycemic distinctions, wherein the apparent value of instantaneous blood glucose is generally perceived as greater for hypoglycemia than hyperglycemia. This issue has made the meters less useful, with precision and ratio of false-positive and -negative outcomes appearing as primary problems. Such constraints decipher a 15% or low imprecision extent as a limiting factor for hyperglycemic conditions. The working poses a slight distinction in the management of 200 and 260 mg•dL$^{-1}$ extents, wherein an error margin of 15% at a low glucose index manifests a greater ambiguity about glucose management.
- The above reference to imprecision is aggravated by the possible false-positive and -negative outcomes in diabetic and nondiabetic populations. The sufferers of type 1 diabetes in general exhibit a wider range of glucose extents, typically within (40–500) mg•dL$^{-1}$ and corresponding to (50–70) mg•dL$^{-1}$ reading, usually hypoglycemic symptoms are accompanied. So, there is a slight uncertainty about a "true positive" representing reading with accompanied minute harm analogous to its being a false positive. Nevertheless, the occurrence of hypoglycemia (for an unaware state), the associated autonomic failure, and faulty counterregulatory response confer greater reliability at low levels, as desperately urgent in type 1 diabetic patients, which is a comparatively rare possibility with the more common form, the type 2 diabetes.
- Contrary to the above, the error in readings of people not suffering from diabetes pertains to periodic hypoglycemia symptoms, which could also be a higher rate of false positives where the meter is rather inaccurate for a possible hypoglycemia diagnosis. The meter presumably provides occasional usefulness in monitoring severe hypoglycemia (such as congenital hyperinsulinism), corresponding to which average glucose in fastening remains $>$70 mg•dL$^{-1}$.

**Handheld pregnancy detection kit**: The first home pregnancy test came into emergence in 1976 when pregnancy tests have become the most common household diagnostic assay. The handheld pregnancy detection provision is a perfect instance of a portable and steadfast biosensor, wherein urine samples are screened for the presence of human chorionic gonadotropin (HCG) using Abs. The choice of HCG as a pregnancy marker pertains to its rapid and consistent rise in early pregnancy, which can be detected in urine. A typical configuration of a handheld pregnancy detection probe is well-equipped to provide women with reliable results just within a few weeks of pregnancy. The working of a pregnancy kit is based on the detection of HCG, which is produced very early in pregnancy by trophoblast cells. On implantation, the placenta begins to develop and generate increasing amounts of HCG,

which is screened in the laboratory and home pregnancy kits. For a fundamental understanding, one must be aware of the genesis factor for HCG as a screening agent to ascertain pregnancy, its features, and functions.

## 7.5 Rationale of Human Chorionic Gonadotropin Measurement for Pregnancy Detection

- The development of the very first biological assay for HCG-driven pregnancy detection can be traced back to 1927 and the combined work of Ascheim and Zondek. In the following 30 years, manifold variations in their procedure have been reported.
- One such modification reported by Tietz in 1965 evaluated the validity in frogs and noticed a 12% positive response in the first week after the missed period. The extent rose to 58 and 93% in the second and third weeks. On being studied in presumably more sensitive rabbits, the response extents of positivity were 77, 90, and 96%.
- A 1973 optimization attempt by Rees and colleagues demonstrate no serious trouble in devising the tests with a higher accuracy level in the first week itself, after the missed period. Nevertheless, a crucial concern of optimized bioassays pertains to cumbersome and expensive procedures that may consume several days before providing the results. Owing to the convenience and cost compromises, bioassays were superseded by immunoassays in 1960.

## 7.6 Biochemistry and Functions of Human Chorionic Gonadotropin

- Belonging to the family of glycoprotein hormones, HCG partners with luteinizing hormone (LH), follicle-stimulating hormone (FSH), and thyrotropin-stimulating hormone (TSH) as the other family members. Each of these hormones comprises two distinct subunits, the first being the 92 amino acid α-subunit, typically similar in all. However, the second subunit (β) makes up the distinctive features of each hormone. In HCG, the β subunit comprises 145 amino acids, with the first 121 N-terminal amino acids having a common involvement for 80% of the sequence with β-LH. Notably, the C-terminus of β-HCG harbors a 24 amino acid extension, unlike the LH. In general, both subunits perform important biological roles, although the specificity of action is determined by the β subunit. The α subunits encoded by a single gene on chromosome 6 while its β counterpart is encoded by a family of seven genes on chromosome 19 (Chard 1992).
- The bulk of HCG exists as intact (α-β dimer) in the human circulation, with only little extents of free α and β domains. Albeit in urine a major extent of material that participates in immunoassays for HCG is a metabolic fragment of the hormone, commonly known as β-core (Chard 1992). This further comprises

two polypeptide chains, derived from the β subunit of HCG, residing in the amino acid sequences 6–40 and 55–92, fused via disulfide bridges.

- The typical β subunit fragment lacks the prominent 30 amino acid carboxy-terminal peptide but does have the constitutional immunological determinants and intact free β subunit. Although significant amounts of β-HCG are located in the urine of pregnant women as well as in some cancer sufferers, it is untraceable in the serum. The rationale for the β-HCG secretion correlates it either via placental circulation after which it is spontaneously excreted by kidneys or anticipate its substantial generator as intracellular degradation of intact HCG β subunit in the renal parenchyma.

## 7.7 Functions of Human Chorionic Gonadotropin

- Typically, chorionic gonadotropin exhibits several biological actions and functions comparable to those of the pituitary luteinizing hormone. Usually, the trophoblast surrounding the blastocyst commences the HCG secretion in the maternal circulation, normally after a week of conception (implantation stage).
- Increasing extents of HCG in a mother's body confer a stimulus to the corpus luteum (CL, the autotrophic hypothesis). Contrary to this, a normal, nonpregnant menstrual cycle has the CL commencement as involuntary at this stage. Besides, the secretions of estradiol and progesterone are much less, resulting in endometrium loss.
- The CL continues to grow under the HCG influence and onsets with the secretion of increasing steroid quantity. Thus, HCG is the principal signal from an early pregnancy leading to CL rescue, postponed menses, and hence, the maintenance of pregnancy.

## 7.8 Human Chorionic Gonadotropin in Early Pregnancy

- In general, HCG detection in a mother's physiology can be done 8 days after conception. A titer of ~10 mI, U•ml$^{-1}$ is observed within the serum on the 9th and 10th days, after the follicular rupture. However, with gradual pregnancy development, the HCG count increases by ~50% per day extent. This reaches a saturation extent of ~100,000 mI, U•ml$^{-1}$ by the 10th week. Henceforth, the HCG secretion declines and slowly attains stability with an extent of ~20,000 mI, U•ml$^{-1}$ for the remaining pregnancy duration.
- Apart from being present in maternal serum, HCG can be detected in the urine of pregnant women, with appearance and rise exhibiting a similar variation as that of maternal circulation. From the ninth day post-conception, HCG concentration normally hovers around 0.93 mI, U•ml$^{-1}$ after which the HCG expression steadily increases and becomes maximum post 45 days of conception.
- Repetitive studies have inferred an increment in urinary HCG up to nearly 50%, wherein a significant uniformity is highlighted, irrespective of ethnicities. The

levels in early pregnancy (16th day onward following assisted reproductive technology) are significantly lower in women with a higher pre-pregnancy body mass index (BMI), which is believed to be due to the effect of adipose tissue-derived signaling molecules on HCG secretion by the implanting embryo.
- Inaccuracies and inconsistency in HCG concentrations could be due to poor recollection of women's LMP. This is supported by the observations of highly low regular monthly cycles (~32%) with a certainty of LMP date. The reasons attributed to this include early pregnancy bleeding, recent hormonal contraceptive use, or breastfeeding. On computing the HCG concentration through surges in LH that stimulate ovulation, this variability is eliminated.

## 7.9 Constitution of Workable Kit Configuration

- A handheld pregnancy kit is arguably the most used and successful protein detection device for pregnancy screening. The assay functions via lateral-flow immuno-chromatography. The typical working operation comprises a nitrocellulose (NC) membrane equipped with sample addition and adsorbent pads at its two terminals. A conjugate pad housing the monoclonal anti-HCG Ab bound with the due label (such as Au NP and the dye-doped polystyrene micro/nanosphere) is placed in between the NC membrane and the sample incorporation pad.
- In the immediate surroundings of the adsorbent pad NC membrane terminal, a test line and a control line, carrying antibodies against HCG and MAb, are immobilized over its surface, respectively. On adding the test urine sample to the sample addition pad, the sample moves toward the adsorbent pad via capillary action.
- The working configuration of the probe necessitates the capture of a dye label in both the test and control lines in the presence of HCG. In the absence of this, only the control line would appear as colored. It is worth noting for the readers that the kit provides a qualitative result that is visualized by naked eyes without a transducer involvement. However, lately, it has been possible to obtain a semi-quantitative result by incorporating a reflectance-based reader (Fig. 23).
- Recent attempts in this relation have aimed at the amalgamation of lateral flow immuno-chromatographic assays with electrochemical detection. A significant study by McNeil and accomplices herein reported the impedimetric detection of antigen–antibody interaction that prevailed on the test line. In place of a dye label, urease was used to label the motional phase of MAb. In course of the assay, urea solution was passed over the test line after the capture of MAb–urease conjugate, to get rid of nonspecific residual materials. Detection was ascertained by urease-driven hydrolysis that led to an increase in the pH. To monitor this, a pH-sensitive electrode was positioned over the test line, so that a pH variation caused a breakdown in the polymeric film and effected a detectable change in electrode capacitance.
- In an attempt to use labels other than those of enzyme, Lin and colleagues demonstrated a high-precision assay comprising QD label (CdS@ZnS), wherein

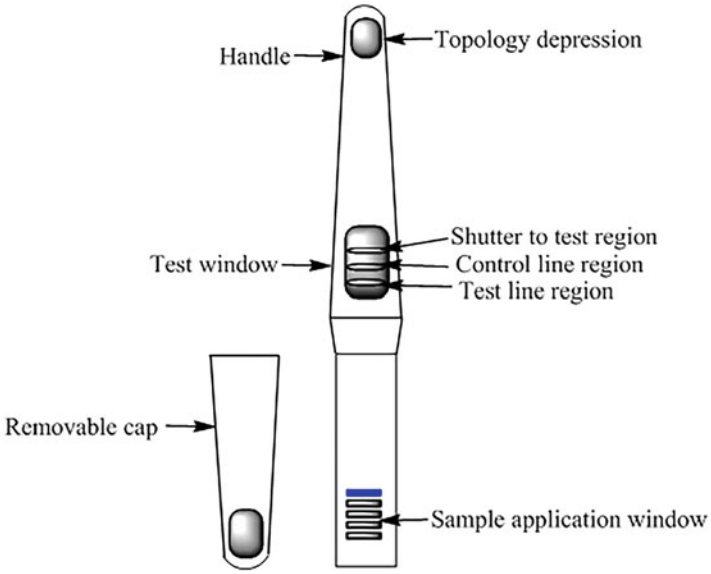


**Fig. 23** Working framework of a handheld pregnancy detection kit

electrochemical detection was made by the initial dissolution of QD via acidic functionalization. Analysis revealed the titer of cadmium ions via stripping voltammetric measurement using a disposable screen-printed electrode. Figure 25 depicts the positioning of this electrode below the test line. Investigators emphasized the rationale of the precise measurements using stripping voltammetric assays, making this technology more sensitive over reflectance-based sensing.

## 7.10 Cautions for Result Interpretation

- Often, it is perceived that pregnancy tests using portable kits are not reliable or are prone to giving negative results before the time of the first period. Nevertheless, a properly and sensitively conducted test with (25–50) IU•$L^{-1}$ sensitivity, a negative result from more than 1 week from the expected missed period can accurately identify the pregnancy.
- Thereby, a fair likelihood prevails of HCG levels in a woman being at the extremely lower end of the normal range leading to its nondetection. Alternatively, it could be possible that conception happened later than expected based on menstrual history. This residual ambiguity can be eliminated by repeating the test after 1 week.
- With current technology, it is quite unlikely to get a positive result in the absence of pregnancy. Still, false-positive results could be obtained, majorly in postmenopausal women. A faint probability mediates such possibilities that are due to low circulating HCG extents in nonpregnant subjects. Several times, it is a

coincidence that the screened HCG levels of the test sample do not fall within the instrumental range and are either low or excessively high. In such cases, the first result is indeed not positive. But a repetition of such issues has resulted in the generalization of $<5$ IU•l$^{-1}$ being confidently stated as negative while those with $>25$ IU•l$^{-1}$ can be confidently declared as positive. The intermediate values are inevitably a doubtful zone, and the values close to 25 IU•l$^{-1}$ need a retesting at the 2-day interval to assure positivity.

- Several factors have been described at varying time instants as the possible interfering agents in a pregnancy test. Such artifacts in the current generation of test kits could be deciphered from the fact that there is no drug or physiological state due to which well-designed ELISA analysis to be carried over a urine sample could be interfered with. A nonfollower herein is the case of a woman who has received HCG therapeutically, usually for ovulation induction. This is because the serum half-life of injected HCG follows a multiphase curve with initial rapid stages of 5 and 24 h, followed by a further moderation to 2.3 days. It is not surprising herewith that exogenous HCG may still be detected in urine up to 14 days after the last dose.
- Another untoward possibility pertains to higher HCG expression following intramuscular compared to subcutaneous injection. In such circumstances, the detection of HCG is not unbiased, and therefore, other tests are suggested. Secondly, in case a pregnant woman undergoes an abortion in the first trimester, it may take as long as 60 days for HCG levels to reduce to zero from the comparatively higher values after 7–10 weeks. Yet another highly rare possibility could be the fact that the screened woman may have an HCG-secreting tumor, gestational trophoblastic disease, a gonadal teratoma, or carcinoma with ectopic HCG secretion.
- Above all, it is highly essential to note that pregnancy or a positive test does not assure getting a baby 9 months later. The net loss of pregnancies between conception and term is highly significant. The modern test kit is more likely to result in a negative response for a pregnancy prediction. Usually, the earlier the pregnancy diagnosis, the more likely the abortion chances. Positive tests may even occur in the luteal phase of an otherwise normal cycle, wherein the pregnancy implants but usually aborts before the termination of the expected period. This kind of situation is also referred to as "occult" or more commonly as "biochemical pregnancy."

## 8 Recent Advances in Biosensor Development for Screening Some Critical Disorders

This section discusses the elect advances of the past 5 years focused on biosensors development of Alzheimer's disease (AD), cystic fibrosis (CF), and tuberculosis (TB). The selection of these diseases has been made based on the alarming adversity affecting healthcare in the recent past. Although this selection is not in its entirety, we believe a thorough understanding of functional principles *vis-a-vis* exclusive

pathogenic markers could be crucial toward accomplishing similar advances toward similar fatalities. All these diseases are known for more than three decades now and therefore population affected by them is quite high, owing to which we have chosen these to discuss whether the biosensors equipped with their prompt diagnosis could make a difference in their fatalities or could better the corrective response. Much has been talked about improving the therapeutic efficacy of delivered drugs in these disorders, and realizing which modified routes to prolong the drug therapeutic activities at the desired site is swiftly gaining momentum across the globe. The discussion does not intend to cover all the recent biosensors evidently, and the focus is more on the distinct configurations optimized via distinct probe modification including functionalization with NMs.

## 8.1 Alzheimer's Disease

- Prevailing as the most common aging disorder, AD has been a consistent element of interest for countless clinicians and scientists. Fundamentally possessing a neurodegenerative origin, AD may remain undistinguished by the affected patients and family members from conventional dementia as a part of the clinical syndrome. Even clinicians not having an exclusive specialization rely on default diagnosis for dementia-affected persons despite negative diagnostic tests. Nevertheless, to specialists, AD is an eventual outcome of cognitive decline and is lesser a diagnosis of exclusion but more a recognizable possibility.
- From a histopathological viewpoint, the extracellular amyloid plaques are the first defined signatures along with the intracellular neurofibrillary tangles (90% prevalence as per the post-AD identification by the pathologists). Perhaps, the hallmarks documented and reported more recently include synaptic degeneration, hippocampal neuronal loss, and aneuploidy. As a matter of interest, even nondemented elderly individuals have been screened by pathologists as to having positive AD signatures. This has led to the genesis of preclinical AD terminology that assumes preceding clinical changes by histopathological changes. Owing to this, a longer lifespan of preclinical AD sufferers is likely to result in dementia (the prevalence of histopathological changes). Though studies explore the reliability of this outcome using in vivo plaque and plaque-tangle imaging, to date consensus considers nondemented elderly cases as equivalent in terms of plaque burdens to those diagnosed clinically with AD.
- A second intriguing aspect of AD molecular biology is it is likely to occur in 95% of persons who are $>100$ years old. Perhaps, a 2005 study noticed some extent of AD histopathology in all the examined brains of $>85$-year-old patients (Polvikoski et al. 2006). Owing to this, there has been an anticipation of all long-living individuals to develop AD. Some yester studies established as many as (75–90)% centenarians of have dementia syndrome with (85–95)% meeting the least histopathological criterion. Thereby, it would not be surprising to

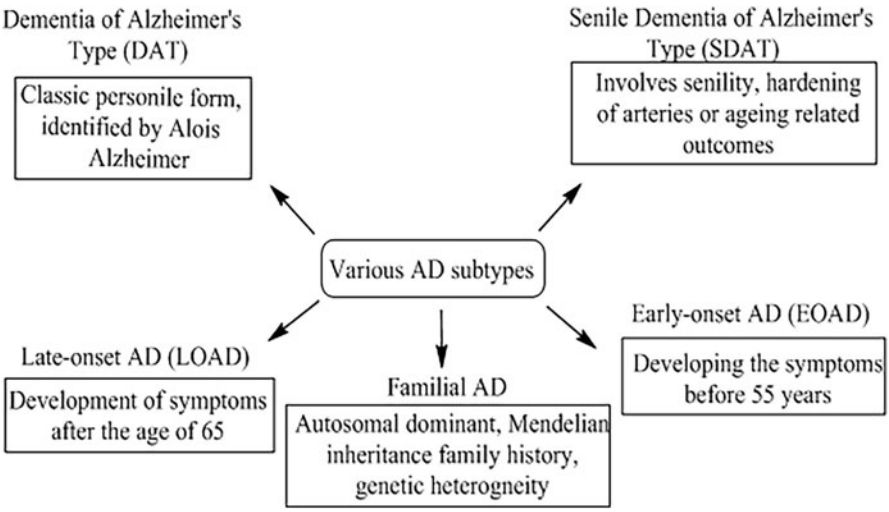


**Fig. 24** Characteristics of the various Alzheimer's disease subtypes

conclude that centenarians are expected to suffer from AD and presumably comprise an exception if they do not have that.

- Another oblivious concern herein relates to a common onset of age-related cognitive skill revival. Yester reports of neuropsychological origin predict that after adulthood attainment insidious cognitive variations begin to manifest. While such changes express through decades but generally represent a decline from the prior more active and adequate functioning contrary to progressive lateral shifts in cognitive strategies. Though such conditions do not pinpoint an AD possession, it would be a big mislead if one does not consider such outcomes as an indication of the AD continuum. The recent notion of mild cognitive impairment (MCI) resolves these issues to a certain extent, identifying a transitional state between normal cognition and dementia. Over the years of continuing improving molecular characterizations now rate MCI as the manifesting AD in their early recognizable extent. An analogous consideration herein is the age-associated cognitive decline (AACD), which exclusively encompasses "benign" cognitive changes.
- Ultimately, it is now considered a norm to include all dementia syndromes, manifested by plaque and tangle accumulation under the AD loop, leading to classify the various AD subtypes. Figure 24 depicts these subtypes, among which senile dementia of Alzheimer's type (SDAT) includes the individuals who have been diagnosed with selenity, hardening of arteries, or just exhibiting an advanced age (since the 1970s). Late-onset AD (LOAD) includes all those sufferers possessing signs and symptoms post 65 years of age. Early-onset AD (EOAD) loosely includes those sufferers who develop signs or symptoms before 55, 60, or 65 years of age. Here, the exact upper age limit is variably defined. Familial AD includes individuals having an autosomal-dominant family history. Though autosomal-dominant inheritance patterns are rare (even among early-onset

cases), the FAD cases prevail with genetic heterogeneity, spanning the mutations in amyloid precursor protein (APP) (located on chromosome 21), presenilin 1 (located on chromosome 14), or presenilin 2 (located on chromosome 1).

## 8.2 Biomarkers and Biosensor-Mediated Early Detection

- As of now, no reliable peripheral and exclusive biomarkers for AD are known for their discrete identification via histological inspection of the brain amidst autopsy. Inspection using PET using the C11-labeled Pittsburg Compound B (a thioflavin T derivative that selectively binds amyloid-β) has resulted in contrasting outcomes.
- Senile plaques and NFTs residing inside the diseased brain are the ubiquitous detection markers for AD screening. Recent efforts have improved the understanding of senile plaques, gradually characterized via manifold subtypes, such as diffused, primitive, neuritic, compact core, and cotton wool. Of these, the neuritic plaques have been screened as pathologically most relevant, many times compared with plaque possession, a consensus aspect for AD diagnosis at the time of autopsy. Readers must note here that as per the CREAD guideline (commonly used plaque relying regulation), standardized brain regions are examined through Bielschowsky silver methodology, typically a nonspecific impregnation responding to all plaque morphologies.
- NFT represents the other major hallmark, occasionally referred to as globose and pretangles, although NFT is not semiquantitative in the standard criteria but prevails under the influence of location-specific residence within the brain. A detailed and more rigorous characterization of a typical AD brain using phosphor-Tau Abs and some other closely related lesions comprise neuropil threads (thread similar phospho-Tau accumulations within neuropil of gray and white matters), and dystrophic neuritis (terminal neuritic swellings) residing within the neuritic plaques.
- Other phenotypes characteristically associated with AD include neuronal and dendritic loss, neuropil threads, dystrophic neurites, granulovacuolar degeneration, Hirano bodies, and cerebrovascular amyloid. The synapse loss was described several years back but has been an exclusive finding in recent literature sources. The more commonly noted "synapse loss" is the most specific identifying feature of AD, thanks to the recent increase in the attempts to link the synapse loss with low n-soluble Aβ. Readers must note herein that inspection of synapse via immunohistochemistry or electron microscopy has no role in AD diagnosis at autopsy, irrespective of its significant association with Aβ or the more general, Tau species.
- A serious issue in distinctive AD identification pertains to the distinction between the pathology of AD and that of aging, in particular, among elderly persons. A recent study highlighting this analyzed the clinical diagnosis with the pathological findings, wherein neuropathologists were blinded to clinical data and observed 76% of cognitively intact elderly brains as AD brains. The identification

of lesions has been an AD hallmark since its 1907 description. The plaque constituent was more stringently associated with senile dementia, even when AD diagnosis was not known. The senile plaque and NFT lesions undoubtedly remain the associated factors for Ad diagnosis, with several other changes also being known that are comparatively less specific (granulovascular degeneration, Hirano bodies, pathologically noninterpretable synapse loss). The clarity on the spectrum of diseases in different age groups enhanced over the years with lesions assuming more and more significance. In 1985, the Khachaturian criterion made this distinction entirely quantitative, with older patients requiring more lesions to confirm the Ad diagnosis. The association was based on the fact that the cases having a positive clinical history might have lesions reduced to half. The identification was finally registered by a consortium after several years, with an intent to facilitate research, establish databases, and simplify the diagnosis procedures, wherein plaques were coined as the most significant factors and for the elderly, more plaques were regarded as the confirming factor. This led to the analysis assuming a semiquantitative version, with the responses of "no, possible, probable, or definite." Herein, the "no and possible" criterion could be deciphered with assumptions that either the older brain is more tolerant of pathological lesions or the lesions have nothing to do with etiology. The fact that both possibilities could not be true at the same time emerged as a mathematical certainty.

- Almost at the same stage, the Braak and Braak criteria came into recognition, which relied more on NFT instead of a senile plaque. These guidelines encompassed comparatively more sophisticated neuroanatomy that was designed as being useful even to those having little or no knowledge. Furthermore, the cases considered while framing these guidelines comprised both demented individuals as well as aged controls, whereas the staging was made irrespective of the disease extent. Keeping this in mind, Braak and Braak noticed neurofibrillary degeneration to proceed in a stepwise manner, from the transentorhinal area (neuronal cells in medial temporal lobe bridge, entorhinal cortex, and temporal neocortex) (stages I and II), to limbic regions (stages II–IV), to isocortical regions (stages V and VI). On being compared to clinical data, the majority of stage I–II cases were revealed as free of cognitive impairment while those from stage V–VI exhibited cognitive impairment. Interestingly, the stage III–IV patients remained more or less evenly distributed within dementia-positive and -negative outcomes. This analysis created apprehensions regarding considering the Braak stage I–II subjects as AD positive. Despite such conflicts, the involvement of neurofibrillary pathology along with a significant neurofibrillary pathology and clinical disease correlation, most neuropathologists favor the Braak approach over the CERAd criterion.
- Relatively more recent NIA-Reagan criteria compromise the CERAD (supporting amyloid cascade) and Braak considerations (primacy of phosphorylated Tau), depending on the pathological extent, and divide the cases into "low likelihood," "immediate likelihood," and "high likelihood" of AD.

The following sections describe the major results of select studies focused on early AD diagnosis using biosensor technology collected from PubMed and features from 2016 to date.

- Realizing the significance of amyloid-beta peptide 42 (Aβ42) as a recognition marker of AD manifestation, Li and colleagues designed a reusable biosensor having magnetically sensitive nitrogen-doped graphene (MNG)-modified Au electrode as the detection surface. The Abs of Aβ1-28 configuration is used as the Aβ42-specific biorecognition element, which was conjugated on the MNG surface. The sensing framework could be robustly made using MNP-coated MNGs, whereby the need for electrode drying could be bypassed, reducing the analysis time and simplifying the overall detection mechanism. The developed configuration exhibited significant reusability with good reproducibility and stability and exhibited a linear correlation within the (5–800) $pg{\bullet}ml^{-1}$ range. The cut-off extent for Aβ42 was well-resolved with a 5 $pg{\bullet}ml^{-1}$ LOD. Briefly, the superparamagnetic magnetite ($Fe_3O_4$) NPs are deposited over nitrogen-doped graphene to form MNG. The MNG surface was labeled with anti-Aβ Abs via sulfosuccinimidyl-4-(*N*-maleimidomethyl)cyclohexane-1-carboxylate (sulfo-SMCC) cross-linking method to form magnetic immunocarriers (Aβ-MNG). Thereafter, the magnetic immunocarriers were dropped over the Au electrode, leading to their entrapment via placing an external magnet beneath the electrode to facilitate electrochemical Aβ detection. Besides improving the detection efficacy, the optimized configuration also moderated the costs and response time, projecting its diagnostic usefulness (Li et al. 2016).
- Through another significant attempt, Azimzadeh and their team developed an ultrasensitive electrochemical nanobiosensor optimized for miR-137 quantification as a distinct AD biomarker. The designed configuration involved electrochemically reduced graphene oxide (ERGO) and Au nanowires to modify the surface of SPCE after the application of an intercalated label, doxorubicin. The fabrication steps were rigorously analyzed using field emission scanning electron microscopy (FE-SEM), energy-dispersive spectroscopy (EDS), cyclic voltammetry (CV), and EIS. It was found that the sensor worked well within the (5–750) fM linear range with 1.7 fM as LOD. Besides, the sensor also exhibited a significant specificity of working, distinguishing the target oligomers from the nonspecific counterparts (nonspecific targets being miR-21 and miR-155) very well. Inspection of working configuration in human serum revealed its potential significance for prompt feasible and robust AD detection (Azimzadeh et al. 2017).
- Another significant 2017 attempt by Yoo and associates involved the design of an IME sensor for impedimetric Aβ protein detection from the blood. The sensing probe was fabricated through a surface micromachining approach, capable of detecting tens to hundreds of $pg{\bullet}ml^{-1}$Aβ contents via medium change from plasma to PBS buffer with signal cancellation and amplification processing (SCAP) configuration. The maintenance of stability amidst medium change was accomplished using a steadfast Ab immobilization method. The probe displayed

significant Aβ detection selectivity due to the specific Aβ affinity to the screening Ab at varying concentrations. To synchronize with the optimized functioning, the medium change was optimized concerning optimized absolute impedance change and differentiated impedance variations for real-scale plasma Aβ detection. The output signal processing system of the developed probe was designed for performance optimization and enhancement of signal interaction between recognition and target materials with cancellation and amplification functions for nullifying the parasitic capacitance, error, and noise. The optimized configuration discriminated the Aβ levels between Aβ protein precursor/presenilin 1 (APP/PS1) transgenic mice and wild-type (normal) mice through screening the Aβ extents in plasma with high sensitivity and reproducibility (Yoo et al. 2017).

- Another notable attempt by Qin and associates designed a label and Ab-free electrochemical biosensor for the exclusive detection of amyloid-beta oligomers (AβO) using an electrically conductive poly(pyrrole-2-carboxylic acid) linking agent and prion protein ($PrP^c$) receptor. The $PrP^c$ was modified to have an $–NH_2$ group terminal that facilitated a covalent linkage with the –COOH group of PPy. The PPyCOOH (poly(pyrrole-2-carboxylic acid)) was electrochemically deposited on Au substrate and subsequently used for immobilizing $PrP^c$. To ensure the effectiveness of the conductive linking agent, a nonconductive self-assembled monolayer (SAM) of 3-mercaptopropionic acid (MPA) was layered on Au substrate to immobilize with $–NH_2$-terminated $PrP^c$. The working principle of optimized configuration was based on the fact that any change in electron transfer through SAM on the electrode surface would be reflected through varied sensor responses. The configuration sensitively detected the Aβ oligomer and developed an insignificant response to the Aβ monomer and fibrils. The working configuration of the sensor was stepwise optimized using EIS and CV, revealing a $10^{-4}$ pM LOD. To validate the specificity, the designed biosensor estimated AβO levels in cerebrospinal fluid of AD-infected mice, the results of which confirmed an accurate and selective detection at sub-pM extents (Qin et al. 2018).
- In a 2019 study from China, Zhang and associates designed an artificial peptide nanonetwork biosensor to combat its natural contemporary pathological peptide aggregates by mimicking their pathogenic response. Precisely, periphery platelet configuration is capable of secreting Aβ and further induced its cross-linking and aggregation to form a surface peptide nanonetwork. The outcome of such a response was the manifold poly-tyrosine strands that were covalently trapped within the network and served as efficient signal amplifiers through electrochemical oxidation of tyrosine. The method is relatively unique, sensitive, and bears proximity to stress-aggravating Aβ configurations. The designed probe enabled a quantitative distinction of normal and pathological periphery platelet distribution, whereby the AD patients could be effectively discriminated through the screened neurodegenerating platelet functioning. The optimized configuration responded well to clinical blood samples and exhibited a larger dynamic range and a lower LOD compared to ELISA. The signal-amplifying ability of covalently trapped poly-tyrosine strands made the fabricated biosensor significantly better than label-free methods (Zhang et al. 2019a).

- Another benign 2019 attempt by Negahdary and the group fabricated a highly sensitive, eco-friendly, and robust aptasensor for Aβ quantification through electrochemical transduction ability of fern leaf similar to Au nanoassembly. This assembly was synthesized by the investigators through electrodeposition using PEG 6000 as a shape-directive agent. The functioning of this probe was characterized both electrochemically and by FE-SEM. The working configuration involved the detection of Aβ binding on a specific RNA aptamer immobilized on the Au nanoassembly using ferro/ferricyanide as a redox marker. The optimized configuration detected Aβ within the (0.002–1.28) ng•ml$^{-1}$ linear range, corresponding to an LOD of 0.4 pg•ml$^{-1}$. The designed configuration functioned well (ruling out any sort of interference), and for assessing the functioning in real samples, human blood serum and artificial cerebrospinal fluid containing Aβ were analyzed (Negahdary and Heli 2019).
- The most recent attempt toward biosensor-mediated early AD diagnosis is a 2020 study by Park and colleagues, who optimized an ultrasensitive and multiplexed detection of $A\beta_{1-42}$ and t-Tau (both prominent AD biomarkers) in biological fluids using a reduced graphene oxide field-effect transistor (gFET). The FET was made by growing a 300 nm $SiO_2$ layer through thermal oxidation on 4-in p-type Si wafers. The $SiO_2$ substrates were cleaned (30 min treatment with a 3:1 $H_2SO_4$ and $H_2O_2$ solution) and surface activated using high-density –OH functional groups. The cleaned surfaces were then treated with 1%, 3-(ethoxydimethylsilyl)propylamine diluted in ethanol for 1 h to give rise to $–NH_2$ linkage. A GO solution was separately prepared using modified Hummer's method and, after being dispersed in water, was spin-coated on APMES-treated $SiO_2$ substrate at 500 rpm for 5 s and 3000 rpm for 60 s. This ensured a strong adhesion through electrostatic interaction between the $–NH_2$ group (of APMES SAM) and –COOH group on GO flakes. The GO thin films were reduced through treatment with HCl vapor at 80 °C for 3 h before being patterned via photolithography and reactive ion etching (RIE) to achieve (40 × 80 μm) dimensions. Lastly, the patterned drain and source electrodes were passivated using a stable SU-8 photoresist, resulting in the partial opening of rGO active layer. The optimized configuration functioned well and enabled a linear detection within ($10^{-1}$ to $10^{-5}$) pg•ml$^{-1}$ and a femtomolar LOD in biofluids (human plasma and artificial cerebrospinal fluid) as well as PBS. Secondly, the screened biomarkers possessed distinct surface charges in the physiological environment based on isoelectric point, leading to the foundation for achieving a distinct biomarker-specific output signal (Park et al. 2020).

## 8.3 Cystic Fibrosis

- CF is the most common autosomal-recessive cause of early mortality in Caucasians across the globe, wherein the occurrence frequency is close to 1 among 3000–4000 live births. Nearly 1 in (25–30) Caucasians are the carriers of pathogenic mutation of the CFTR gene. In the United States, as many as 1000

individuals are diagnosed with CF each year. Before the presently followed newborn screening (NBS), the CF diagnosis proceeded either through symptomatic presentation or via family history. In 2004, the Centre for Diseases Control and Prevention (CDC) recommended all states implement the NBS for CF, which resulted in diagnosed extent being enhanced to 2/3rd of all cases. Surveys and databases reveal the NBS-driven early CF diagnosis as the factor behind improved nutritional outcomes that further resulted in improved pulmonary functioning.

- Lung disease is the major source of morbidity and mortality in CF-affected persons, characterized by the most commonly tracked parameter of exhaled air volume in the first second of forced exhalation ($FEV_1$). Depending on age, gender, race, and height, the $FEV_1$ can be measured at the earliest in children approaching school age. Children below 6 years are uncertain for reliable spirometry, along with a poor $FEV_1$ sensitivity for early CF. The noted complementary tests that compensate for these hurdles include infant pulmonary function tests (PFTs), chest imaging, and lung clearance index (LCI), a parameter that identifies abnormalities in the ventilation distribution. Monitoring of such measures by the collaborative efforts of the Australian Respiratory Early Surveillance Team for CF and London CF Collaborative has revealed a nonsuitability of PFT in nearly 25% of 3-month-olds and as much as 50% of 2-year-olds suffering from CF. LCI is abnormal even in 3-month-old children, wherein the early abnormalities are likely to be related to subsequent abnormalities on chest CT scans and are likely to be stronger in abnormality than traditional spirometry in early school years. Thus far, it is highly urgent to search for authentic and reliable early-stage CF detection procedures that could strengthen the treatment efficacy alongside moderating mortality.
- Chronic endobronchial infections have been viciously recognized as contributing factors to CF morbidity and mortality. The recognition of pro-inflammatory organisms, including *Pseudomonas aeruginosa*, *Staphylococcus aureus*, *Haemophilus influenza*, *Streptococcus pneumonia*, and *Aspergillus* species, in the first 2 years is associated with worse spirometry in school-going children. *S. aureus* is usually the first respiratory pathogen identified in respiratory secretions of young children suffering from CF, albeit there remains controversy regarding the treatment via antibiotic prophylaxis. In adults infected with CF, *P. aeruginosa* is the most commonly encountered pathogen with its mucoid phenotype playing a decisive role in the manifestation of lung disease. In recent years, *P. aeruginosa* prevalence has been signed in a decline, which could be due to improved control of infection. The methicillin-resistant *S. aureus* is usually associated with deteriorating lung disease with increased mortality. There has been a consistent increment in its existence over the past two decades, similar to that of the non-CF population. Similarly, the *Burkholderia cepacia* complex prevalence has decreased, whereas that of non-tuberculous *Mycobacteria* has increased since 2010. The recent emergence of bacterial detection techniques that do not rely on routine microbial culture assays has identified the diversity and complexity of microbes invading the CF-infected airways.

- Apart from poor nutrition and progressively critical lung diseases, many other manifestations including CFTR dysfunctioning, wherein chronic sinusitis is reported in 30% of all CF patients, lead to poor life quality and require surgical intervention for elimination. Likewise, liver disease is known to affect (15–30)% of CF sufferers with an associated minimal clinical consequence, although, if ignored, it may lead to cirrhosis, along with a liver transplant requirement in severe cases.
- A positive correlation has been noted for CF-related diabetes (CFRD) with progressive aging of patients and gradual destruction of pancreatic islet cells, culminating in insulin deficiency. Lately, CFRD has been associated with more severe lung disease, frequent pulmonary exacerbations, and poor nutritional status. Familiar observations in CF sufferers and their caretakers are depression and anxiety, as a caution of which routine screening is unanimously suggested. The typical presence of depression or anxiety is usually associated with suppressed adherence, enhanced pulmonary exacerbations, and worsened lung disorders. The CF complications are more common in individuals having severe genotypes and pancreatic inactivity. The sufferers with mild cystic fibrosis transmembrane conductance regulator (CFTR) gene mutations are typically pancreatic okay with no demonstrable lung diseases or at least having displayed a multitude of measurable abnormalities. Such individuals may suffer from male infertility or recurrent/chronic pancreatitis.
- The most observed cause of CF to date are the mutations in the gene encoding CFTR protein, an ion channel regulating chloride, bicarbonate, sodium, and fluid fluxes at epithelial surfaces. CF lung disease is identified through impaired ion transport, mucociliary clearance, inflammation, bacterial infection, and airway remodeling, together resulting in bronchiectasis and respiratory failure. CFTR may also cause intrinsic abnormalities in host defense cells, including epithelia, neutrophils, and macrophages.
- Change in $FEV_1$ has emerged as the most well-known endpoint for demonstrating the clinical efficacy of CF clinical trials. Pulmonary exacerbations also serve as primary clinical efficacy endpoints, but generally require elaborate analysis to demonstrate the treatment impact. The notable secondary measures that have supported approval and clinical use of pulmonary therapies include patient-reported outcomes, weight gain, and bacterial density. Surprisingly, to date, no CF-implicit anti-inflammatory drug has been accorded regulatory approval, whereby knowledge about accepted clinical efficacy measures for these agents is relatively scarce.
- Concerning ionic movement, sweat chloride titer, nasal potential difference (NPD), and intestinal current measurement (ICM) are the major in vivo biomarkers to ascertain the normalcy of CFTR functioning. Of these, sweat chloride is a comparatively easier, portable, and reliable procedure to screen the CFTR operation and discriminate the patients based on minimal, partial, and complete CFTR functions. This method is entirely standardized for clinical applications and is being studied in multiple clinical trials, comprising a formidable mechanism of CF diagnosis. The quantified CFTR functions by the sweat chloride test

are ably supported by the altered titers of prominent markers for disease severity, viz., age at the time of diagnosis, pancreatic stability, isolated male fertility, and the typical lung disease severity. Nearly all studies of ivacaftor monotherapy in CF patients (having a gating abnormality) exhibit considerable reductions in sweat chloride. Erstwhile investigations in this reference have reported intermediate effects for ivacaftor in CF sufferers having R117H mutation while moderate consequences were observed in the patients having two copies of F508del CFTR mutation. In general, the consequences of CFTR modulators on the sweat chloride test remain analogous to the clinical benefits for minimal, partial, and complete CFTR functioning. Though discrete variations in sweat chloride have not been yet directly correlated with FEV1 improvements, available aggregate observations signify a distinctly improved assay performance for detaining the biological activity.

- NPD is a direct measurement source of CFTR functioning in the respiratory epithelium, isolating CFTR activity across the nasal mucosa independent of sodium transport and the functioning of other chloride transporters. In general, the NPD is more difficult to perform than the sweat chloride test and mandates a need for specialized equipment and specific training. Recent interests have standardized the NPD performance and analysis across the United States and Europe, driven through SOPs and centralized coordination and interpretation of trial data. The standardized NPD has been incorporated into small investigator-initiated CFTR, other ion transport modulator trials, and also onto the early-phase trials of CFTR modulators for which regulatory approval needs to be sought. In multicenter trials, NPD assessments exhibited adequate sensitivity to detect dose-dependent ivacaftor bioactivity in patients possessing the G551D CFTR mutation but could not detect the bioactivity of systemic ataluren or lower dose lumacaftor monotherapy in phase 2 and 3 studies conducted on patients having PTC and F508del mutations, respectively. Neither of the attempted interventions could enhance the clinical benefits to a measurable level, inferring the specificity for clinically relevant modulator bioactivity.
- Another assay equipped with the elimination of CFTR functioning is the ICM, exhibiting the distinction of a large dynamic range between CF and non-CF. The typical working comprises a dissection of rectal biopsies that are subsequently analyzed using chambers to monitor the CFTR-dependent ion transport in the ex vivo conditions. Akin to NPD, many illustrious efforts are presently being made to obtain standardized ICM performance and practical suitability, currently in the phase of a universal SOP development by the European centers and US clinical laboratories for centralized data interpretation. An added advantage of ICM is its discrimination of variable extents of CFTR defects, typically based on the characteristic CFTR genotype (nonfunctional, partial, and fully functional) with clinical correlates emerging dependent on CFTR expression. The applicability of an ICM assay is restricted to centers with expertise in electrophysiological measurements. These restrictions have reduced the ICM screening as an early phase CFTR biomarker in molecular diagnosis.

- **Biomarkers of infection**: Markers in this domain pertain to viral and fungal infections, wherein infection by some defined bacterial species (mentioned before) results in CF morbidity and mortality. Most evident infection biomarkers reside in the lower respiratory tract (bronchoalveolar lavage, BAL fluid, sputum) while other sources including cough swabs, oropharyngeal swabs, and nasopharyngeal samples are used in nonexpectant patients. The inconclusive sensitivity and specificity for lower airway tract infection generally limit their applicability in drug development.
- Frequently analyzed markers for antimicrobial rationale are the bacterial density (determined in $cfu \bullet g^{-1}$ for sputum while in $cfu \bullet ml^{-1}$ for BAL fluid) and the monitored CF pathogens (primary or secondary endpoints). As of now, the chronic *Pseudomonas* infection-ramifying drugs have been approved by the regulatory agencies, working via reduced microbial density as its endpoint. In several trials, variations in FEV1 are noted as the primary endpoint that may not coincide with the decrements in *Pseudomonas* density. Lately though, targeted PCR-facilitated detection (used for viruses) is being improvised upon for an accurate quantitative estimation of CF bacteria. Detection panels for repeatedly infecting bacterial species are being standardized, relying on the prospect that bacterial enzymes or virulence factors may aid in the early detection of resisted responses.

- **Biomarkers of inflammation**: Markers of this category are suspected to play decisive roles in the development of anti-inflammatory drugs that shape the downstream improvements in CF lung disease for disease modification. These markers could be used in early-phase studies to confirm the known action mechanism of drug candidates. The studies made via yester CF clinical trials convey that anti-inflammatory therapies may not induce immediate improvements in pulmonary function and can only moderate the deteriorating lung functioning. The conventional method to monitor CF lung inflammation is through bronchoscopy using BAL. BAL inflammatory markers have been used as clinical endpoints in pathophysiological investigations and clinical trials of inhaled tobramycin as well as recombinant human DNAse. The bottlenecks of using bronchoscopy (recently recommended by the European CF Society Clinical Trial Network for limiting the use to early-phase clinical trials) have rendered blood and sputum as the commonly collected biospecimens for assessing inflammation.
- Spontaneous sputum expectoration is generally confined to screening the more advanced lung disease (in adolescents and adults). Sputum induction (inhalation of hypertonic saline) improves the sample obtained in the sufferers who do not normally expectorate the sputum; the biomarker assessments are generally comparable in both cases. Noted sputum biomarkers for CF are neutrophil elastase (NE), whose activity provides an idea about the bronchiectasis in CF, and predicts a possibility of likelihood future lung deterioration. The NE assessment has been a consistent indicator of treatment response to pulmonary exacerbations,

emerging significant to ascertain a future risk too. Elevated BAL NE also serves as a predictive biomarker of impaired lung functioning and bronchiectasis in young children suffering from CF. Other noted sputum biomarkers significant toward CF clinical aspects include calprotectin, myeloperoxidase, high-mobility group box 1, and YKL-40. Though sputum markers have been known for long, recent conflicts in their observations for a possible CF possession make it challenging to rely upon them *vis-a-vis* drug evaluation for shorter periods. The sputum biomarkers therefore would only be sufficient for their sensitivity to anti-inflammatory effects in longer trials.

- Reliance on systemic inflammatory biomarkers has been a recent upsurge owing to easier standardized, repeatable, age and disease severity-dependence moderate blood measurements. Systemic inflammation may also link pulmonary and non-pulmonary CF morbidities, although the availability of data linking systemic inflammation with clinical outcomes in CF is scarce. A considerable variation in circulating biomarkers (contrary to sputum biomarkers) of inflammation after exacerbation treatment is a vital inference of a higher sensitivity of systemic inflammatory signatures, highlighting their usefulness in short-term interventional studies aimed at mitigating exacerbations. For example, a multicenter exacerbation study noted suppressed serum CRP, amyloid A, and calprotectin expressions in response to azithromycin treatment during a CF interventional trial. The reductions correlated well with improvised lung functioning and weight gain, suggesting the changes to be associated with clinically meaningful outcomes. Other potential systemic biomarkers relating clinical status to CF outcomes comprise neutrophil elastase antiprotease complexes, several cytokines such as IL-6, IgG, and circulating mononuclear cell RNA transcripts. Readers are suggested to have a look at more focused literature sources to know about the further possibilities of improving the biomarker-predictive CF intensity and the possible future challenges. The following points discuss the salient biosensor mediated earlier and faster CF diagnosis of the recent past.
- In a noted attempt in 2015, the study by Toren and associates proposed a microtoroid surface (as a biosensor) for screening the early-stage bacterial mutations. The specific context referred to herein was for screening the DNA alterations of *Pseudomonas aeruginosa*, the major CF pathogen that suffers from a poor prognosis through manifested mutations in course of virulence and drug-resistance development. The optimized configuration involved the fabrication of high-quality factors microtoroids, after which their surfaces were coated with 3-aminopropyl triethoxysilane (APTES)/trimethyl methoxy silane (TMMS)-mixed silane solution. Subsequently, the engineered toroid surfaces were again coated with EDC/NHS linkages to facilitate the covalent conjugation of DNA probes. Nonspecific interactions were prevented through ethanolamine capping while the homogenous functionalization of the toroid surface was inferred from confocal studies. The bacterial DNA hybridization at each step was observed as dependent on probe length, where a significant response of nearly 22 pm was obtained in response to the complementary strand of mutated *P. aeruginosa* DNA, while that toward the mismatched strand was substantially low and late (~5 pm).

The LOD for the complementary strand was 2.32 nM, whereas no significant response toward the noncomplementary strand was developed. Thereby, it was validated that engineered microtoroid surfaces were capable of distinguishing DNA alterations and CF-specific *Pseudomonas* recognition (Toren et al. 2015).

- In a 2018 study reported from Saudi Arabia, Eissa and colleagues proposed a multiplexed biosensor for the detection of hyper immunoglobulin E syndromes (HIES), the rare immunodeficiency disorder. The biosensor working domain spanned a simultaneous detection of signal transducer and activator of transcription 3 (STAT3), dedicator of cytokinesis 8 (DOCK8), and phosphoglucomutase 3 (PGM3) proteins. The sensing probe was constructed on carbon array electrodes that were initially modified through electrodeposition of Au NPs. The array electrodes were thereafter used to immobilize specific Abs for the three proteins after the electrode functionalization with cysteamine/glutaraldehyde linkers. The sensor enabled simultaneous detection of DOCK8, PGM3, and STAT3 proteins with the respective limits of 3.1, 2.2, and 3.5 pg•ml$^{-1}$. The sensing exhibited good selectivity and sensitivity toward other proteins (along with DOCK8, PGM3, and STAT3), that is, CFTR and Duchenne muscular dystrophy (DMD). The sensor also displayed a distinctive HIES identification from human serum. So, although the designed configuration was not aimed toward screening CF, the identification of CFTR protein attributes to its ability for efficient screening of CF (Eissa et al. 2018b).
- Another attempt from a similar research group demonstrated a disposable carbon nanofiber (CNF)-based electrochemical immunosensor for simultaneous detection of survival motor neuron 1 (SMN1), CFTR, and DMD proteins. The intent behind choosing these analytes was to accomplish a point-of-care detection mechanism for identifying the specific biomarkers of spinal muscular atrophy (SMA), CF, and DMD, all hereditary disorders possessing rising morbidity and mortality. To design the biosensor, initially, the CNF-modified array electrodes were functionalized by the electroreduction of a carboxyphenyl diazonium salt. Thereafter, the sensing probe was designed through a covalent immobilization of three Abs on the working electrodes via EDC/NHS chemistry. The optimized configuration enabled simultaneous detection of CFTR, DMD, and SMN1 with high sensitivity and 0.9, 0.7, and 0.74 pg•ml$^{-1}$ LOD. Apart from this, the sensor also enabled a high recovery percentage on being applied to spiked whole blood samples. Thus, the voltammetric immunosensor configuration provided a cost-effective, easy-to-use, rapid and high-throughput SMA, CF, and DMD detection using merely a few blood drops (Eissa et al. 2018a).
- A second attempt from the Toren research group is a 2018 study that featured in *ACS Sensors* and aimed at the early detection of pathogens or their virulence factors in complex media, suspecting its key role in the early diagnosis and treatment of multiple diseases. The working configuration enabled a nanomolar-selective Exotoxin A, a virulence factor secreted by *Pseudomonas aeruginosa* in the sputum of CF patients. The study described an account of preliminary investigation toward the feasibility evaluation of optical sensing of *P. aeruginosa* in diluted artificial sputum, which mimicked the CF respiratory

environment. The probe design enabled a high-throughput screening by exploiting anti-Exotoxin A-conjugated microtoroidal optical resonators. The optimized surface engineering enabled an effective biointerface toward a highly selective Exotoxin A detection in the complex media using monoclonal anti-Exotoxin A-functionalized microtoroids. The engineered surface was screened as highly resistive to other sputum constituents and enabled exclusive Exotoxin A identification with reproducible measurements, with an LOD of 2.45 nM (Toren et al. 2018).

- A recent attempt from 2020 is a study by Ghaderinezhad and his group, who fabricated a paper-based sensor for quantitative screening of sodium, potassium, calcium, chloride, and nitrite in the urine. The designed sensor configuration was quantified using a smartphone-enabled platform. The probe comprised of a fluorescent-sensitive platform for $Na^{+}$, $K^{+}$, and $Ca^{+2}$ detection and a colorimetric method for $Cl^{-}$ and $NO_2^{-}$ detection. To make the biosensor, the reagents were added to a paper matrix after which the sample was deposited. This was succeeded by reading the fluorescent and color intensities for quantifying the target ion concentration. The application screening of the optimized configuration enabled the $Na^{+}$, $K^{+}$, and $Ca^{+2}$ estimation in their physiological extents, $Cl^{-}$ from 50 to 300 mM and $NO_2^{-}$ from 0.05 to 2 mM in the artificial urine (Ghaderinezhad et al. 2020).

## 8.4 Tuberculosis

- One of the most dreaded life-threatening disorders, tuberculosis (TN) is caused by *Mycobacterium tuberculosis* (Mtb) and is transmitted by aerosols released from the upper respiratory tract of an infected person to a healthy counterpart. As per the WHO 2016 global TB report, 10.4 million TB cases were reported across the globe in 2015, of which 1.8 million died in the same year. More startlingly, as much as one-third of the world's population is presently infected with Mtb bacilli. It is a further concerning aspect that despite registering a 22% decline in TB deaths during 2000–2015 the disease remains well-settled among the top 10 leading causes of death across the world.
- The exclusive traits of Gram-negative bacillus, Mtb, make TB one of the major prevalent diseases at present. TB can remain in a dormant state for years without expressing symptoms or getting spread to other subjects, but immediately after a host-immune system is weakened, the bacteria become active and exclusively affects the lungs and other body parts.
- The TB sufferers are further aggravated owing to the immune system affecting illnesses that affects the immune system, such as HIV, whose condition is highly precarious in many developing and underdeveloped economies of the world. The bacilli exist in the lungs in the instant just after entering a host's body, when they are contained by the host's immune system, resulting in moderation and latency of infection, without noticeable symptoms. That's why early diagnosis and

treatment of latent TB infection is a pivotal step in TB cure and is a decisive factor for preventing the dissemination to healthy individuals.

- The major obstacles to successful field detection and treatment of TB are spearheaded by the omnipresence of pathogens and diseases across different continents, thereby complicating the management and eradication programs. Interestingly, nearly 98% of reported cases are from developing countries, resulting in TB being coined as a disease of poverty, wherein as much as two-thirds of infections are reported within the (15–59) age group, typical adulthood.
- The next curtailing factor is the high cost of first-line anti-TB drugs (isoniazid, rifampicin, pyrazinamide, and ethambutol) that restricts their usage and aggravates the frequent resistance episodes. This factor has been the limiting cause of inadequate progress in emerging TB treatments and has vitally affected countries like India and others.
- The resistance episodes in Mtb toward the major first-line chemotherapeutic agents have marred the treatment of TB cases. The last but not least issue relates to a major extent of date of diagnosis procedures as being immunoassay-driven, resulting in reduced specificity. It is worth mentioning here that Mtb shares antigens with several other Mycobacterium species, owing to which the incidence of false-positive testing is noted in as much as 35% of active sufferers. Besides immunoassays, several other techniques such as flow cytometry, radiometric detection, and latex agglutination are also used but all suffer from one or more disadvantages about time-consuming detection procedure, skilled manpower requirement, nonreproducibility of measurements, costly probe configuration, etc.
- **Current diagnosis**: Present-stage TB diagnosis is done via immunological-cum-microbiological and genotypic tests. The following sections discuss the major characteristics of these techniques with a focus on their inadequacies.
- **Immunological-cum-microbiological tests**: The different configurations of these tests are available for TB diagnosis, mentioned next in chronological order:
  - **Smear microscopy**: Microscopy-based smear tests are very rapid, inexpensive, simple, and relatively easy-to-perform procedures for the detection of acid-fast bacterium such as Mtb. Usually, the Ziehl–Neelsen staining is employed needing at least $10^4$ bacteria per ml sputum. The fluorescence microscope using auramine-rhodamine staining is comparatively more sensitive despite being expensive, owing to its necessity of a fluorescence microscope. A higher sensitivity of this method is attributed to the feasible examination suitability of slides at lower magnification. This method processes results within hours.
  - **Immunological assays (latex agglutination, ELISA, and Mantoux tests)**: These tests are based on the typical binding of serum antibodies to Mtb antigen. For instance, in latex agglutination tests, the latex (as polystyrene) beads are functionalized with antigens extracted from a pathogenic Mtb, which are subsequently reacted with serum samples. The completion of the reaction results in coagulation of latex beads demarcating a positive response. These

tests do not have a high sensitivity, owing to which these often meet failure whenever the bacterial load is lower than a threshold. Furthermore, the presence of antibodies in the serum could also interfere with the analysis and aggravate the error-prone inferences.

- **Radiometric detection test**: This test estimates the Mtb metabolic activity through radiological means. For instance, the *Mycobacterium* species are well known to generate $CO_2$ from the carbon sources like glycerol or acetate. The important selective criterion concerning Mtb herein pertains to its inability of generating $CO_2$ from glucose. Using this selective $CO_2$-generating characteristic, the Mtb capability in generating $14CO_2$ from 14C-U-glycerol or 14C-U-acetate but not from 14C-U-glucose is estimated. This method draws very low responses from developing countries owing to the technical complexity.
- **Flow cytometry test**: Over the past few years, this technique has swiftly witnessed an increment in the detection of TB cases. The method herein exploits the ability of viable Mtb to absorb fluorescein diacetate (FDA) and hydrolyze it into fluorescein, which on being accumulated in the metabolically active bacterium could be viably detected. The reproducibility of this method is high, along with null active mycobacterial cell division. The technique, however, desperately needs a sophisticated infrastructure and skilled manpower, which are seldom accomplished in developing countries.
- **Cultivation detection tests (like BACTEC MGIT 960 systems)**: In these techniques, biological samples are selectively cultured on solid media to detect and quantify Mtb. Though operationally quite accurate, a (9–42)-day growth period is required by this method. The method also requires a laboratory backup, which complicates applications under field conditions in developing countries.
- **Genotypic tests**: DNA-based techniques are rapidly assuming significance, in particular for the Mtb-resistant stain detection. These tests mandate a laboratory-scale optimization and therefore do not represent an apt option. The following are the most important variations of these tests:
  1. **Assays based on polymerase chain reaction**: Of the well-documented and studied molecular assays, PCR-mediated Mtb screening relies on the recognition of specific gene sequences (from the mixture of all host genes fragments) using the complimentary primers. The PCR-based assays are the most sensitive techniques for screening the codons responsible for Mtb resistance. The DNA fragments amplified by PCR protocol [better termed as restriction fragment length polymorphisms (RFLPs)] are thereafter analyzed using electrophoresis or hybridization-based assays.

     ***The following are the brief operational steps of these techniques***:
  2. **Electrophoresis**: This analytical technique works based on charge-modulated electrophoretic mobility of the mutated Mtb fragments, especially those of resistant strains. The analysis is made via comparison of PCR-amplified DNA with the electrophoretic mobility of wild/reference Mtb DNA to screen the resistant genotype. In the past few years, a heteroduplex assay has also been reported for the identification of single-

base mismatched strands. The strands are isolated from the null mismatched containing strands using the confirmatory gel electrophoresis assay.

3. **Hybridization-based methods**: These methods are based on the hybridization of clinical DNA fragments with those of complementary DNA. The concomitant binding is thereafter compared with the outcomes of wild/reference Mtb DNA. The binding of clinical DNA can be ascertained via ELISA readers in case of the significant homologous complementary strand. The hybridization could be accomplished with the help of strips, microtiter plates, and microarrays.

– **Real-time polymerase chain reaction**: It is feasible to visualize the increasing concentration of a DNA strand in real time using fluorescently labeled DNA strands. Several fluorescent labels are applied in an adverse range of real-time PCR techniques, such as TaqMan probes, Beacons, and FRET probes.
– Exclusive demerits of PCR tests comprise relatively high equipment and reagent costs. The method also mandates the requirement of skilled personnel along with dedicated pre- and post-PCR rooms to keep the contamination at bay. Furthermore, the technological dependence and sample preparation complexity make these procedures inappropriate in resource-poor economies.

## 8.5 Biomarkers for Tuberculosis Detection

- Figure 25 distinguishes the pathogen and host-based biomarkers, primed for TB diagnosis. From a pathogenic perspective, Mtb products could be aptly distinguished in the blood, sputum, or urine. The blood and urinal detections can be made with a higher sensitivity contrary to that of Mtb culture from the analogous

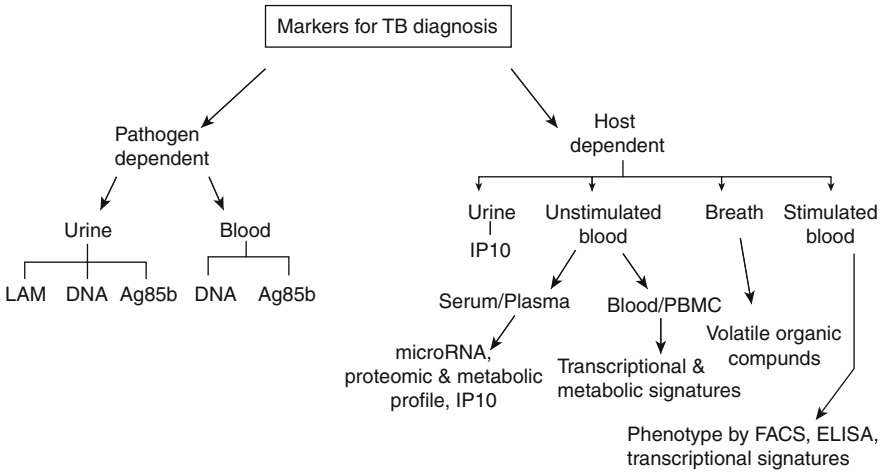


**Fig. 25** Diversity of TB diagnosis biomarkers. The current regime has more reliability for pathogen-dependent screening as the detection is exact and prompt

biological fluid. The Mtb cell wall constituent, lipoarabinomannan (LAM), is reported as a discrete TB biomarker in light of the low sensitivity of the conventional urinal analysis.

- Although well below par the conventional standards recommended to date, the Mtb DNA and LAM detection in the urinal samples of HIV-infected patients could be a decisive approach for the detection of advanced TB with low CD4 T-cell counts. Of note, Mtb Ag85 complex is a (30–32) kD family of three proteins, namely, Ag85A, Ag85B, and Ag85C, characterized by the mycolyl transferase-mediated coupling of mycolic acids to arabinogalactan of the *Mycobacterium* cell wall and in the biological formation of cord factor. Multiple studies pinpoint the significance of Ag85 (in blood and urine) as an Mtb detection marker.
- Among the host biomarkers, several non-sputum-based assays for active TB screening are validated using serum, plasma, urine, or stimulated or unstimulated blood. In light of serum or plasma products, Mtb-specific Ab detection is not an accurate diagnostic method due to a heterogeneous Mtb response pattern. Apart from this, the WHO guidelines also voiced against the use of these tests for active TB diagnosis. Studies on serum microRNAs have been reported with variable success for active TB diagnosis in drug-sensitive and drug-resistant subjects.
- A broad range of potential transcriptional biomarkers have also been reported, including neutrophil-driven interferon (IFN)-inducible gene profiles comprising both type 2 IFNγ and type I (IFNαβ). IFN signaling represents a significant TB signature traceable in peripheral blood from pulmonary TB patients. Such findings have been complemented in the analysis of other populations and in several other studies where the manifestation of TB could be distinguished from other respiratory infections and inflammatory diseases. Correlations with IFN expression have inferred enhanced activity for the diseased state, which decreased for the treatment state.
- Diagnostic indications of a TB distinction from other diseases and LTBI were noticed in children from South Africa, Malawi, and Kenya. Disappointingly, a persistent challenge in the detection of new childhood TB pertains to missing references due to a cumbersome microbiological diagnosis of active disease. Analysis complexity and expensive operational requirements (related to transcriptional profiles) make the diagnosis difficult and urgently require the development of easier technologies.
- IFNγ-inducible protein 10 (IP10) has been studied as being enhanced in the unstimulated plasma of children and adults having active TB. This has been screened using different methodologies based on lateral flow assays using the interference-free, fluorescent upconverting phosphor extents. Of significant interest is the fact that IP10 could also be detected in the urine of adult patients. A study conducted on Ugandan children infected with TB revealed decreased IP10 expressions in response to efficacious therapy.
- Potential breakthroughs in TB diagnosis have also been enabled by the advanced mode functioning of multiparametric flow cytometry, allowing simultaneous screening of manifold immune functions in single cells, such as cytokine

generation and memory status. Polyfunctional T-cells are capable of generating more than one cytokine at the same instant and are the active components of the immune response toward different pathogenic species. The T-cells producing IFNγ, TNFα, and IL12 are associated with guarding immune responses in HIV nonprogressing subjects. Studies focused on analyzing the role of polyfunctional T-cells in TB do not decipher a homogenous conclusive outlook. Active TB has been linked either with monofunctional TNFα-$CD4^+$ T-cells or double-functional $IFN\gamma^+$ $TNF\alpha^+$ $CD4^+$ T-cells. Contrary to this, the activation and memory states of Mtb-specific T-cells are generally more in agreement, even when comparing patient populations at different sites.

- While the effector T-cells grow amidst Mtb replication, the memory cells regulate the arrest and elimination of Mtb infection. It is pertinent to mention here that active TB infection is profusely estimated by suppressed CD27 surface expression over the circulating Mtb-antigen-stimulated $CD4^+$ T-cells. More recently, an erstwhile T-cell activation marker, (TAM-TB) assay has been demonstrated for active TB recognition in children. This assay relied on the stoichiometric variations of median fluorescence intensity of all $CD4^+$ and $CD27^+$ T-cells to those of Mtb-explicit $CD4^+CD27^+$ T-cells (CD27 MF1 ratio). This marker has been evaluated in adults from a low TB-endemic country, where it successfully distinguished the various stages of a TB infection.
- A breakthrough study based on blood analysis showed the expression of immune activation markers, CD38, HLA-DR, and proliferation marker, Ki-67 on Mtb-specific $CD4^+$ T-cells, involved with Mtb load. It was noticed that modulation of these markers adequately distinguished active TB cases from those of LTBI with 100% specificity and over 96% specificity. These markers also classified the individuals who had completed TB therapy, indicating a correlation with the decrease in mycobacterial load after treatment. Of eminence is the recent finding of T-cell activation as an immune correlate of risk for TB development in BCG-vaccinated infants.
- Nontargeted methods to screen and identify novel markers for TB sufferers are primed on transcriptomic, proteomic, and metabolomics hypotheses. A noted attempt herein analyzed the transcriptomic and metabolic contour of patients infected with two distinct Mtb lineages (Maf and Mtb), before and after anti-TB therapy. The main aim of the investigation was to identify and enumerate the distinctions in host factors and biological events associated with diseased pathology and the corresponding explicit treatment response. It was noticed that peripheral blood gene expressions were not significantly distinct between the Maf- and Mtb-infected patients at the pretreated stage. However, the extents considerably differed at the post-treatment stage. On the whole, the investigation summarized that the pre- and post-treatment genotypes were exclusive functions of the characteristic immune response.
- It is urgent to mention herein that the upstream regulator hepatocyte nuclear factor 4-α regulated ~15% of distinctively expressed genes in the post-treatment groups. Surprisingly, the serum metabolic profiles of Maf and Mtb strain-infected sufferers remained unchanged both at pre- and post-treatment stages. Subsequently,

the advent of analytical tools like mass spectrometry or protein chip technology enabled the distinctive analysis of the proteomic profile of TB sufferers and healthy individuals. The noted host markers that distinguished the TB sufferers from those suffering from erstwhile infections and inflammatory disorders included transthyretin, CRP, and neopterin. Interestingly, the sputum analysis also distinguished the sufferers via analyzing the proteomic profiles based on smear-positive and -negative TB patients contrary to those of control models.

- The biomarkers specific for active pulmonary TB may prevail in the volatile organic compounds (VOCs) in the breath, both from the infecting organism and the infected host. These signatures could be the outcomes of concomitant oxidative stress. For a definitive screening, a breath test for the presence of VOCs could be done, wherein potential biomarkers of active pulmonary TB could be ascertained with ~85% accuracy in symptomatic high-risk individuals. The presence of VOCs in the picomolar range complicates their screening, typically remaining out of the measurable extents of the majority of conventionally used instruments.

## 8.6 Biosensor-Mediated Early Tuberculosis Diagnosis

Knowing that 98% of all TB cases prevail in developing countries, where access to specialized and advanced facilities in a laboratory setup is scarce, there is a dire necessity to develop alternative, simpler, and low-cost techniques for TB diagnosis. The varying sensing and transduction modes of a biosensor facilitate prompt detection of these responses through simplistic and efficient measurement of optical, thermal, and electrical signals. Major advances in biosensors for a faster TB diagnosis are as follows:

- **Technical advantage**: Biosensors empower a high level of device and capture, followed by integration achieved through single-step detection.
- **Quick response**: The typical response time of a biosensor analysis is within the range of a few minutes in most configurations, together enabling rapid and significant measurement control.
- **Ease of use**: Many designed and optimized biosensor configurations are equipped with user-friendly interfaces for connection with advanced instrumentation.

The following points discuss the most recent biosensor studies aimed at a faster and more efficient TB diagnosis. The salient aspects of performance analysis aspects are briefed.

- A recent attempt focusing on the practical demerits (longer detection time than the conventional approaches for MTb detection) is the 2020 study by Zhang and associates. The investigation reported an electrochemical biosensor using a 16S rDNA fragment of Mtb, H37Ra as the target marker. Peptide nucleic acid (PNA) was used as a capture probe while 2D $Ti_3C_2$MXenes (having high conductance)

were used for signal transduction. Amidst the assay development, the PNA and 16S rDNA-specific fragment was hybridized on the substrate of the PNA-Au NPs network electrode, after which the target fragments were directly conjugated with $Ti_3C_2$MXenes. This linkage was stabilized by the strong interactions between zirconium cross-linked $Ti_3C_2$MXenes and the phosphate moieties of target fragments, which bridged the gaps of interrupted Au NPs in the nanogap network electrode, giving rise to a conductive passage to monitor the conductance variation across the electrodes. The conductance variation was monitored for Mtb screening, which was completed in 2 h with an LOD of 20 cfu•ml$^{-1}$. The PNA used in the analysis was an unnatural DNA analog, comprising repeating neutral, N-(2-aminoethyl) glycine functionality, linked together via peptide bonds and having nucleotide bases. The as-designed sensor configuration functioned well and enabled the Mtb detection in 40 stimulated sputum samples. Thereby, this study explained the success of the shift from PNA to highly Ti3C2MXenes, across the nanogap network electrodes, enabling the detection using a sharp conductance change (Zhang et al. 2020).

- Another rigorous 2020 attempt from Pelaez and colleagues reported a portable, user-friendly, and low-cost biosensor working in a label-free manner and using SPR sensitivity. The configuration was a direct immunoassay for spontaneous detection and quantification of the heat shock protein X (HspX), a standard biomarker of Mtb, prevailing in pretreated sputum samples. The sensing mechanism relies on highly specific MAbs that were previously immobilized on the plasmonic sensor surface. The optimized configuration enabled direct detection of Hsp without amplification, with a 0.63 ng•ml$^{-1}$ LOD and 2.12 ng•ml$^{-1}$ as the limit of quantification (LOQ). Also, the inspection of pretreated sputum samples revealed significant differences in the Hsp patient concentration, for those infected with TB, (116–175) ng•ml$^{-1}$ concentration extents compared to below LOQ for the uninfected subjects (Pelaez et al. 2020).
- A highly significant attempt by Gupta and colleagues used a magnetic biosensor relying on giant magnetoresistance (GMR) for on-field TB detection through assessing an Mtb-specific protein, ESAT-6 (early secretory antigenic target). The specific reason to choose ESAT-6 as the MTB detection protein was its secretion at the initial infection stage besides a prominence in progressive TB infection. The investigators opined that due to a molecular weight of 6 kDa, ESAT-6 is a small protein that can bind to toll-like receptor-2 (TLR-2) directly and also exhibits an inhibiting capability toward the downstream transduction of signaling events. Furthermore, ESAT-6 can form a heterodimer with culture filtrate protein (CFP-10), another MTB-secreted antigenic protein, having a molecular weight of 10 kDa. The portable configuration served as a highly sensitive diagnostic tool and detects MTB with a low turnaround time and a pg•ml$^{-1}$ ranged LOD. The use of DARPins (designed ankyrin repeat proteins) in the optimized configuration confers a high specificity and aids in prompt detection, thereby enabling early treatment onset with reduced mortality. The comparison with conventional and Au NPs-assisted ELISA inferred the developed configuration as more sensitive. Utility analysis revealed a likelihood of sensitivity improvement through

variation in the structural composition and size of MNPs, with the larger-sized NPs (40 nm radius) exhibiting higher signal strengths for low concentrations compared to small-sized NP (5 nm radius). Besides, there is the feasibility of real integration of GMR biosensors with several other standardized procedures; it was found that this technique could be sued for the detection of malignant pathogens such as HIV and drug-resistant mutants (Gupta and Kakkar 2019).

- Another significant attempt by the same group (Zhang et al, the first being the discussed 2020 investigation) illustrated the design of an electrochemical biosensor for screening of MTB reference strain, H37Rv. Optimized configuration used H37Rv aptamer (as recognition probe) and oligonucleotides engineered using Au NPs. Detection was made via monitoring the frequency variations, conferred by Au NPs conjugated with DNA, in the presence of H37Rv, with the aid of a multi-channel series piezoelectric quartz-crystal (MSPQC) system. Three oligonucleotides were engineered with Au NPs and were hybridized with 37 nucleotides comprising H37Rv aptamer, which was immobilized over the Au electrode using Au–S linkages. A conductive layer was henceforth generated by the sequential hybridization of the aptamer with the Au NPs-functionalized DNA segments. The binding of the pathogenic (Mtb) strain to the aptamer took place in the presence of H37Rv and resulted in the detachment of Au NPs-conjugated DNA from the electrode surface. The conductive film was thereafter replaced by an insulating aptamer-conjugated bacterial complex. The discrete variations were recorded by the MSPQC system. The optimized configuration facilitated a rapid, implicit, and sensitive detection and provided the response in 2 h with a 100 CFU•ml$^{-1}$ LOD (Zhang et al. 2019b).
- Another elegant study of 2019 itself was reported by Bai and colleagues from China, wherein detection of IS6110 MTB fragment was made using novel sensing mechanisms of an electrochemical DNA biosensor. The sensor probe comprised of a nanohybrid of Au NPs-decorated fullerene NPs/nitrogen-doped graphene nanosheet, which directly served as a new signal tag. This probe generated a signal response without additional redox molecules and was thereafter labeled with signal probes to form a tracer label for accomplishing signal amplification. In an attempt to further improve the diagnosis sensitivity, biotin–avidin conjugation was configured to immobilize abundant capture probes. On the fabrication of typical sandwich hybridization, the designed biosensor was incubated with tetraoctylammonium bromide (TOAB). This TOAB incubation boosted the induced intrinsic redox activity of the tracer label and generated a discriminating current response. The optimized configuration exhibited a broad linear range functioning for 10 fM to 10 nM Mtb determination with a 3 fM LOD. In terms of selectivity, the designed sensor distinguished a mismatched DNA sequence and also differentiates Mtb from other pathogenic agents. The preliminary scrutiny of the clinical analysis revealed an excellent ability to recognize the PCR products of clinical samples. Thus, after the Hsp and ESAT-6 protein identification in earlier 2020 and 2019 studies, this is the third attempt toward identifying Mtb using its IS6110 fragment (Bai et al. 2019).

- In a noted 2018 study from the collaboration of Kazakhstan and the United Kingdom, Sypabekova and colleagues optimized the feasibility of a synthetic receptor in the form of an aptamer (a short stretch of oligonucleotides) for the detection of secreted protein MPT64, which is an acutely immunogenic polypeptide of *MTB*. Toward the sensing efficacy, the investigators screened the combinatorial effects of an aptamer linker and a co-adsorbent over an Au electrode for optimal binding efficiency and reduced nonspecific interactions for label-free MPT64 detection using EIS. Two configurations of co-adsorbents and aptamer linkers were studied and high specificity and sensitivity to MPT64 were noticed for a surface prepared with a thiol PEGylated aptamer, HS-$(CH_2)_6$-$OP(O)_2O$-$(CH_2CH_2O)_6$-TTTTT-aptamer and 6-mercaptohexanol in 1:10 stoichiometry. The optimized configuration was evaluated for real-time significance via access to a spiked human serum sample with an LOD of 81 pM. This study, therefore, demonstrated the application suitability of MPT64 aptamer as a low-cost, accurate, and stable replacement of antibodies for the development of point-of-care TB biosensors, decreasing the detection time from several days or hours to 30 min (Sypabekova et al. 2018).
- Another study of 2018 is the study by Phan and colleagues, who designed a highly specific and accurate dot-blot immunoassay for the detection of culture filtrate protein ($M_w$: 10 kDa, CFP-10) through the formation of a Cu nanoshell on Au NPs surface. The optimized assay configuration worked through a $Cu^{+2}$ reduction on the GBP-CFP10G2-Au NPs conjugate, possessing Au binding and antigen-binding affinities simultaneously, appearing as a red dot that could be noticed with the naked eye. The dot intensity was found proportional to CFP-10 TB antigen, with a 7.6 pg•$ml^{-1}$ LOD. The analytical performance of optimized dot-blot configuration was studied as superior to that of a conventional Ag nanoshell. The probe efficacy toward real-life detection ability was also monitored via identification of CFP-10 antigen in urine samples, wherein minimum steps, high sensitivity, and specificity were observed (Tu Phan et al. 2018).
- Yet another 2018 attempt comprises an attempt from Malaysia, wherein yet again CFP-10 identification was made using a robust sandwich electrochemical immunosensor working through fabricated graphene/polyaniline (GP/PANI) nanocomposite over the screen-printed Au electrode. The configuration enabled an efficient detection of CFP10, with the Gp/PANI probe being characterized using FT-IR spectroscopy and FE-SEM. The morphology and chemical bonding pattern of GP/PANI nanocomposite were studied using FE-SEM and Raman spectroscopy revealed a successful coating of GP/PANI composite on the SPGE using a drop-cast technique. The coating of nanocomposite enhanced the SPGE surface area by nearly five times than the uncoated SPGE. The probe functioning was monitored and validated using CV and DPV analysis, wherein the CFP10 detection could be optimized. The optimized configuration exhibited a wide linear range (20–100) ng•$ml^{-1}$ with an LOD of 15 ng•$ml^{-1}$, thereby conveying the sensitivity, rapidity, and disposable suitability of the designed configuration for TB detection within the real samples (Azmi et al. 2018). Studies like these serve as valuable databases for biosensing advances of graphene and related

compounds. The results of this investigation must be compared with NPs' functionalized graphene to understand whether the composite framework could substitute an NP under certain conditions.

- Yet another significant attempt by Bakhori and colleagues reported a plasmonic ELISA method to study the antigen–antibody interaction using an ultrasensitive and affordable naked eye TB detection and diagnosis. The detection mechanism made use of the biocatalytic cycle of intracellular enzymes, which induces the formation and successive growth of Au NPs. The detection of TB analytes in the sample solution was inferred by the formation of differently colored solutions by the plasmonic NPs in the presence of enzyme labels. The detection of disease was made using the standardized ELISA working that used catalase-labeled Abs, the enzymes consumed $H_2O_2$ and further generate Au NPs on the inclusion of $AuCl_3$. The blue or red color of the Au NPs-containing solution as a confirmatory indication for naked eye detection of TB analytes was determined based on the leftover $H_2O_2$ amount in the solution. This feature distinguished the optimized assay from conventional ELISA, which only develops tonal colors and requires a high analyte concentration to achieve distinguishing naked eye detection. The investigators also incorporated the MTB-specific ESAT-6 protein fragment in the optimized configuration for the detection of TB using plasmonic ELISA. The technique enabled the CFP-10 detection limit to as low as 0.01 $\mu g \cdot ml^{-1}$ on being visualized by the naked eye. The designed sensor was also studied on a confirmatory scale with the sputum samples from TB-positive patients, thereby providing enough evidence for a manifested suitability for early TB diagnosis (Bakhori et al. 2018).

## 9 Conclusions

Biomaterials exhibit immense potential for being used as sensing the interactions of the biological platforms. The structure-activity-specific functioning of these entities makes them competent for diversified activities. With advancements in characterization techniques and the emergence of shape and size-dependent functioning of NMs, the potential of biological sensing has evolved over a new horizon. The natural flexibility and self-assembly-driven sensing of biomaterials are widely instrumental in their roles as implicit detection moieties. Tailoring of NMs with biocompatible probes has been a major achievement of the emerging nanoscale phenomenon, wherein a precise detection of the slightest deviations in the properties has become possible. Many studies are in the final phase of being put on the commercialization scale, but there is no second path to meeting the set ethical guidelines, for which the procedures regarding reproducible outcomes have to be met. Such imbibitions manifest an urgent need of bridging the material sciences, electronics, and biological sciences so that smart biofunctional materials with steadfast and accurate responses could be developed. About mammalian cells, the whole tissues or specific regions are equally capable of being used as sensors, but appropriate measures must be considered to prevent any possible cross-reactions.

## 10 Cross-References


- ▶ Emerging Interest in the Use of Au and Ag NPs for Drug Delivery
- ▶ Focused on Compatible Biological Interactions of Nanomaterials
- ▶ How Nanomaterials Could be Used in Precise Biological Imaging


## References


Azimzadeh M, Nasirizadeh N, Rahaie M, Naderi-Manesh H. Early detection of Alzheimer's disease using a biosensor based on electrochemically-reduced graphene oxide and gold nanowires for the quantification of serum microRNA-137. RSC Adv. 2017;7:55709.

Azmi UZM, Yusof NA, Kusnin N, Abdullah J, Suraiya S, Ong PS, et al. Sandwich electrochemical immunosensor for early detection of tuberculosis based on graphene/polyanline-modified screen-printed gold electrode. Sensors. 2018;18:3926.

Bai L, Chen Y, Liu X, Zhou J, Cao J, Hou L, et al. Ultrasensitive electrochemical detolvedection of Mycobacterium tuberculosis IS6110 fragment using gold nanoparticles decorated fullerene nanoparticles/nitrogen doped graphene nanosheet as signal tags. Anal Chim Acta. 2019;1080: 75–83.

Bakhori NM, Yusof NA, Abdullah J, Wasoh H, Noor SSM, Raston NHA, et al. Immunonanosensor for the ultrasensitive naked eye detection of tuberculosis. Sensors. 2018;18:1932.

Biju V. Chemical modifications and bioconjugate reactions of nanomaterials for sensing, imaging, drug delivery and therapy. Chem Soc Rev. 2014;43:744–64.

Cai X, Weng S, Guo R, Lin L, Chen W, Zheng Z, et al. Ratiometric electrochemical immunoassay based on internal reference value for reproducible and sensitive detection of tumor marker. Biosens Bioelectron. 2016;81:173–80.

Chard T. Pregnancy tests: a review. Hum Reprod. 1992;7:701–10.

Dembski S, Graf C, Kruger T, Gbureck U, Ewald A, Bock A, et al. Photoactivation of CdSe/Zns quantum dots embedded in silica colloids. Small. 2008;4:1516–26.

DeSantis C, Ma J, Bryan L, Jemal A. Breast cancer statistics, 2013. CA Cancer J Clin. 2014;64: 52–62.

Drbohlavova J, Adam V, Kizek R, Hubalek J. Quantum dots-characterization, preparation and usage in biological systems. Int J Mol Sci. 2009;10:656–73.

Eissa S, Abdulkarim H, Dasouki M, Mousa HA, Amout R, Saud BA, et al. Multiplexed detection of DOCK8, PGM3 and STAT3 proteins for the diagnosis of Hyper-Immunoglobulin E syndrome using gold nanoparticles-based immunosensor array platform. Biosens Bioelectron. 2018a;117: 613. https://doi.org/10.1016/j.bios.2018.06.058.

Eissa S, Alshehri N, Abduljabbar M, Rahman AMA, Dasouki M, Nizami IY, et al. Carbon nanofiber-based multiplexed immunosensor for the detection of Survival Motor Neuron 1, Cystic Fibrosis Transmembrane Conductance Regulator and Duchenne Muscular Dystrophy proteins. Biosens Bioelectron. 2018b;117:84. https://doi.org/10.1016/j.bios.2018.05.048.

Ghaderinezhad F, Koydemir HC, Tseng D, Karnica D, Liang K, Ozcan A, et al. Sensing of electrolytes in urine using a miniaturized paper-based device. Sci Rep. 2020;10:13620.

Griffin EG, Nelson JM. The influence of certain substances on the activity of invertase. J Am Chem Soc. 1916;38:722–30.

Guilbault GG, Montalvo JG Jr. Urea-specific enzyme electrode. J Am Chem Soc. 1969;91:2164–5.

Gupta S, Kakkar V. DARPin based GMR biosensor for the detection of ESAT-6 tuberculosis protein. Tuberculosis. 2019;118:101852.

Hackshaw AK, Law MR, Wald NJ. The accumulated evidence on lung cancer and environmental tobacco smoke. BMJ. 1997;315:980–8.

Haddour N, Cosnier S, Gondran C. Electrogeneration of a poly(pyrrole)-NTA chelator film for a reversible oriented immobilization of histidine-tagged proteins. J Am Chem Soc. 2005;127:5752–3.
Heineman WR, Jensen WB, Clark Jr. LC. (1918–2005). Biosens Bioelectron. 2006;21:1403–4.
Holzinger M, Goff AL, Cosnier S. Nanomaterials for biosensing applications: a review. Front Chem. 2014;2:Article 63, 1–10
Hughes WS. The potential difference between glass and electrolytes in contact with the glass. J Am Chem Soc. 1922;44:2860–7.
Issa B, Obaidat IM, Albiss BA, Haik Y. Magnetic nanoparticles: surface effects and properties related to biomedicine applications. Int J Mol Sci. 2013;14:21266–305.
Li F, Feng Y, Wang Z, Yang L, Zhuo L, Tang B, et al. Direct electrochemistry of horseradish peroxidase immobilized on the layered calcium carbonate-gold nanoparticles inorganic hybrid composite. Biosens Bioelectron. 2010;25:2244–8.
Li S-S, Lin C-W, Wei K-C, Huang C-Y, Hsu P-H, Liu H-L, et al. Non-invasive screening for early Alzheimer's disease diagnosis by a sensitively immunomagnetic biosensor. Sci Rep. 2016;6:25155.
Michalet X, Pinaud FF, Bentolila LA, Tsay JM, Doose S, Li JJ, et al. Quantum dots for live cells, in vivo imaging and diagnostics. Science. 2005;307:538–44.
Mittal S, Kaur H, Gautam N, Mantha AK. Biosensors for breast cancer diagnosis: a review of bioreceptors, biotransducers and signal amplification strategies. Biosens Bioelectron. 2017;88:217–31.
Negahdary M, Heli H. An ultrasensitive electrochemical aptasensor for early diagnosis of Alzheimer's disease, using a fern leaves-like gold nanostructure. Talanta. 2019;198:510–7.
Park D, Kim JH, Kim HJ, Lee DS, Yoon DS, Hwang KS. Multiplexed femtomolar detection of Alzheimer's disease biomarkers in biofluids using a graphene oxide field-effect transistor. Biosens Bioelectron. 2020;167:112505.
Parker AR, McPhedran RC, McKenzie DR, Botten LC, Nicorovici N-AP. Aphrodite's iridescence. Nature. 2001;409:36–7.
Pelaez EC, Estevez MC, Mongui A, Menendez MC, Toro C, Herrera-Sandoval OL, et al. Detection and quantification of HspX antigen in sputum samples usingplasmonic biosensing: towards a real point of care (POC) for tuberculosis diagnosis. ACS Infect Dis. 2020;6:1110–20.
Pereira AC, Sales MGF, Rodrihues LR. Biosensors for rapid detection of breast cancer biomarkers, Chapter-3. In: Advanced biosensors for health care applications. 2019. https://doi.org/10.1016/B978-0-12-815743-5.00003-2.
Phan LMT, Rafique R, Baek SH, Nguyen TP, Park KY, Kim EB, et al. Gold-copper nanoshell dot-blot immunoassay for naked-eye sensitive detection of tuberculosis specific CFP-10 antigen. Biosens Bioelectron. 2018. https://doi.org/10.1016/j.bios.2018.08.068.
Polvikoski T, Sulkava R, Rastas S, Sutela A, Niinistö L, Notkola IL. Incidence of dementia in very elderly individuals: a clinical, neuropathological and molecular genetic study. Neuroepidemiology. 2006;26:76–82.
Poznyak SK, Talapin DV, Shevchenko EV, Weller H. Quantum dot chemiluminescence. Nano Lett. 2004;4:693–8.
Qin J, Jo DG, Cho M, Lee Y. Monitoring of early diagnosis of Alzheimer's disease using the cellular prion protein and poly(pyrrole-2-carboxylic acid) modified electrode. Biosens Bioelectron. 2018;113:82. https://doi.org/10.1016/j.bios.2018.04.061.
Resch-Genger U, Grabolle M, Cavaliere-Jaricot S, Nitschke R, Nann T. Quantum dots versus organic dyes as fluorescent labels. Nat Methods. 2008;5:763–75.
Rocha-Santos TAP. Sensors and biosensors based on magnetic nanoparticles. Trends Anal Chem. 2014;62:28–36.
Russell P. Photonic crystal fibers. Science. 2003;299:358–62.
Siddique RH, Gornard G, Holscher H. The role of random nanostructures for the omnidirectional anti-reflection properties of the glasswing butterfly. Nat Commun. 2015;6:6909.

Sin MLY, Mach KE, Wong PK, Liao JC. Advances and challenges in biosensor-based diagnosis of infectious diseases. Exp Rev Mol Diagn. 2014;14:225–44.

Sirisha VL, Jain A, Jain A. Enzyme immobilization: an overview on methods, support, materials and applications of immobilized enzymes. In: Advances in food and nutrition research. Amsterdam: Academic; 2016. ISSN: 1043-4526.

Sypabekova M, Jolly P, Estrela P, Kanayeva D. Electrochemical aptasensor using optimized surface chemistry for the detection of *Mycobacterium tuberculosis* secreted protein MPT64 in human serum. Biosens Bioelectron. 2018;123:141. https://doi.org/10.1016/j.bios.2018.07.053.

Toren P, Ozgur E, Bayindir M. Real-time and selective detection of single nucleotide DNA mutations using surface engineered microtoroids. Anal Chem. 2015;87:10920. https://doi.org/10.1021/acs.analchem.5b02664.

Toren P, Ozgur E, Bayindir M. Label-free biodetection of pathogen virulence factors in complex media using microtoroids with multifunctional surface functionality. ACS Sensors. 2018;3:352. https://doi.org/10.1021/acssensors.7b00775.

Turkevich J, Stevenson PC, Hillier J. A study of the nucleation and growth processes in the synthesis of colloidal gold. Discuss Faraday Soc. 1951;11:55–75.

Wang L, Chen D, Jiang K, Shen G. New insights and perspectives into biological materials for flexible electronics. Chem Soc Rev. 2017;46:6764.

Wilchek M, Bayer E. The avidin-biotin complex in bioanalytical applications. Anal Biochem. 1988;171:1–32.

Wu H-T, Chen Y-L, Huang Y-C, Liu W-C, Yaw NM, Hseih B-Y, et al. Colloid-gold nanoparticle enhanced detection sensitivity of paired surface plasma waves biosensor. In: Proceedings of SPIE – the international society for optical engineering, vol. 6447. 2007.

Yang G, Xiao Z, Tang C, Deng Y, Huang H, He Z. Recent advances in biosensor for detection of lung cancer biomarkers. Biosens Bioelectron. 2019;141:111416.

Yoo YK, Kim J, Kim G, Kim YS, Kim HY, Lee S, et al. A highly sensitive plasma-based amyloid-β detection system through medium-changing and noise cancellation system for early diagnosis of the Alzheimer's disease. Sci Rep. 2017;7:8882.

Zhang K, Yang Q, Fan Z, Zhao J, Li H. Platelet-driven formation of interface peptide nano-network biosensor enabling a non-invasive means for early detection of Alzheimer's disease. Biosens Bioelectron. 2019a;145:111701.

Zhang X, Feng Y, Duan S, Su L, Zhang J, He F. *Mycobacterium tuberculosis* strain H37Rv electrochemical sensor mediated by aptamer and AuNPs-DNA. ACS Sensors. 2019b;4:849–55.

Zhang J, Li Y, Duan S, He F. Highly electrically conductive two-dimensionsl $Ti_3C_2$Mxenes-based 16S rDNA electrochemical sensor for detecting *Mycobacterium tuberculosis*. Anal Chim Acta. 2020;1123:9–17.